UNIVERSITÀ DEGLI STUDI DI PADOVA

TÉCNICO LISBOA

Università degli Studi di Padova
Centro interdipartimentale "Centro Ricerche Fusione"

Universidade de Lisboa
Instituto Superior Técnico (IST)

JOINT RESEARCH DOCTORATE IN FUSION SCIENCE AND ENGINEERING
Cycle XXVIII

Interaction between neutral beam fast particles and plasma in fusion experiments

Coordinator: Prof. Paolo Bettini

Supervisors: Dr. Tommaso Bolzonella, Prof. Francesco Gnesotto

Ph.D. student: Pietro Vincenzi

Padova, January 2016

JOINT Doctorate and NETWORK in Fusion Science and Engineering.
Network Partners:

- Instituto Superior Técnico (IST) Lisboa, Portugal
- Universitá degli studi di Padova, Italy
- Ludwig Maximilians University Munich, Germany

In collaboration with:

- Consorzio RFX, Italy
- IPP Garching, Germany

"I ought to know by this time that when a fact appears opposed to a long train of deductions it invariably proves to be capable of bearing some other interpretation."

Sherlock Holmes "A Study in Scarlet" (1887) by Sir Arthur Conan Doyle

CONTENTS

1 INTRODUCTION 1
- 1.1 The energy supply problem 1
- 1.2 A promising candidate for future energy supply: nuclear fusion 2
- 1.3 Thermonuclear fusion by magnetic confinement 4
- 1.4 General structure of the work 7

2 BASICS OF NEUTRAL BEAM INJECTION (NBI) 9
- 2.1 NB system: the generation of the beam 11
- 2.2 Basics NBI-plasma interaction physics 14
  - 2.2.1 Plasma heating by NBI 14
  - 2.2.2 NB current drive 18
  - 2.2.3 Not only heating and CD: further considerations 20
- 2.3 Tools for NBI-plasma interaction modelling 21

3 STAND-ALONE NBI-PLASMA SIMULATIONS 23
- 3.1 NBI-plasma interaction at JET 23
  - 3.1.1 JET Tokamak and NB system 23
  - 3.1.2 NBI modelling at JET: ASCOT and PENCIL 26
  - 3.1.3 Ion temperature reconstruction in JET ILW discharge with dominant NB heating 27
  - 3.1.4 Isotope effect studies at JET: D NBI vs H NBI 30
- 3.2 NBI-plasma interaction at LHD 35
  - 3.2.1 LHD device and NB system 35
  - 3.2.2 TASK3D-a integrated transport suite for LHD experiment analysis 37
  - 3.2.3 FIT3D upgrades for LHD D operation: discussion of physics models and implementation in the code 38
  - 3.2.4 Application of the upgraded FIT3D code to NBI-plasma interaction studies for similar H and He discharges 52

4 INTEGRATED NBI-PLASMA SIMULATIONS 59
- 4.1 EU DEMO studies 59
- 4.2 Not only EU DEMO: other DEMO concepts 62
- 4.3 EU DEMO scenario modelling 68
  - 4.3.1 DEMO designs analysed: 2012, 2013 and 2015 releases 69
  - 4.3.2 Integrated DEMO scenario simulations: effect of NBI and auxiliary heating systems 71
  - 4.3.3 Flattop studies 74
  - 4.3.4 Investigation of transient phases for DEMO1: ramp-up and ramp-down 83
  - 4.3.5 The role of NBI in DEMO scenarios 98

5 CONCLUSIONS AND LIST OF PUBLICATIONS 101
- 5.1 List of my publications 103

A APPENDIX 105

BIBLIOGRAPHY 109

ABSTRACT

Neutral beam injection (NBI) is one of the most used and reliable methods to heat plasmas in magnetically confined fusion devices. NBI is used in most of the present experiments, it will be used as dominant auxiliary power system in ITER experiment and studies are ongoing for DEMO reactor pre-conceptual designs with neutral beam (NB) systems. NBI is an essential actuator for plasma scenarios in terms of heating and driven current.

This thesis presents the work performed during the 3 years of my Ph.D.. It focuses on numerical studies of the interaction between energetic particles coming from NBI and magnetically confined hot plasmas. The main aspects discussed in this thesis are the neutral beam ionization, fast ion confinement, fast ion losses, power deposition and driven current. A brief discussion of NBI as fuelling source is also presented. NBI modelling tools have been applied to study different devices with dominant NB power: the largest tokamak in operation (JET), the largest helical device in operation (LHD) and DEMO tokamak reactor concept.

Detailed modelling of NBI by means of a Monte Carlo orbit following code has been provided for JET discharge analyses. A predictive simulation aimed at reconstructing the ion temperature profile with strong ion heating from NBI has been performed, resulting in a reliable prediction when the experimental measurement was not available due to a diagnostic fault. JET NBI-plasma interaction has been studied by predictive simulations for H discharges starting from reference D discharges in support of JET isotope studies. The isotopic change and the consequent effect on NBI-plasma interaction has been discussed also for LHD helical device, where studies in preparation of future D experiments (instead of H) are ongoing.

NBI is one of the options as additional power system for a demonstrative fusion power plant (DEMO), and a pre-conceptual design of the reactor is ongoing within EUROfusion activities. DEMO scenario simulations have been carried out both for pulsed and steady-state concepts. The role of NBI as dominant heating and current drive system has been investigated by sensitivity studies, comparisons with other heating systems and transport investigations of transient phases (plasma ramp-up and ramp-down).

SOMMARIO

L'iniezione di fasci di particelle neutre (neutral beam injection NBI) é uno dei metodi piú utilizzati e affidabili per scaldare il plasma in esperimenti sulla fusione termonucleare confinata magneticamente. L'NBI é utilizzato nella maggior parte degli attuali esperimenti, verrá applicato come riscaldamento dominante in ITER e studi sono in corso per implementare l'NBI nel progetto europeo del futuro reattore dimostrativo DEMO. L'NBI gioca un ruolo fondamentale per i plasmi fusionistici in termini di riscaldamento e capacitá di indurre corrente nel plasma.

Questa tesi presenta il lavoro svolto durante i tre anni del mio dottorato e si focalizza su studi numerici dell'interazione tra particelle energetiche provenienti dall'NBI e plasmi confinati magneticamente. Gli aspetti principali

discussi sono la ionizzazione del fascio di neutri nel plasma, il confinamento e le perdite degli ioni veloci, la deposizione di potenza e la corrente di plasma indotta dal fascio. Viene inoltre presentata una breve discussione sull'NBI come sorgente di particelle. Diversi codici numerici sono stati applicati per lo studio di esperimenti caratterizzati da un riscaldamento dominante tramite NBI: sono stati studiati il piú grande tokamak attivo al mondo (JET), il piú grande stellarator attivo al mondo (LHD) e il progetto del reattore dimostrativo europeo DEMO.

Accurate simulazioni dell'iniezione del fascio neutro sono state elaborate grazie ad un codice Monte Carlo per l'analisi di esperimenti di JET. Una simulazione predittiva é stata condotta con l'intento di ricostruire il profilo di temperature ionica del plasma nel caso di rilevante riscaldamento ionico da parte dell'NBI. Ció ha prodotto un'attendibile ricostruzione in un caso in cui le misure sperimentali non erano disponibili a causa di un problema con lo strumento di misura. L'interazione tra NBI e plasma al JET é stata studiata tramite simulazioni predittive anche per scariche in idrogeno, partendo da scariche di riferimento in deuterio, con l'obbiettivo di studiare gli effetti che il cambiamento isotopico provoca sul plasma di JET. Studi sugli effetti isotopici sono stati effettuati anche per LHD, esperimento a configurazione elicoidale, dove si stanno preparando i futuri esperimenti in deuterio al posto degli usuali esperimenti in idrogeno.

L'iniezione di particelle neutre é una delle opzioni come riscaldamento addizionale del plasma per il futuro reattore dimostrativo DEMO. Attualmente uno studio pre-concettuale di questo reattore é in corso a livello europeo. Simulazioni degli scenari di DEMO sono state effettuate sia per il progetto di un DEMO pulsato, sia per un DEMO a funzionamento stazionario. Il ruolo dell'NBI come riscaldamento principale e sistema per indurre la corrente di plasma é stato investigato tramite studi di sensibilitá, confronti con altri sistemi di riscaldamento e simulazioni delle fasi transitorie del plasma (accensione - ramp-up - e spegnimento - ramp-down - della scarica).

1 INTRODUCTION

1.1 THE ENERGY SUPPLY PROBLEM

Human activities seem to have a clear influence on climate system, and recent climate changes had and are having relevant impacts on human and natural systems. Global warming is an undoubted trend of the last century, and this coincided with the increase of greenhouse gas emissions from human activities. Human activities are extremely likely to have been the dominant cause of the observed warming since the mid-20th century. This conclusion is included in "Climate change 2014: impacts, adaptation, and vulnerability" [1], where climate changes and their causes are analysed.

Human emissions, beside all direct emissions from industries and transportation, are also connected to the way the energy is produced, and to the amount of energy consumed. Energy scenario forecasts reveal an increasing energy demand in the next future, as it is reported in e.g. IEA "World Energy Outlook" [2]. Depending on environmental policies adopted, different energy scenario with different energy mixes can be envisaged, implying different impacts on global warming and hopefully on climate changes. Public opinion also influences the energetic policies, as it has been seen for nuclear fission energy. Anyway, human need of energy is increasing, and this has an impact on the environment. Figure 1 shows the extrapolation of the energy consumption in 2035 divided by fuel as presented in "BP energy outlook 2035" [3]. Although an increase of renewable energies, most of the energy

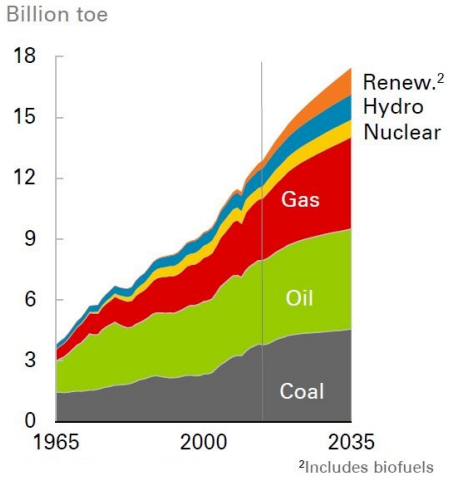

Figure 1.: Energy consumption forecast by fuel in billion toe (tonne of oil equivalent), from [3].

supply will still consist of coal, oil and gas. It has to be considered that energy from sun, wind or similar renewable sources cannot most likely sustain the whole energy demand, being bound to particular environmental conditions. Anyway their contribution to a more sustainable energy mix is fundamental. Sustainable however must mean environmentally, socially and economically sustainable. The main challenge is therefore to find a new

main energy source able to gradually replace fossil fuels: hopefully long lasting, environmental-friendly, inherently safe, economically competitive and publicly accepted. A promising candidate is fusion energy.

1.2 A PROMISING CANDIDATE FOR FUTURE ENERGY SUPPLY: NUCLEAR FUSION

Fusion is a nuclear process in which two light nuclei merge to form a heavier element. In order to reach a fusion reaction, two positive charged nuclei have to overcome the mutual Coulomb repulsion. They have hence to be closer than a distance in the order of 10^{-15}m [4]. A vast knowledge about fusion comes from stars, which are the oldest and biggest fusion "plants" existing. Studying the sun, the proton-proton fusion chain has been discovered. In this reaction helium is formed out of hydrogen, releasing an energy of 26.7MeV for each reaction. In the sun, this fusion process is possible due to the high core density (~$10^{31}\,\frac{\mathrm{particles}}{\mathrm{m}^3}$), sustained by the gravitational force. This is not attainable on earth, since densities in this range cannot be reached. In order to exploit fusion processes on earth, the most feasible reaction is employing two hydrogen isotopes, namely deuterium and tritium (reaction 1). They are used because of their fusion cross section, which is larger with respect to other possible reactions (reactions 2,3,4, see figure 2).

$$^2\mathrm{D} +^3 \mathrm{T} \rightarrow^4 \mathrm{He} +^1 \mathrm{n} + 17.6\mathrm{MeV} \tag{1}$$

$$^2\mathrm{D} +^2 \mathrm{D} \rightarrow^3 \mathrm{He} +^1 \mathrm{n} + 3.27\mathrm{MeV} \tag{2}$$

$$^2\mathrm{D} +^2 \mathrm{D} \rightarrow^3 \mathrm{T} +^1 \mathrm{H} + 4.03\mathrm{MeV} \tag{3}$$

$$^2\mathrm{D} +^3 \mathrm{He} \rightarrow^4 \mathrm{He} +^1 \mathrm{H} + 18.3\mathrm{MeV} \tag{4}$$

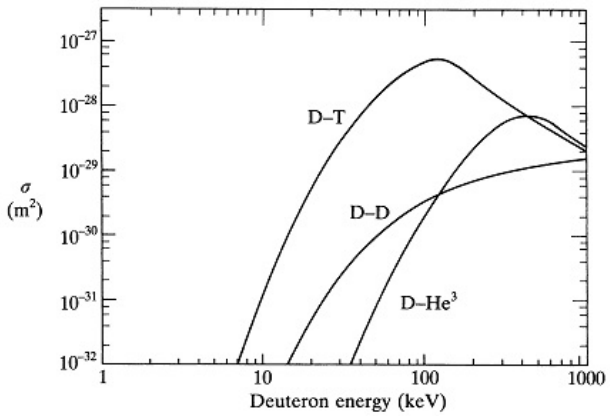

Figure 2.: Fusion cross-sections for the reactions D-T, D-D and D-^{3}He. The D-D curve is the sum of the cross sections of the two D-D reaction listed in reactions 2 and 3. From [4].

Despite the D-T curve has a maximum around a particle energy of ~100keV, the mean temperature needed to have a sufficient number of reactions in a

future fusion reactor is 10keV. At this temperature there are enough energetic ions populating the high energy tail of the particle velocity distribution which can reach fusion. A concise way to express the condition needed to achieve ignition is that of the Lawson criteria: temperature (T), density (n) and energy confinement time (τ_E) have to satisfy the relation 5. Figure 3 shows the ignition curve, as function of triple product parameters. Ignition means a self-sustaining burning plasma heated without any external system, but just with the energy coming from fusion reactions.

$$nT\tau_E > 3 \times 10^{21} \frac{keVs}{m^3} \tag{5}$$

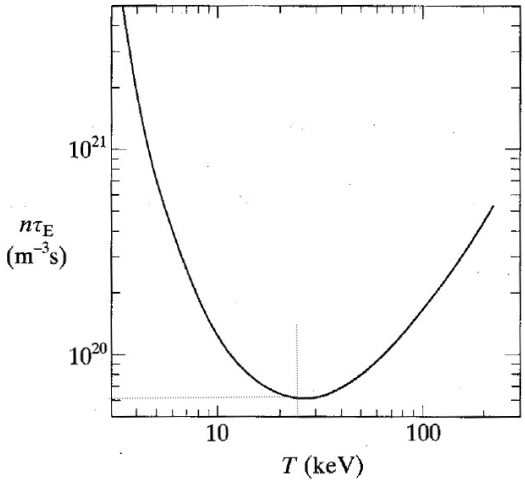

Figure 3.: The value of $n\tau_E$ required to obtain ignition, as a function of temperature [4].

The temperature required is about ten times the core temperature of the sun: at this temperature atoms are ionized. The state of this hot, ionized gas is called "plasma": it consists in a globally neutral system of many charged particles, which is characterized by presenting collective properties (somehow as a fluid).

Fusion with D-T fuel is very advantageous in terms of energy density: a comparison with fossil and fission fuels shows its great potential.

fossil	fission	fusion
10^6 tonne oil	0.8 tonne uranium	0.14 tonne deuterium

Table 1.: Comparison of energy equivalence among different resources [5].

Deuterium is a stable isotope of hydrogen and is widespread in nature (0,015% of the total hydrogen). Tritium on the contrary, is radioactive and has a half-life of approximately 12 years. For this reason it does not occur in nature and it has to be produced directly inside the reactor. Neutrons coming from fusion reactions in the plasma will be used to breed tritium out of lithium (with reactions 6, 7).

$$^6Li + ^1n \rightarrow T + ^4He + 4.8MeV \tag{6}$$

$$^7Li + ^1n \rightarrow T + ^4He + n - 2.5MeV \tag{7}$$

Future fusion plants can also be considered inherently safe: given the strict constraints to maintain burning plasmas, any accident in the reactor will lead to a stop in the reaction chain, on the contrary to fission plants. But due to the difficult conditions to reach ignition, the track to commercial fusion plants is still long.

1.3 THERMONUCLEAR FUSION BY MAGNETIC CONFINEMENT

At the moment, two mechanisms to achieve fusion processes are being studied. The Inertial Confinement Fusion (ICF) approach intends to reach a very high density and temperature of a Deuterium-Tritium target using high power lasers, causing an implosion. The other way, which is treated in this thesis, is the magnetic confinement of a high temperature plasma.

Since a plasma consists of an charged particles, it is possible confine it in a device with strong magnetic fields avoiding any contact with facing materials. When a magnetic field is present, the Lorentz force imposes to charged particles a circular motion around the field lines ("gyro-motion"). In this way the particles are strictly confined to the magnetic field. Anyway, with this kind of confinement, the particles can move freely along the magnetic field line (e.g. due to an electric field). In a linear magnetic field setup (e.g. a magnetic bottle configuration), the particles are lost at the ends, therefore a closed configuration for the magnetic field lines has been chosen, and the devices are currently shaped as a torus. The torus is enclosed by coils, in order to generate a confining toroidal magnetic field. However this field is not enough: to prevent the loss of the plasma to the wall due to drift effects, the magnetic field configuration is set to be helically twisted. A poloidal component is therefore added, so the main particle trajectory becomes helical, keeping most of the plasma in the central part of the torus. The magnetic field generates nested surfaces characterized by constant magnetic flux and pressure ("flux surfaces"), as shown in figure 4. The pressure increases perpendicularly to the flux surfaces confining the hot plasma in the centre of the torus. In the core region of a fusion reactor, it is thus possible to achieve the conditions necessary to heat the plasma up to about 10keV with a density in the order of $10^{20}\,\frac{particles}{m^3}$, as required by the Lawson criteria 5. Since this

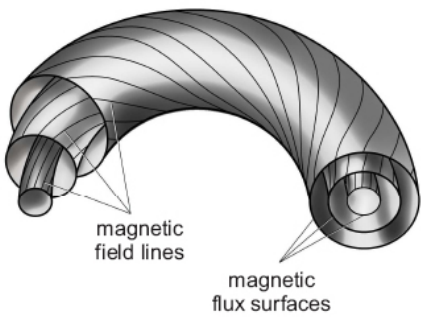

Figure 4.: Helically twisted field lines and flux surfaces in a tokamak

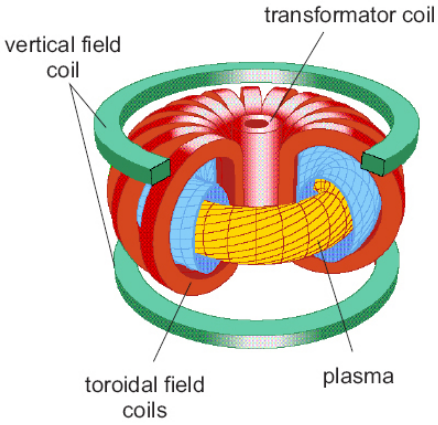

Figure 5.: General design of a tokamak. The plasma column is in yellow, while the magnetic field coils are shown in red (toroidal field) and green (vertical field). A vertical field is necessary to control the position of the plasma column. In the centre of the torus the transformer coil is illustrated, which is needed to generate the plasma current.

value of density is lower than that in the atmosphere of a factor 10^6, plasma is contained in a vacuum vessel.

Among magnetic confinement devices, three main configurations can be distinguished: tokamak (figure 5), reversed field pinch (RFP, figure 6a) and stellarator (figure 6b). The first two create the poloidal magnetic field with an induced plasma current, the latter uses complex shaping of the magnetic field coils to generate directly helically twisted magnetic field lines.

The tokamak (from **to**roidal'naya **ka**mera s **ma**gnitnymi **k**atushkami - toroidal chamber with magnetic coils in Russian) represents the most advanced fusion concept. It is the most used and studied configuration, and, at the moment, the most promising one for next step fusion reactors. With this configuration, parameters needed for fusion have been reached, but not all at the same time for a sufficient duration to obtain an energy gain. The largest operating tokamak is JET in Oxford (GB): more details on JET can be found in section 3.1. In tokamak configuration, magnetic fields consist of an externally applied toroidal field and a poloidal field which is generated by a toroidal current flowing through the plasma. The plasma current is induced using a voltage ramp in a central solenoid, which causes a change in the magnetic flux in the central gap of the torus. The solenoid acts as

(a) Reversed field pinch (RFP) **(b)** Stellarator

Figure 6.: Representations of helical plasma configurations in RFP (quasi-single helicity (QSH) regime in RFX-mod, Padova [6]) and stellarator (Wendelstein 7-X, Greifswald [7]). These are alternative magnetic configurations to tokamak.

the primary winding of a transformer with the plasma itself acting as the secondary, and a current is hence induced in the plasma. Plasma is heated by Ohmic power and external heating systems, as it is described in chapter 2.

On the way to commercial fusion reactors, the next step is the ITER experiment [8] (see figure 7), under construction in Cadarache (FR). This will be the largest tokamak in the world. It has been designed to demonstrate the feasibility of a high-gain fusion reactor, with long lasting burning plasma and with effective energy gain. ITER is supported by a worldwide collaboration among China, EU, India, Japan, Korea, Russia and USA. The next step after ITER is supposed to be DEMO (DEMOnstration Power Plant), the prototype of a commercial fusion reactor. The European fusion roadmap, and different international DEMO concepts are presented in chapter 4.

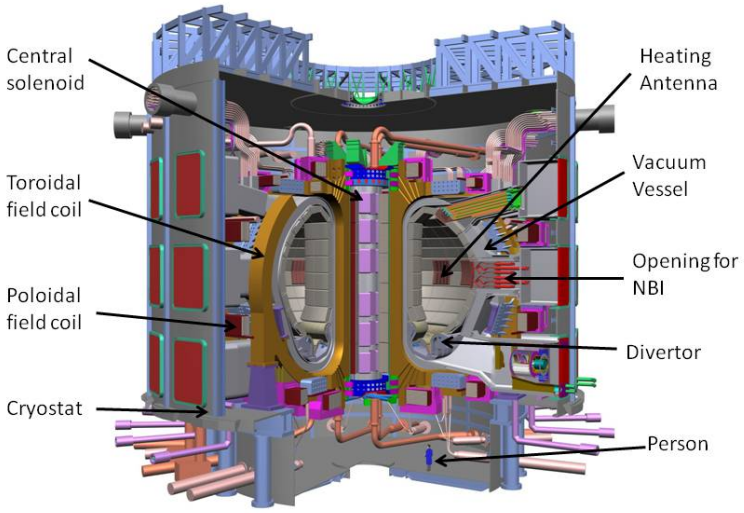

Figure 7.: ITER tokamak design. Artist's drawing of the entire ITER device (*ITER Final Design Report*.(2001). Vienna:IAEA).

The other promising configuration relevant for fusion reactors is the stellarator concept, which includes all the helical configurations. The underlying idea is that the magnetic field is externally generated by specifically shaped coils. The contribution of the plasma to the confining magnetic field is null. In stellarators, plasma is therefore (almost) current-free, and it is heated only by external systems. Stellarators are intrinsically steady-state devices, and they do not suffer current-driven instabilities and disruptions. They also have very high density limits (no Greenwald limit). On the other hand they need a very complex 3-D magnetic configuration, which requires a careful optimization process in the design phase. Stellarator configurations tend to provide a poor particle confinement, presenting also very complex divertor and plasma facing components. Due to these difficulties, research on stellarators is unfortunately ~$1\frac{1}{2}$ generations behind tokamaks. The biggest helical experiments are LHD at NIFS, Japan (see section 3.2) and the recently built Wendelstein 7-X at IPP Greifswald, Germany [7].

RFP devices are not treated in this thesis, but they represent another possible magnetic configuration to confine plasmas, although less reactor-relevant. They rely on high plasma currents, which create strong confining magnetic fields in addition to a relatively small toroidal magnetic field. They are very interesting from physics point of view, since RFPs exploit self-organized plasma states. The biggest operating RFP in the world is RFX-mod, in Padova (IT) [6].

1.4 GENERAL STRUCTURE OF THE WORK

NB systems are one of the most used external heating systems, both for tokamaks and stellarators. Moreover NBI is planned to be used in ITER and studies are ongoing for DEMO. The success of NBI in terms of fulfilling scenario requirements and contributing to scenario achievements depends on the physics of the interaction of NBI and plasma. The general aim of this thesis is to investigate the interaction of neutral beam fast particles with different plasmas, including existing tokamak and stellarator devices and predictions for EU DEMO concepts. These studies are based on NBI modelling, which has been the main tool to perform the presented work. The motivations of the single activities on JET, LHD and DEMO will be illustrated in the related chapters.

The thesis is organized as follows. In chapter 2, NBI is introduced, from the technological and physics point of view. Studies carried out on standalone NBI-plasma interaction are presented in chapter 3, for JET tokamak (section 3.1) and for LHD helical device (section 3.2). The work performed on DEMO is presented in chapter 4. Finally, summary and conclusion are presented in chapter 5.

2 BASICS OF NEUTRAL BEAM INJECTION (NBI)

In this chapter, neutral beam injection (NBI) is introduced. First, a simple explanation of the need of auxiliary heating systems is given, with a brief overview on the most used heating systems. In the next sections, the NBI system is firstly described (section 2.1), then a description of the physics basics of NBI-plasma interaction (section 2.2) is presented, including plasma heating, current drive and other considerations. In the last section (2.3) an overview of computational possibilities for NBI-plasma interaction modelling is reported. Bibliographic references for the topics presented in this chapter are the main books on fusion science [4, 9, 10], in addition to other specific works that will be cited.

The requirements on plasma pressure and confinement time to reach ignition find a minimum for a plasma temperature of ~15keV [5], resulting from a simplified calculation without taking into account bremsstrahlung radiation losses. Consistently with this calculation, alpha heating becomes dominant for $T > 5 - 7keV$, while below the contribution from fusion power is almost negligible. In order to reach this temperature, other heating sources are essential. The simplest one, but unfortunately insufficient, is ohmic heating (for tokamaks). Plasma is a conductor, and the flowing of a plasma current produce heating ($P = \eta j^2$ with η the resistivity and j the current density). However plasma resistivity decreases with temperature ($\eta \propto T^{-\frac{3}{2}}$) and this limits the efficiency of ohmic heating, which alone may lead to a maximum plasma temperature of ~3keV for typical reactor parameters. The resulting temperature gap must be filled by auxiliary heating systems: without them it is not possible to ignite a reactor (exemplified in figure 8a). Figure 8b shows a schematic view of ohmic and external heating sources for a toroidal plasma. Different options for plasma heating are used nowadays and can be divided in coupling electromagnetic waves to the plasma or injecting high energy particles in the plasma. The former includes elec-

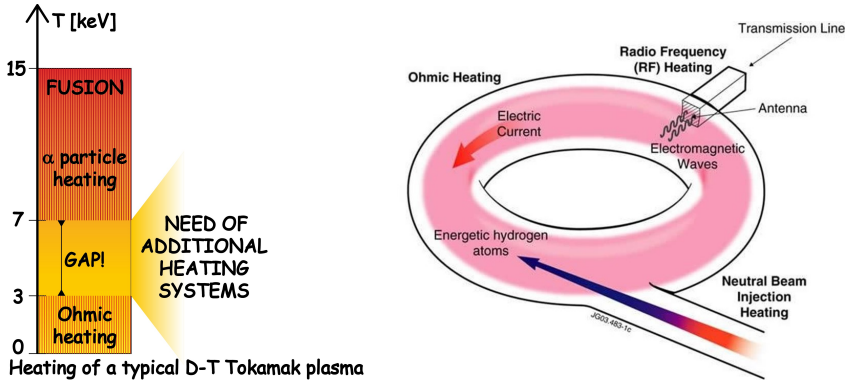

(a) Tokamak reactor: need of auxiliary systems

(b) Ohmic and external heating sources

Figure 8.: Exemplification of the need of auxiliary heating systems in tokamak reactors and schematic overview of ohmic and external heating sources.

tron and ion cyclotron resonance heating (ECRH and ICRH respectively), and lower hybrid (LH) heating. The latter refers to neutral beam injection (NBI) heating. These systems not only heat the plasma, but are also able to drive plasma current if expressly designed. This feature is particularly important for steady-state tokamak scenarios (advanced scenarios), where fully non-inductive currents flow in the plasma. In these advanced scenarios, auxiliary heating systems are the main actors for non-inductive current generation, together with the contribution of the bootstrap current, which is an off-axis current generated by the natural radial plasma transport and which depends on density and temperature gradients. Auxiliary heating systems are therefore the main actuators for plasma heating and current drive (CD). ECRH, ICRH and LH systems are based on launching electromagnetic waves into the plasma, set to match plasma resonant frequencies in order to maximize the energy absorption. This, at a fixed frequency, depends on plasma characteristics, such as magnetic field, plasma density and temperature. Typical frequencies are in the range of 30-100MHZ for ICRH, 1-10GHz for LH and 50-170GHz for ECRH.

Ion cyclotron resonant heating (ICRH) is normally used for plasma ion heating, but it can be used also for central current drive, although with poor efficiency. IC systems can be used to heat a minority ion population in the plasma (typical example is ^3He minority heating). Other RF systems capable of electron heating have been developed, and are called fast wave (FW) and ion Bernstein wave systems. The source of the IC wave is a high-power vacuum tube. The presence of an antenna (which is the launcher of IC waves) very close to the plasma in order to have a good coupling represents a problem for reactor relevant experiments, as the high voltage required to launch large amounts of power may cause arching between the metal structure of the antenna and the plasma, leading then to breakdown. Studies on reactor-relevant IC systems are ongoing, and a solution has been presented in the last International Toki Conference 25, Toki(JP), Nov. 2015 [11].

Electron cyclotron resonant heating (ECRH) is a system which heats plasma electrons. EC systems are used to provide central heating, but they can also drive very localized currents, and EC represents an optimum system for MHD control (e.g. NTM stabilisation). ECRH presents some technological difficulties due to the lack of high power steady-state gyrotron sources (sub-millimeter waves). The launcher of EC waves is a mirroring system, which acts as interface between the transmission circuit and the plasma itself.

Lower hybrid (LH) energy transfer is based on Landau damping, which is a method to basically accelerate plasma electrons using waves at specific frequencies. This system has a very high current drive efficiency, although the difficult plasma penetration makes this system useful mainly for off-axis current drive. LH sources are klystrons (microwaves). The launcher, which is composed of an array of wave-guides, has to be close to the plasma for a good matching of wave energy to plasma, and this creates issues in severe edge conditions. The limited wave penetration poses some limitations for the use in future reactors.

Neutral beam injection (NBI) is based on the injection of energetic neutral particles which are then ionized and, during the thermalization process, heat the plasma. Injected particles must be neutral to penetrate the magnetic fields before entering the plasma. Fast ions heat prevalently electrons at high energy, ions at low energy. NBI can also drive current with good efficiency, if the injection is tangential to the plasma. Tangential injection

provides also toroidal torque to the plasma. NB is also a source of particles. Neutral beam injection is a robust method for heating and current drive (CD) because it does not depend on any resonance or coupling conditions (as it is for waves). The only limitation is low plasma densities, for the risk that shine-through power losses exceed first wall material limitations. NBI will be deeply described in next sections.

NB systems are used since 1970s, and the first proof on NB heating principle was published in 1979 [12]. NBI provided the necessary heating power to the experiments in ASDEX tokamak which enabled the discovery of the H-mode (1982 [13]). A dominant NB heating characterised the D-T experiments of TFTR and JET tokamaks during 1990s, which resulted in the first considerable production of fusion power [14, 15]. Nowadays, NBI is the highest power heating system in construction for ITER and it will be the highest energy beam (1MeV) ever built, for which R&D is ongoing [16]. At the moment, NBI is also considered for the next step reactor after ITER, DEMO [17].

2.1 NB SYSTEM: THE GENERATION OF THE BEAM

A NB injector is made of four parts: a source of ions, an electrostatic accelerating, a neutralizer and a residual ion dump (see sketch in figure 9). A calorimeter can be inserted for diagnostic purposes. Most of the present

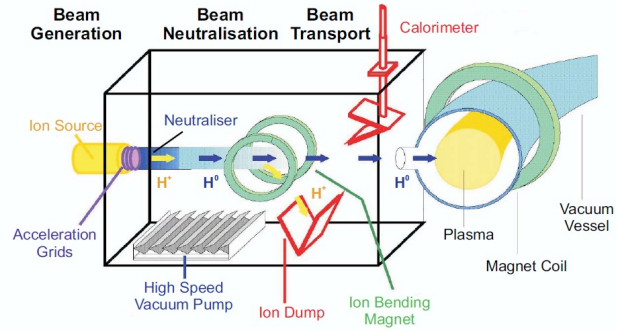

Figure 9.: Sketch of a positive NB injector: the source, the acceleration grids, the neutralizer and the ion dump (©MPI für Plasmaphysik, Garching).

NB systems accelerate positive ions, but, for high energy beams, negative ion sources are needed. The reason is that in case of a positive ion source, the beam neutralization efficiency rapidly decreases above ~50keV/amu (see figure 10). In case of negative beams, the neutralization efficiency remains almost constant also at high energies. The different parts of the NB system are now described, first for a positive ion based beam, then for a NB system with a negative ion source.

Positive ions in the source are extracted from a plasma, characterized by good uniformity and a density high enough to provide the required ion current. The overall acceleration voltage is set to satisfy the requested beam energy, which is directly related to beam penetration in the plasma. The plasma in the source can be generated in two ways: either with an arc or with a radio frequency (RF) source. In the former electrons are thermally emitted by hot tungsten filament cathodes, then accelerated into a chamber where they ionize the gas creating a plasma. The second method is realized by coils wound around the source and powered by a RF source. The induced

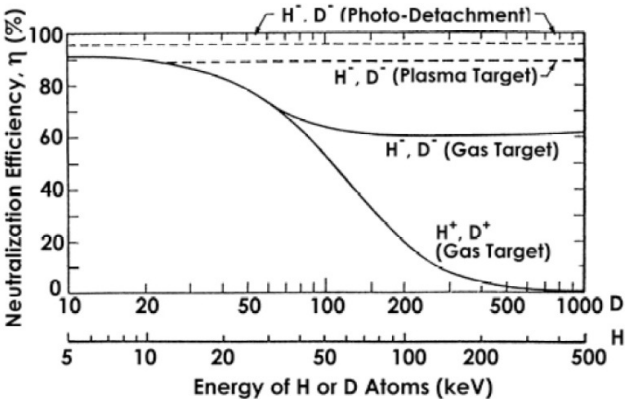

Figure 10.: Neutralization efficiency of positive and negative beam sources for different targets as a function of energy [10].

oscillating fields generate an acceleration of free electrons, leading to the ionization of the gas. This method is more advantageous as it is possible to easily control the extraction current by setting the RF power. With respect to arc sources, it has less needs of maintenance. The generation of ionized molecules (e.g. H_2^+ or H_3^+ in case of H source) is possible but not desirable, as these ions will carry half or one third of the beam energy per H.

The extraction system is made of several metallic grids. The first one separates the source from the accelerator (usually called *plasma grid*, with an applied voltage in the order of 100 kV). Then there is the *grounded grid*, and the acceleration potential is created between this and the plasma grid. In between there is the *decel grid*, which is negative biased by a few kV to prevent electrons from being accelerated towards the source. The total acceleration can be provided by several steps, in a so-called multi-stage system, which prevents electrical breakdown problems that are possible in a single-stage acceleration system especially for high voltages. Moreover multi-stage systems distribute heat loads among different stages. Incident ions on the structure generate indeed heating and a cooling system is required. After the extraction grids, the beam is focused to the neutralizer.

The gas neutralization is made via charge-exchange collisions with cold H (or D, depending on the accelerated species) molecules contained in a drift tube connected directly to the ion source. The pressure is kept constant by a continuous inflow of the gas. The length of the neutralizer is set to have a balance between the neutralization and re-ionization processes. The neutral fraction of the beam at the end is called neutralizer efficiency.

The last part of the NB system permits the residual ion removal (*RID*, Residual Ion dump). The resulting beam is not in fact totally neutralized and a fraction is still ionized. Thanks to a magnetic field from a bending magnet, the residual ions are deviated into the ion dump, which can be made e.g. of copper panels with cooling channels. Instead of a magnetic RID, also an electrostatic RID can be used. A movable calorimeter can be placed at the end of the NB, to measure the energy of the beam. Beyond the neutralizer the pressure should be kept low in order to minimize neutral particle losses due to re-ionization or scattering processes. Moreover it has to be avoided a gas inflow into the tours chamber. This condition is guaranteed by vacuum pumps.

In case of high energy beams, negative ions sources are needed. For the ITER case, it is foreseen the use of a 1MeV D NBI with 16.5MW of power

(2 ITER NB injectors for a total of 33MW). In this case negative ion sources must be used, but so high energy negative beams have in fact never been produced. R&D activities are therefore on-going, and ITER NB research is the main aim of PRIMA (Padova Research on ITER Megavolt Accelerator) which foresees the development of the ITER ion source (SPIDER - Source for the Production of Ions of Deuterium Extracted from an RF plasma) and the full ITER NBI prototype MITICA (Megavolt ITER Injector & Concept Advancement) [16]. Two methods are available for negative ion generation: the surface production and the volume production [18]. The first process is the most relevant for ITER NB source: neutral (or positively ionized) H particles (in case of H source, the same is for D) captures one (or two) electrons via backscattering on a surface with a material characterized by a low working function. In order to lower the working function of the surface, the metal surface is covered with a thin layer of Caesium, which allows up to $0.67H^-$ created per incident particle. Caesium coating is done by evaporating it into the chamber, being then redistributed by the plasma. The source must be close to the extraction holes (i.e. on the plasma grid surface) because of the low mean free path of H^- ions. Operating with low gas pressure is desirable in order to minimize the loss of H^- due to collisions. The other method to produce negative ions (volume production) is based on the fact that under specific conditions (i.e. gas pressure) the fraction of negative ions in a plasma can be high enough to be used as a source. The production of negative ions happens in two steps: first exciting a molecule with a fast electron (energy of several tens of eV) and then generating the ion by a collision with a slow electron (energy less than 1 eV). In order to separate the two temperature region with fast and slow electrons respectively, a magnetic field is used, and the device is called *tandem source*. Caesium seeding in the source enhances the yield of negative ions, and therefore can be used to increase the negative ion current. With respect to positive ion beams, it is more difficult to extract high current densities from the source, and this has to be compensated by a larger extraction area. Moreover the weakly bound electron of the negative ion is easily stripped away, and H^- (similarly for D^-) can be destroyed by three processes:

$$H^- + e^- \rightarrow H + 2e^- \text{ electron stripping (or detachment)} \tag{8}$$

$$H^- + H^+ \rightarrow 2H \text{ mutual neutralization} \tag{9}$$

$$H^- + H \rightarrow H_2 + e^- \text{ or } 2H + e^- \text{ associative detachment} \tag{10}$$

Electron stripping is very effective for T_e of a few eV and can be lowered decreasing the density of energetic electrons. Mutual neutralization is the most important, and depends slightly on T_i, while associative detachment presents a weak dependence on T_H.

A problem arises from the co-extraction of electrons with the negative ions. They of course cannot be part of the final neutral beam and the acceleration of unwanted particles represent a loss of energy for the beam. The first step of the acceleration grid is therefore set at low voltage with respect to the other step. This is done to eliminate immediately the electrons, before they gain higher energies, by specific bending magnets on the extraction grid. The increase of neutralizer efficiency is indeed connected to the minimization of the co-extracted electron current. Another way to increase the neutralizer efficiency is to exploit the photo-detachment of negative ions

using photons of a laser in an optical cavity or using a plasma target (see figure 10). These options are under investigation for a high efficiency NB source for DEMO.

The beam production influences the NBI-plasma interaction in many terms, in addition to the characteristic power and energy of the NB system. The first is the beam dimension together with the beam divergence, which is fixed by the acceleration grid design. Then the beam composition can change, depending on the possible co-accelerated molecular particles, which carry less energy per single atom. Once the NB system has been built, also the beam trajectory in the plasma is fixed. The NBI can indeed be set to have either tangential or perpendicular injection with respect to the torus. The former can give torque to the plasma and drive current, while the latter, whose placement between coils is geometrically simpler, can strongly heat the central part of plasma but at the risk of undesired phenomena as loss of high energy particles (with high $v_{\perp B}$) due to neoclassical transport if toroidal field ripple is too high and due to possible higher shine-through losses. For the tangential case, the injection can be in the direction of the plasma current (Co-injection) or counter current (Counter-injection). The NB can aim to the plasma magnetic axis (on-axis injection), or to the outer plasma region (off-axis injection). The injection possibilities are depicted in figure 11.

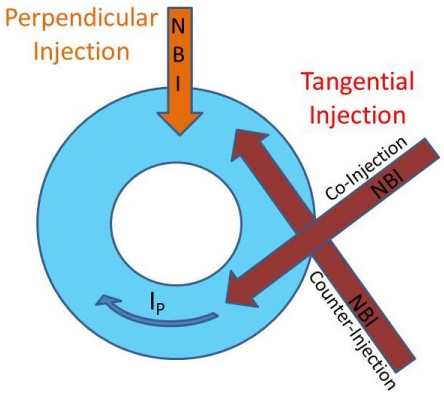

Figure 11.: Possible NBI geometries.

2.2 BASICS NBI–PLASMA INTERACTION PHYSICS

In addition to heating, NBI can be also a source of current, particles, plasma torque, supra-thermal ion population and fusion reactions in case of reactive species. In the next subsections, a physics introduction on NBI-plasma interaction is provided.

2.2.1 Plasma heating by NBI

The interaction between the energetic neutral beam and plasma can be divided in two processes: the beam ionization with the creation of energetic ions, and the thermalization of the fast ions (also called slowing down process).

The beam ionization is the process happening when the fast neutral particles are converted into fast ions due to the interaction with the plasma,

and this happens mainly thanks to three processes (the same for H,D or T particles):

$$H^0 + H^+ \rightarrow H^+ + H^0 \text{ charge exchange (CX)} \tag{11}$$

$$H^0 + H^+ \rightarrow H^+ + H^+ + e^- \text{ ionization by ions} \tag{12}$$

$$H^0 + e^- \rightarrow H^+ + 2e^- \text{ ionization by electrons} \tag{13}$$

Fast neutrals can also be ionized by plasma impurities. The cross section of these processes (σ_{cx}, σ_{ii}, σ_{ie}) depend on the beam particle energy, and are plotted in figure 12. Above 40keV/amu, ionization by plasma ions is

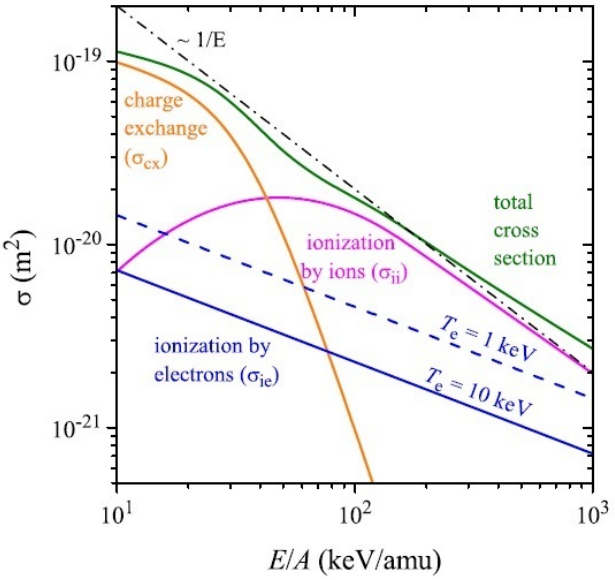

Figure 12.: Beam ionization cross sections due to plasma ions and electrons (re-elaborated from [19]).

dominant, while below 40keV/amu CX process dominates. The total cross section shows approximately a 1/E trend. The total cross section can be written as the sum of the three above-mentioned processes:

$$\sigma_{tot} = \sum_{k=cx,ii,ie} \frac{\langle \sigma_k v \rangle}{v_{beam}} \text{ with } \langle \sigma_k v \rangle = \frac{\int \sigma_k(v_{rel}) v_{rel} f(v_{rel}) dv_{rel}}{\int f(v_{rel}) dv_{rel}} \tag{14}$$

In case of relevant presence of impurities, the impurity cross section term can be added. $\langle \sigma_k v \rangle$ is called "rate coefficient" and represents the cross section averaged over all the relative velocities. If plasma rotation is not small, it has to be considered in the relative velocity and hence we have $v_{rel} = |\vec{v}_{beam} - \vec{v}_{rotation}|$. Since $v_i \ll v_{beam} \ll v_e$, the total cross section σ_{tot} can be approximated as follows:

$$\sigma_{tot} = \sigma_{cx}(v_{beam}) + \sigma_{ii}(v_{beam}) + \frac{\langle \sigma_{ie} v \rangle}{v_{beam}} \tag{15}$$

Fast neutral particles can also be ionized from plasma ions in excited states. The processes are (for H ions):

$$H^0 + (H^+ \text{ or } e^-) \rightarrow H^{0*} + (H^+ \text{ or } e^-) \rightarrow H^+ + e^- + (H^+ \text{ or } e^-) \tag{16}$$

This kind of ionization process is called "multi-step ionization (MSI)" and it enhances the total beam ionization cross section by an enhancement factor δ:

$$\sigma_{tot_{MSI}} = \sigma_{tot}(1 + \delta) \tag{17}$$

For current experiments we have $\delta < 0.4$.

Beam ionization is therefore determined by different processes: the ionization by plasma ions and electrons (including CX processes and MSI), and ionization by impurities (which is usually taken into account as a enhancement factor, see e.g. discussions in section 3.2). Once having the total beam ionization cross section, it is possible to write the mean free path of the neutral beam assuming $n = n_e = n_i$ as:

$$\lambda = \frac{1}{n\sigma_{tot}} \tag{18}$$

The beam energy is therefore a parameter which determines the beam mean free path (since the total ionization cross section depends on the NB energy) and, on first approximation, $\lambda \approx E$.

Even though the beam energy is carefully set, a part of the beam may be not ionized, especially in case of low plasma density. This is referred to as shine through losses, which represent the fraction of the beam not ionized. Other fast particle losses can characterize the beam-plasma interaction. It is possible to have scrape-off layer losses, corresponding to fast ions born outside the confined plasma. This can happen especially if external neutral particles collide with the neutral beam before entering the plasma. Then we can have first orbit losses, which represent fast ions born on non-confined orbits (e.g. plasma edge). An analytical calculation for first orbit losses is presented in [20], where, depending on the ion birth position and injection trajectory, the loss cone of the ions, i.e. the region in $v_{\parallel}/v_{\perp}$ space where ions are lost due to non-confined orbits, is calculated. Inside the confined plasma, charge-exchange processes between fast ions and background neutrals can result in fast neutrals escaping the plasma (CX losses). Finally, orbit losses can happen when a fast ion is lost due to a scattering process. All these processes represent power losses before the fast ion complete thermalization.

The radial distribution of newly born fast ions (fast ion birth profile H(r)) is usually calculated by numerical codes. The population of newly born ions is then slowed down by Coulomb collisions with the background plasma. In this thermalization process the energy injected by the NB is transferred to the plasma. Assuming $v_i \ll v_{beam} \ll v_e$, the fast ion energy transfer can be written as:

$$\frac{dE}{dx} = -\underbrace{\frac{\alpha}{E}}_{\text{to ions}} - \underbrace{\beta\sqrt{E}}_{\text{to electrons}} \tag{19}$$

where $\frac{dE}{dx}$ has been divided into two terms, one representing the energy going to plasma ions, the other to plasma electrons. α and β are coefficients which depend on atomic mass number A and charge Z of fast ions and of plasma ion species, density of ions and electrons in the plasma and electron plasma temperature. It is possible to define a critical energy, where stopping

by electrons and ions is equal. E_c has been calculated e.g. in Stix's paper [21] (where also α and β coefficients are described).

$$E_c = \left(\frac{\alpha}{\beta}\right)^{\frac{2}{3}} \text{ or:}$$

$$E_c[keV] = \left(\frac{9\pi m_p}{16 m_e}\right)^{1/3} \left[\sum_j \frac{n_j Z_j^2}{n_e A_j}\right]^{2/3} A_b T_e = 14.8 \overline{Z}^{2/3} \overline{A_b}^{1/3} T_e[keV] \tag{20}$$

where subscripts p, e, j, b are respectively for proton, electron, plasma species and beam. When the beam energy is greater than E_c the energy transfer to electrons is dominant, when is less the energy transfer to ions dominates. For instance, for pure hydrogen plasma:

$$H^0 \rightarrow H^+ : E_c[keV] = 14.8 T_e[keV] \tag{21}$$

$$D^0 \rightarrow D^+ : E_c[keV] = 18.6 T_e[keV] \tag{22}$$

The slowing down time is defined as the fast ion thermalization time, i.e. the time a fast ion spends to pass from initial energy E_0 to plasma background energy E_{therm}, and can be expressed by:

$$\begin{aligned} \tau_{sd} = &\int_{t(E_0)}^{t(E=0)} dt = \int_{E_0}^{E=0} \left[\frac{dE}{dx}\frac{dx}{dt}\right]^{-1} dE = \int_0^{E_0} \left[-\frac{dE}{dx}\sqrt{\frac{2E}{m}}\right]^{-1} dE = \\ = &\frac{t_s}{3} \ln\left[1 + \left(\frac{E_0}{E_c}\right)^{\frac{3}{2}}\right] \end{aligned} \tag{23}$$

where t_s is the Spitzer slowing down time, which is defined as:

$$t_s[s] = \frac{\sqrt{2 m_i}}{\beta} = 6.28 \times 10^{14} \cdot \frac{A T_e[eV]^{\frac{3}{2}}}{Z^2 n_e[m^{-3}] \ln\Lambda} \tag{24}$$

with the Coulomb logarithm $\ln\Lambda \approx 17$. For present day NBIs ($E_0 < 100$ keV, $n_e = 5 \times 10^{19} m^{-3}$) the slowing down time has typically values of $\tau_{sd} \approx 20 - 100$ms, time which is less than the typical particle confinement time. For future reactors, higher τ_{sd} values are expected, even in the order of 1s. The fast ion $\frac{dE}{dt}$ can be expressed by the following relation (E is the beam energy):

$$\frac{dE}{dt} = -\frac{2}{t_s} E \left(\frac{E_c^{\frac{3}{2}}}{E^{\frac{3}{2}}} + 1\right) \tag{25}$$

with the first addend representing the energy transferred to ions, while the second to electrons. In particular, the power transferred to ions is:

$$P_i = -\frac{2}{t_s} E \left(\frac{E_c^{\frac{3}{2}}}{E^{\frac{3}{2}}}\right) \tag{26}$$

and rewriting $\frac{dE}{dt}$ as:

$$\frac{dE}{dt} = -\frac{2}{t_s} E \left(\frac{E_c^{\frac{3}{2}} + E^{\frac{3}{2}}}{E^{\frac{3}{2}}} \right) \tag{27}$$

one obtains:

$$\frac{2}{t_s} E = \frac{-E^{\frac{3}{2}}}{E_c^{\frac{3}{2}} + E^{\frac{3}{2}}} \frac{dE}{dt} \tag{28}$$

which is useful to rewrite P_i:

$$P_i = \frac{-E_c^{\frac{3}{2}}}{E_c^{\frac{3}{2}} + E^{\frac{3}{2}}} \frac{dE}{dt} \tag{29}$$

Now it is possible to calculate the fraction of beam energy going to ions by the following formula:

$$G_i = -\frac{1}{E_0} \int_0^{\tau_{sd}} P_i \, dt = \frac{E_c^{\frac{3}{2}}}{E_0} \int_0^{E_0} \frac{dE}{E_c^{\frac{3}{2}} + E^{\frac{3}{2}}} = \frac{E_c}{E_0} \int_0^{E_0 \backslash E_c} \frac{dy}{1 + y^{\frac{3}{2}}} \tag{30}$$

where $y = \frac{E}{E_c}$. For electrons we have:

$$G_e = 1 - G_i \tag{31}$$

Figure 13 illustrates G_i (power fraction to ions) and G_e (power fraction to electrons) as a function of E_0/E_c.

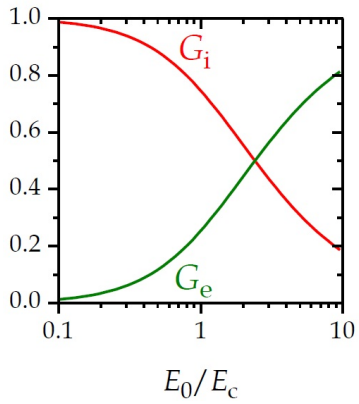

Figure 13.: Fraction of beam energy to ions (G_i) and to electrons (G_e).

In order to assess the fast ion slowing down for real cases, numerical codes are necessary. As it will be described in section 2.3, different approaches can be used, from simple analytical approximations to full Monte Carlo orbit following codes.

2.2.2 NB current drive

NB systems with tangential injection are able to drive plasma current with good efficiency. A description of the underlying physics for the current drive (CD) process is now presented. In case of tangential injection, the ionization of the beam generates a circulating fast ion current, which can be written with a simply and approximated formula as:

$$I_{circ} = I_0 \frac{\langle v_{\parallel} \rangle \tau_{sd}}{2\pi R_0} \tag{32}$$

where $I_0 = \frac{P_{NBI}}{U_0}$ is the injected current, $\langle v_{\parallel} \rangle \approx \frac{v_0}{2}$, $\langle v_{\parallel} \rangle \tau_{sd}$ is the toroidal path length during the slowing down and finally the whole fraction in equation 32 represents the average number of toroidal lap for ions. This formula is useful for simple estimations. A more detailed treatment has to take into account the correct averaging over the slowing down process and considers the pitch angle scattering processes (the initial pitch angle is defined as $\xi_0 = \frac{v_{\parallel 0}}{v_0}$). In this case the circulating current is expressed as:

$$I_{circ} = Z_{beam} I_0 \frac{v_0 t_s}{2\pi R_0} \xi_0 J(x, y) \tag{33}$$

with:

$$J(x, y) = \frac{1}{x} \left(\frac{1 + x^3}{x^3} \right)^y \int_0^x \left(\frac{u^3}{1 + u^3} \right)^{y+1} du \tag{34}$$

where $x = \sqrt{\frac{E_0}{E_c}}$ and $y = \frac{4 Z_{eff}}{5 A_{beam}}$ (with $Z_{eff} = \frac{\sum_j Z_j^2 n_j}{\sum_j Z_j n_j}$ and j representing plasma species), with y called pitch-angle scattering parameter. However I_{circ} is not the real current driven by NBI, because circulating fast ions drag electrons (via collisions) and the electron motion tends to cancel the ion current. The NB driven current is therefore decreased by the "back electron current" (I_{be}):

$$I_{NBCD} = I_{circ} - I_{be} \tag{35}$$

If $Z_{beam} = Z_{eff}$ and without considering toroidal effects, then $I_{NBCD} = 0$, so there is not current drive. If Z_{eff} is different from Z_{beam}, then electrons experience a higher resistance and the NB driven current becomes:

$$I_{NBCD} = I_{circ} \left(1 - \frac{Z_{beam}}{Z_{eff}} \right) \tag{36}$$

Electrons on trapped orbits cannot participate in the net toroidal movement, and therefore they do not contribute to I_{be}. Considering trapped electrons, I_{NBCD} becomes:

$$I_{NBCD} = I_{circ} \left(1 - \frac{Z_{beam}}{Z_{eff}} (1 - G(Z_{eff}, \epsilon)) \right) \tag{37}$$

with:

$$G = \left(1.55 + \frac{0.85}{Z_{eff}} \right) \sqrt{\epsilon} - \left(0.22 + \frac{1.55}{Z_{eff}} \right) \epsilon \tag{38}$$

where $\epsilon = \frac{r}{R_0}$ is the inverse aspect ratio. In order to calculate the density profile of the driven current $j_{NBCD}(r)[A/m^2]$ the fast ion birth profile $H(r)$ has to be considered. The circulating current density profile can be written in the following way:

$$j_{circ}(r) = Z_{beam} v_0 t_s(r) \epsilon_0(r) J\big(x(r), y\big) \frac{I_0}{V_p} H(r) \tag{39}$$

where the dependences on minor radius r are stressed. Similar to the total current, the driven current density profile $j_{NBCD}(r)$ is hence given by:

$$j_{NBCD}(r) = j_{circ}(r)\left(1 - \frac{Z_{beam}}{Z_{eff}}\left[1 - G\left(Z_{eff}, \epsilon(r)\right)\right]\right) \tag{40}$$

These equations are valid assuming that ions born at minor radius r stay on that radius during the slowing down, which is reasonable for tangential injection without banana orbits. Again, for a consistent estimation of the driven current numerical codes are necessary. It is indeed difficult to measure the driven current from the experiment: one should compare the loop voltage between current drive (CD) discharges and reference discharges. Of course, it has to be taken into account other contributions to non inductive currents, as bootstrap currents, which is possible only by modelling.

Once calculated the driven current, it is possible to estimate the CD efficiency of the system, i.e. the current driven per power coupled to the plasma ($\frac{I_{CD}}{P}\left[\frac{A}{W}\right]$). Since for all the CD systems $I_{CD} \propto P\frac{1}{R_0 n_e}$ (R_0 is the major radius of the torus, n_e is the line-averaged density), the CD efficiency is defined as:

$$\eta_{CD} = R_0 n_e \frac{I_{CD}}{P} \text{ usually in } \left[\frac{10^{20}A}{Wm^2}\right] \tag{41}$$

In case of a comparison of different NB injection trajectories for a given toroidal device, it is possible to substitute in the definition R_0 with the NB tangency radius R_T (the major radius at the tangency point with respect to the injection trajectory).

2.2.3 Not only heating and CD: further considerations

NB systems inject particles in the confined plasma, therefore it is a source of particles. The number of injected particles in time can be estimated from:

$$\frac{dN_{NBI}}{dt} = \frac{P_{NBI}}{U_0 e} \tag{42}$$

If in present day experiments this source can be not negligible, for ITER and future reactors the beam fuelling may be negligible, due to the big plasma volume at the foreseen injection power values. This topic will be shortly discussed in chapter 4 for DEMO case. The tangential injection of the beam provides also a toroidal torque to the plasma and induces plasma rotation. The resulting momentum M is:

$$M = \frac{I_0}{e} A_{beam} m_p v_0 R_T e_\phi \tag{43}$$

where R_T is the tangency radius, e_ϕ is the toroidal unit vector and v_0 is the component of the velocity parallel to the direction of the tangential injection. The rotation velocity of the plasma depends on M. However for large machine as ITER or future reactors, the induced momentum will be modest since we have that $\frac{M}{P_{NBI}} \propto U_0^{-1/2}$.

NBI provides a supra-thermal ion population in plasma which can be useful to study fast ion properties, as e.g. fast particle confinement which can be helpful for confinement prediction studies of α particles in burning devices as ITER. Moreover NB fast ions drive fusion reactions if reactive species are used. In the above mentioned D-T experiments at JET and TFTR, fusion neutrons came mostly from beam-plasma interactions. This contribution will be anyway less important for high Q reactors. Further discussion on fusion reaction estimation including NB driven reactions is presented in section 3.2.

2.3 TOOLS FOR NBI–PLASMA INTERACTION MODELLING

Many NBI modelling tools exist nowadays, integrated within different modelling suites. Modern modelling suites are organized by modules. A transport suite is based on a transport code which communicates with other modules accomplishing specific tasks: from plasma transport including impurities and neutrals to plasma-wall interactions, from equilibrium reconstruction to MHD calculations, and, of course, also NBI-plasma interaction calculations. Many NBI modules were born as a part of an omnicomprehensive transport code, and then evolved until they became their self stand-alone modules possibly integrated in transport suites. These transport codes, including all the related modules, can be run in two ways, with different purposes. The first regards "predictive" simulations, which evolves the heat and particle sources self-consistently, evolving the kinetic profiles according to the transport model. This can be used for non existing devices, to explore present machines in unachievable regions or to overcome diagnostic faults, or even to validate different transport models. The other way is called "interpretative" simulation, which uses actual experimental measurements (e.g. source terms) as input, or ”frozen” plasma profiles (i.e. not consistently evolved by the transport code). This is useful to investigate specific topics, assuming the validity of the rest of the prescribed inputs. CPU time of transport simulations can vary between seconds and weeks or more, depending on the amount of calculations required. The simplest and fastest transport codes (order of seconds) treat average quantities and are usually called 0-D codes. 0.5-D codes (CPU time in the order of minutes) are named in this way to stress that they do not use 1-D profiles (e.g. $T(r)$) but they include more sophisticated calculation than 0-D ones, using e.g. a simplified magnetic equilibrium, handling profile peakings instead of whole profiles and considering the time evolution of the parameters. More precise codes are called 1.5-D (CPU time from hours to days or more): they deal with the evolution of 1-D profiles (e.g. $n_e, T_e, T_i, j, \ldots$) and 2-D magnetic equilibrium. Among 1.5-D codes, "fixed boundary equilibrium" ones compute **B** field in the plasma for given plasma boundaries. In 1.5-D "free boundary equilibrium" codes **B** field is computed inside and outside the plasma directly from coil currents. In this thesis, JINTRAC 1.5-D transport suite has been used (see section 3.1.2 for a description), and it has also been coupled with CREATE free boundary code (see section 4.3.2). 0.5-D transport simulations have also been performed with the fast tokamak simulator METIS (see section 4.3.2 for a description).

Focusing on NBI modelling, it is possible to divide NB simulations in two types. The first is composed by stand-alone NB simulations, i.e. simulations where only the NB module is active and acts on a ”frozen” (prescribed) background. The second consists of ”integrated” simulations, where the transport simulation is evolved taking into account consistently the NB calculations. NB codes use different approaches, which influence the computational effort required. Simple and fast codes exploit analytical formulations and approximations, while detailed and computational ”heavy” codes evolve fast ion quantities by means of Monte Carlo, orbit following codes. In this thesis, FIT3D NB code has been used, and it exploits a mix of analytical formulas and Monte Carlo methods to evaluate NBI-plasma interaction (description in section 3.2.2). METIS includes also an NB module, which uses only analytical approximations for NB calculations (section 4.3.2). An-

alytical calculations are used also in PENCIL code, integrated in JINTRAC suite. For JINTRAC modelling, a detailed NB code is available: ASCOT. ASCOT is a full orbit following Monte Carlo code, which has been used in this work for detailed NB analysis. PENCIL and ASCOT are described in section 3.1.2.

3 STAND-ALONE NBI-PLASMA SIMULATIONS

In this chapter, different NBI-plasma interaction models are applied to existing experiments, in order to interpret and predict the beam ionization, heat deposition and fast ion confinement in different situations. For these cases, the focus of the modelling is to accurately reproduce the NB physics for selected time intervals and selected tasks. Therefore we perform here "stand-alone" simulations, in which, for instance, we take as input experimental kinetic profiles, and we investigate the NB absorption and slowing down process.

Two tasks for JET experiment are presented in section 3.1. After an introduction on the NBI modelling tools at JET (subsection 3.1.2), the modelling of a JET experiment is presented in subsection 3.1.3. In this case, from a reference simulation which matches the experimental measurements, an accurate NBI modelling simulation is used to predict the ion temperature profile, since it was not available from experimental measurements due to a fault of a diagnostic. In subsection 3.1.4 JET isotope studies are introduced, and a prediction of performances of H plasma with H NBI is shown starting from similar D cases. In this case an interpretative simulation is run starting from D profiles, which are "frozen" in the simulation, i.e. not evolved during the modelling. In this subsection, a comparison between two different NBI modelling tools is also presented.

In section 3.2 LHD experiment and modelling tools are introduced. In view of the future D experiments instead of usual H discharges, the NBI modelling tool "FIT3D" has been upgraded to enable D experiment analyses and the underlying physics models and the consequent modifications are discussed in subsection 3.2.3. Subsection 3.2.4 shows an application of the upgraded FIT3D code for the analysis of LHD experiments, where different plasma composition required detailed NBI-plasma interaction analyses. In this case the simulated NBI acts on frozen kinetic profiles, and the results are valid in stationary approximation.

All these subjects have in common the use of the NBI modelling in stand-alone mode, therefore not integrated in a fully consistently evolving transport simulation. In the next chapter 4, a different philosophy of NBI simulations will be presented: in that case integrated scenario simulations with dominant NBI are described, and the focus will be not on detailed NBI modelling for selected intervals or tasks, but on the whole evolving plasma with dominant NBI heating, whose behaviour is predicted by complete transport simulations.

3.1 NBI-PLASMA INTERACTION AT JET

3.1.1 JET Tokamak and NB system

JET (Joint European Torus) is a tokamak device in operation at Culham, U.K. . It has been built in the 1970s, and after various modifications it is still in operation, being actually the largest Tokamak in operation world-

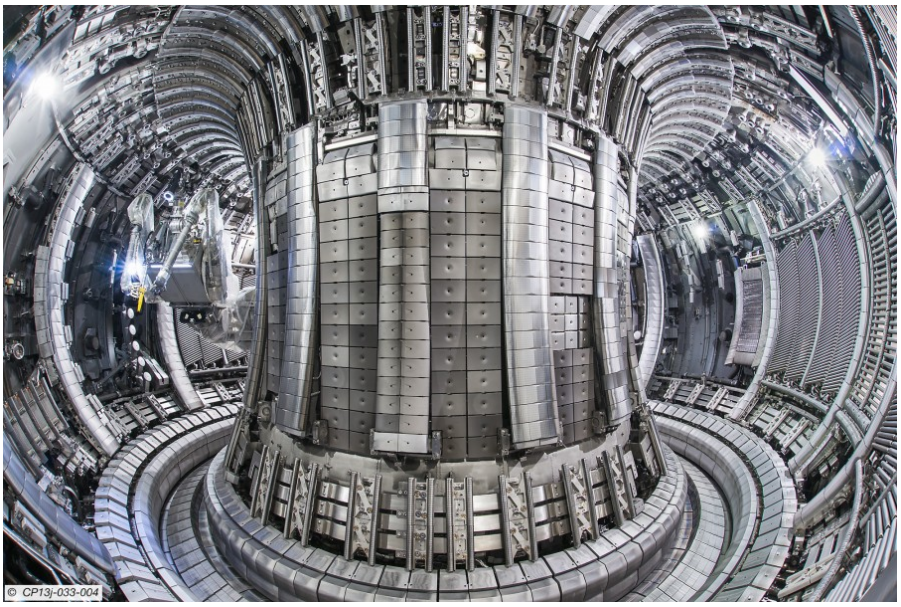

Figure 14.: ITER-like wall (ILW) at JET, from www.euro-fusion.org

wide. The operation has been conducted under EURATOM first, then under EFDA (European Fusion Development Agreement) from 2000 and finally from 2014 under EUROfusion (the "European Consortium for the Development of Fusion Energy") [22]. Main parameters of JET device are reported in table 2.

JET parameters	
Major plasma radius	2.96m
Minor plasma radius	1.25m
Magnetic field	3.45T
Plasma current	4.8MA
NBI power	34MW
ICRH power	10MW
LH power	7MW

Table 2.: Parameters of JET tokamak. Magnetic field value is referred to the magnetic axis.

JET has a D-shaped poloidal cross section, and operates in divertor configuration. Since 2004 JET actively supports the preparation of ITER operation, mainly by three actions:

1. the installation of a ITER-like wall (ILW) in order to have similar plasma facing components (Tungsten and Beryllium instead of Carbon plasma facing components) [23]
2. plasma operation to explore ITER configuration [24, 25]
3. D-T experiments (from 2017)

Since 2011, JET operates with ILW [26], which is shown in figure 14. A strong effort has been devoted to investigate plasma performances with ILW, because unexpected differences and performance issues have been observed with respect to Carbon wall operations [27, 28]. A summary of the most

recent results of ILW campaigns, such as the re-establishment of high performance scenarios after the first wall modifications, can be found in [29].

JET plasma can be heated by 3 different systems (NBI, ICRH, LH), and among them NBI is the most powerful one. NB system is formed by two positive injectors, each of them equipped with up to 8 PINIs (**P**ositive **I**on **N**eutral **I**njectors), as sketched in figure 15. Four PINIs on each injector are grouped into two banks: one having tangential injection with a tangency radius of $R_T = 1.85m$ and one normal bank. JET injection scheme is depicted in figure 16.

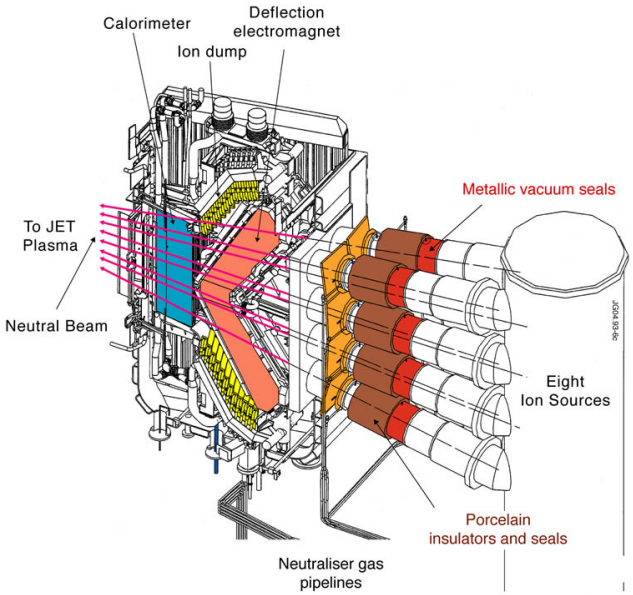

Figure 15.: Sketch of a JET neutral beam injector.

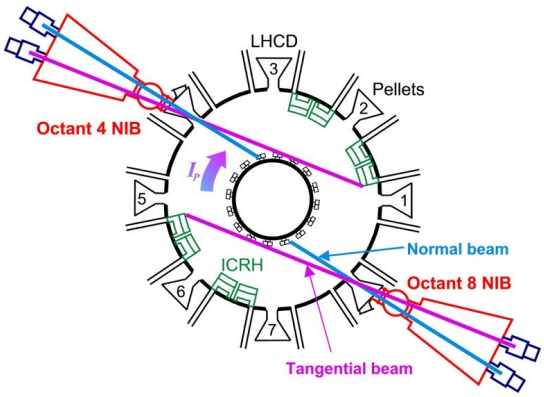

Figure 16.: NBI trajectories and position of other heating systems at JET.

In the last years the NB system has been upgraded to reach 34MW (from the previous 24MW), to increase the NB pulse duration (up to 20s at full power) and to increase the overall availability and reliability of the system [30]. The upgraded PINIs are operated at 125kV/65A in deuterium, providing a 125 keV beam.

3.1.2 NBI modelling at JET: ASCOT and PENCIL

As it can be seen from table 2, NBI is the most powerful additional heating system, and careful NBI modelling is needed to perform JET simulations. JET NBI modelling is integrated in a wider modelling framework named JINTRAC (Jet INtegrated TRAnsport Code) [31], which is a transport suite of codes developed at JET. It is based on 1.5D transport code JETTO [32], which can be coupled with NCLASS [33] for neoclassical transport calculations and GLF-23 [34] which is a complex code for anomalous core heat and particle transport. Other models in JINTRAC suite which are often coupled are EDGE2D [35] for 2D divertor plasma edge modelling, SANCO [36] for impurity transport, EIRENE [37] for transport of neutrals and HPI2 [38] code for pellet injection. Different other models can be coupled depending on the modelling needs. The equilibrium inside the plasma boundary is typically solved with the 2D solver ESCO [32], which is able to consider the pressure contribution from NB fast particles and fusion-born alphas. For NBI modelling in JINTRAC, PENCIL and ASCOT codes are available, and are now described.

PENCIL

PENCIL [39] is a fast NBI code developed during 1980's originally for NB current drive estimation and used also for NB heating estimation. It uses a "fluid approach" with some approximations, running a "bounce-averaged" Fokker-Planck solver. It calculates the deposition profile by summing the deposition profiles of a set of pencil beams (i.e. zero cross section). The ionization of fast neutral particles in plasma takes into account cross sections which includes ionization by charge exchange, by plasma electrons and by plasma ions. Impurities are also taken into account by the effective charge value. Fokker-Planck equation for fast ion dynamics is solved as said with some approximations, which are now summarized. The fast ion density is assumed to be small enough to neglect fast ion self-collisions. The effects of toroidal electric field and bulk plasma rotation are neglected in fast ion dynamics calculations. Larmor motion and drift effects are considered to be negligible with respect to the radial width of the power deposition profile: this approximation permits to neglect the cross-field transport of fast ions. Finally the code is insensitive to beam pitch angle.

This code is less accurate than a Monte Carlo code, especially in case of transient phases. On the other hand it is a very fast tool: in JINTRAC simulations it consumes a negligible CPU time with respect to other transport modules (e.g. ~0.1% of CPU time in a typical integrated transport simulation).

ASCOT

ASCOT [40] is a Monte Carlo code which uses the so-called "kinetic approach". It has been developed in Aalto University, Finland, and it has been applied to all the most relevant devices. ASCOT solves kinetic equations for fast ions and impurity species, and it can be generally used to model minority species in plasma (e.g. [41]). The code follows the test particles integrating numerically the equations, and it can take into account guiding centre approximation or it can consider the full gyro-orbits. It uses a 5^{th}

order Runge-Kutta algorithm. The code is able to simulate also the region outside the separatrix up to the first wall.

ASCOT solves the distribution function for minority species and the kinetic equation for an ensemble of Monte Carlo test particles is:

$$\frac{\partial f}{\partial t} + \dot{\mathbf{z}}\frac{\partial f}{\partial \mathbf{z}} = \left(\frac{\partial f}{\partial t}\right)_{coll} \tag{44}$$

where $f(\mathbf{z}, t)$ is the distribution function, $\mathbf{z} = (\mathbf{r}, \mathbf{v})$ is the particles' phase space, $\dot{\mathbf{z}}$ stands for the equations of motion and $\left(\frac{\partial f}{\partial t}\right)_{coll}$ is the collisional term. According to the Liouville theorem, the phase space volume is conserved by the equations of motion and the kinetic equation can be therefore expressed as the Kolmogorov or Fokker-Planck equation:

$$\frac{\partial f}{\partial t}(\mathbf{z}, t) = -\frac{\partial}{\partial \mathbf{z}}\left[\mathbf{a}(\mathbf{z}, t) f(\mathbf{z}, t)\right] + \frac{\partial}{\partial \mathbf{z}}\frac{\partial}{\partial \mathbf{z}}\left[\mathbf{c}(\mathbf{z}, t) f(\mathbf{z}, t)\right] \tag{45}$$

where the quantity $\mathbf{a}$ contains also the equations of motion $\dot{\mathbf{z}}$. Equation 45 describes the evolution of the probability of finding a test particle in $\mathbf{z}$ when its motion is described by a stochastic process. The solution of the kinetic equation is given by averaging on many paths of random test particles. Guiding centre approximation is then taken into account to reduce the computational effort. Further details can be found in [40].

ASCOT is a fully 3-D code providing accurate NBI simulations (e.g. PENCIL does not include fast ion orbit effects) and it is able to include the wall geometry. It can be applied therefore to study non-axysimmetric configurations in Tokamaks (e.g. ITER power loads due to asymmetries [42]) or even stellarator physics (ASCOT is being currently implemented for W7-X stellarator transport analyses). As drawback, it is slower than analytical codes and typical simulation time is from hours to days. For instance, in an integrated JINTRAC transport simulation with ASCOT of 2.5s with 50000 Monte Carlo test particles, the code took 98% of CPU time.

3.1.3 Ion temperature reconstruction in JET ILW discharge with dominant NB heating

As mentioned in section 3.1.1 JET ILW experiments have been analysed and compared to similar experiments with Carbon wall: with this purpose a systematic modelling activity has been carried out within JET core transport modelling group. The group has studied the ILW deuterium discharge 83479 (JET campaign C29) similar to discharge 77955 of Carbon wall (C-wall) campaign: they are both baseline H-mode discharges with low triangularity and high plasma current. Shot 83479 has $I_p = 3.5MA$, $B_T = 3.3T$ and $q_{95} = 3$.

In ILW shot 83479, due to a fault of the charge-exchange diagnostic, the ion temperature measurement was not reliable. To overcome this issue, predictive JINTRAC simulations has been run with the aim of reproducing available experimental measurements in a relatively stable phase during flattop while predicting at the same time the ion temperature profile evolution. In this shot, NBI was the dominant additional heating with $P_{NBI} = 23MW$, while ICRH provided $P_{RF} = 2.5MW$.

In the reference simulation of this shot done by JET core transport modelling group, the power deposition from NBI has been prescribed to typical profiles in similar shots (normalized to the actual injected power). Since neutral beam injection at typical JET NBI energies heats strongly ions and this

shot was strongly dominated by NB heating, a more accurate simulation of NB power deposition was recommended to reconstruct reliably the ion temperature profiles. For this reason NBI modelling with JINTRAC+ASCOT for shot 83479 has been carried out, and it is here presented.

JINTRAC has been run in predictive mode for 2.5s, reading as input the plasma current and injected additional power from the experimental data and using EFIT for plasma equilibrium reconstruction. Transport has been modelled with JETTO + NCLASS (for neoclassical contributions) + continuous ELM model with prescribed target density and temperature at top of the pedestal. A feedback control on gas puff has been set to reproduce experimental average density values. Sawtheet have been simulated with Kadomtsev model [43]. Impurities (W and Be) have been modelled with SANCO code, trying to reproduce experimental Z_{eff} values. Neutrals have been modelled by FRANTIC code, and in reference simulation both RF and NB power deposition have been prescribed and not directly modelled. In the new simulation here presented, ASCOT has been used to model neutral beam injection. Figure 17 shows the evolution of the measured and simulated line averaged n_e, input I_p and input P_{NBI} during the simulated interval.

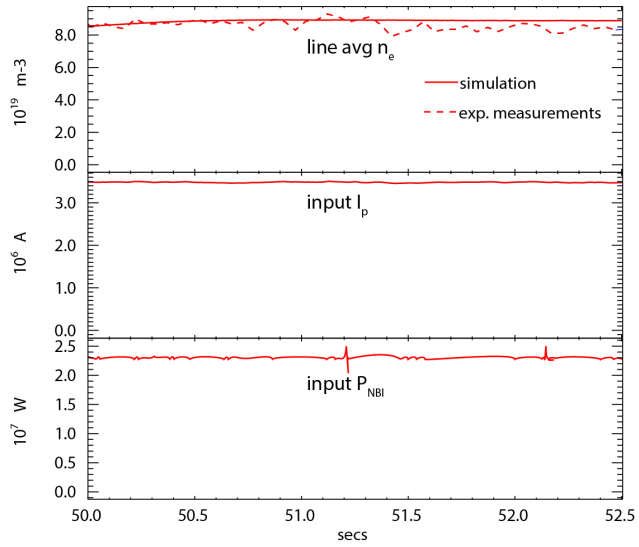

Figure 17.: Line averaged n_e, I_p and P_{NBI} evolution during the simulated interval.

In figure 18 a comparison of high resolution Thomson scattering (HRTS) measurements (marked as "HRTS exp") and simulated profiles with JINTRAC (marked as "simulation") for shot 83479 is shown for time 51s and 52s: a good match can be observed between the experiment and the modelling.

As shown in figures 17 and 18, the simulation correctly follows the available experimental data, and this validates the reconstruction of ion temperature profile which cannot be compared with experimental measurements. Figure 19 shows ion temperature profiles for time 51s and 52s, both from the reference simulation with prescribe NB power deposition (marked as "ref") and from reconstruction with accurate NBI modelling with ASCOT code specifically carried out for this task. In the same figure also the power deposition to ions and to electrons is shown, and, as said, it can be confirmed that the majority of NB heating goes to plasma ions.

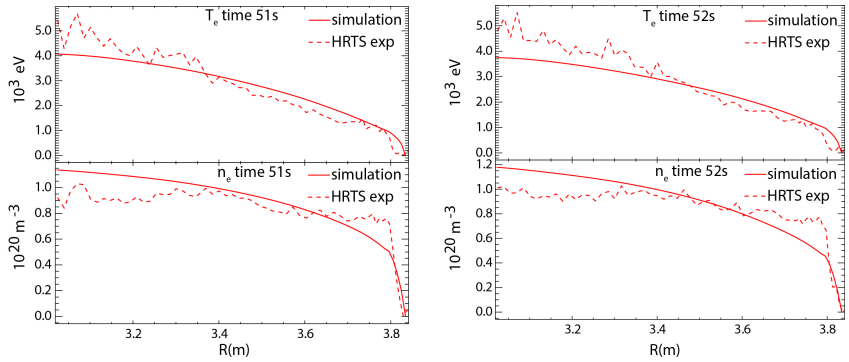

(a) t=51s **(b)** t=52s

Figure 18.: T_e and n_e profiles: comparison of experimental data (from high resolution Thomson scattering -HRTS- diagnostic) and simulation for shot 83479.

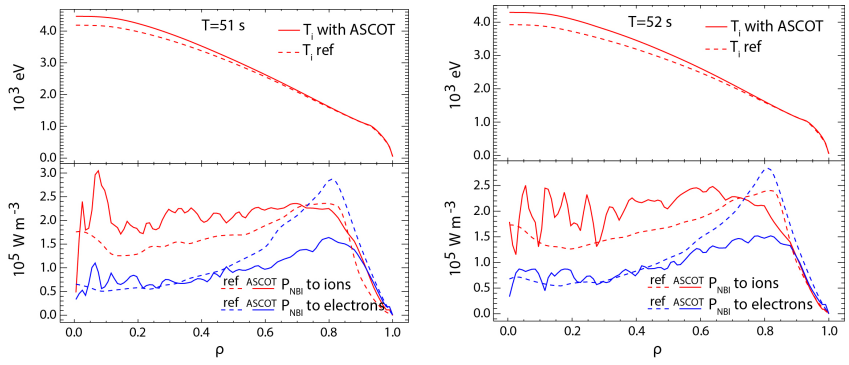

(a) t=51s **(b)** t=52s

Figure 19.: Profiles of T_i and P_{NBI} to electrons and ions: comparison of simulation with prescribed NB power deposition ("ref", dashed lines) and simulation (solid lines) with NB power deposition calculated with ASCOT code for shot 83479.

From figure 19 we can observe that the prescribed NB power density profiles are different from the modelling results with ASCOT code. Electron power deposition is quite different at plasma edge, while ion power deposition differs more remarkably in plasma core. The difference in ion power density causes a different ion temperature profile in JINTRAC+ASCOT simulation with respect to reference JINTRAC+prescribed NBI simulations. We can observe an higher ion temperature in plasma core with accurate NBI modelling. This has been taken into account also for other JET ILW shots of campaigns C28-C30, where ion temperature profile was not reliably measured, and accurate NBI modelling has been carried out within JET core transport modelling group.

An example of these studies is reported in e.g. ref. [44], where the shot here studied together with other ILW and C-wall shots have been modelled, with particular attention to NBI modelling. It is shown that even with PENCIL code modelling of these shots the NB power deposition is not matching the more accurate ASCOT modelling. This means that orbit effects in NB slowing down are important in these cases and that generally in complex simulations, like the comparisons of plasma performance between ILW

and C-wall, where many aspects play a role (e.g. impurities distribution, radiation, neutrals distribution, plasma rotation ...), careful NBI modelling is needed in order to provide accurate results.

3.1.4 Isotope effect studies at JET: D NBI vs H NBI

Another project undertaken at JET in support of ITER is the study of the isotope effect towards a new D-T campaign. In order to prepare the future D-T campaign (2017) and to predict the plasma performances with different hydrogenic plasmas respect to usual D operations, an investigation on isotope effect (for H and D plasmas) has started in the last years. This effort aims to review and extend the isotope effect studies on plasma confinement, pedestal and performance carried out at JET in late 1990s with H, D, D-T and T plasmas [45–49]. Identity experiments with same profiles of dimensionless physics parameters ($\rho^* \propto \frac{\sqrt{MT}}{aB}$, $\beta \propto \frac{nT}{B^2}$, $\nu \propto \frac{na}{T^2}$ and safety factor q) were performed, and the effect of the isotope mass was highlighted, although the scaling appeared to be different for edge and core plasma. In general, the energy confinement increased with the isotope mass, while L-H power threshold and ELM frequency decreased with the isotope mass. These studies were confirmed also for JT-60U Tokamak, where H and D pulses were compared and the results are reported in ref. [50–52]. In this case, beside identity experiments with same profiles of dimensionless physics parameters, a study was conducted keeping the same density and temperature profiles for both H and D plasmas, although the required power clearly increased for H case. A recent work on L-H power threshold dependence on isotope mass is presented in [53], where the ITPA L-H power threshold scaling is discussed, given new results from ILW JET experiments.

In JET experimental campaign C34, experiments with H plasma and H NBI were planned in order to compare them with reference D shots. The aim of experiment H14-03 "Pedestal and confinement in H vs D plasmas" was to study the isotopic dependence of pedestal height and width, ELM size, H-mode characteristic at identical ρ^*, confinement and transport properties. The experiments were based on reference D pulses to be repeated in identical H pulses. The aim of the work here presented has been to support the preparation of these experiments with core plasma modelling, providing detailed analyses of NBI-plasma interaction analysing reference D plasmas and predicting the behaviour of identical H pulses, in order to evaluate possible differences. In general, for NBI-plasma interaction we can expect some dependencies on plasma/beam particle mass, as shown in the equations presented in section 2.2. The first difference is in the beam acceleration: increasing the isotope mass of the accelerated beam particle, keeping the same voltage i.e. beam energy, the velocity of the final beam particle will be lower, and this has an impact on neutral beam ionization. The ionization cross sections, as shown e.g. in [54], depends in fact on beam particle mass, while it weakly depends on main plasma composition. Neutral beam ionization cross section and differences for D and H beams are further discussed in section 3.2.3. We can expect also a dependence of fast ion slowing down on both beam particle mass and plasma ion mass, as shown in equations in section 2.2: for instance the slowing down time increases with isotope mass at same NB energy. All this physics is of course included in PENCIL and ASCOT codes, and they have been used to predict NBI-plasma interaction in H plasma with H NBI starting from the selected reference pulses with D plasmas and D NBI.

The reference D pulse with D NBI chosen for this analysis is 84796, part of power scan experiments in hybrid scenario. The main parameters for this shot are: $I_p = 1.4MA$, $B_T = 1.7T$ with low triangularity. A stable phase of the pulse long enough to allow a detailed analysis ($\backsim$1.5s) has been identified, having in this interval $P_{NBI} = 10.5MW$, $E_{NBI} = 100keV$ and an average $n_e = 3.5 \cdot 10^{19} m^{-3}$. An interpretative simulation has been run with JINTRAC, reading the data (e.g. kinetic profiles, I_p, equilibrium, injected heating power, NB energy...) from the experiment, and modelling with ASCOT the NB absorption in a "frozen" plasma. From this simulation we can extract information for the reference D pulse on NB power deposition profiles, driven current, fast ion birth profile, fast ion density and shine through losses. Starting from this simulation, the main plasma has been switched to H, and NB injection too, keeping the rest of the simulation identical (e.g. kinetic profiles and all other inputs). The density and temperature profiles are shown in figure 20a.

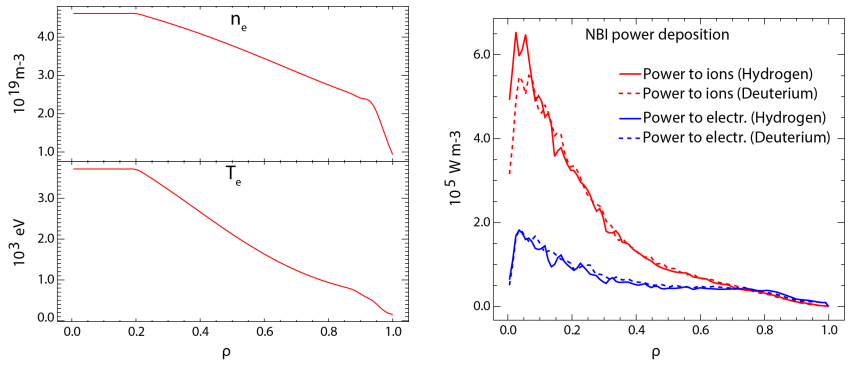

(a) Profiles of T_e and n_e **(b)** NB power depositions for D and H cases

Figure 20.: Profiles of T_e and n_e used as input in the interpretative simulation of the reference D pulse and in the simulated H pulse and comparison of NB power deposition profiles to ions and electrons for D and H cases.

Since for H discharges at JET the maximum NB energy for reliable operations has been fixed to 90keV, E_{NBI} has been set to this value in H simulations, while NB power has been kept identical (maximum allowed P_{NBI} for H pulses is 16MW). This makes a little difference in the two simulations, since keeping the same power and lowering the energy implies that the source of particle is different, being lower for D and higher for H. An interpretative simulation of 0.5s with H plasma and H NBI has been run, longer than the fast ion slowing down time. The power deposition to ions and electrons is shown in figure 20b: the final deposition is not much affected from the isotopic change.

Nevertheless some differences can be seen in the fast ion source profile ("birth" profile) and in fast ion confinement. Figure 21 shows the ion birth profile, the fast ion density and the driven current profile. From the plot of the fast ion birth profiles, we can see that the total source (i.e. the volume integral of the profiles) of H fast ions is lager than D fast ions, as it has been explained above. However the fast ion density (which takes into account the slowing down process) is higher for D than H, and the same behaviour is observed for the driven current profile. This can be partly explained by the fact that slowing down time for D fast ions is longer than for H fast ions, and remembering also that, as highlighted in the above-mentioned JET isotopic studies, confinement increases with isotope mass, we can expect worse con-

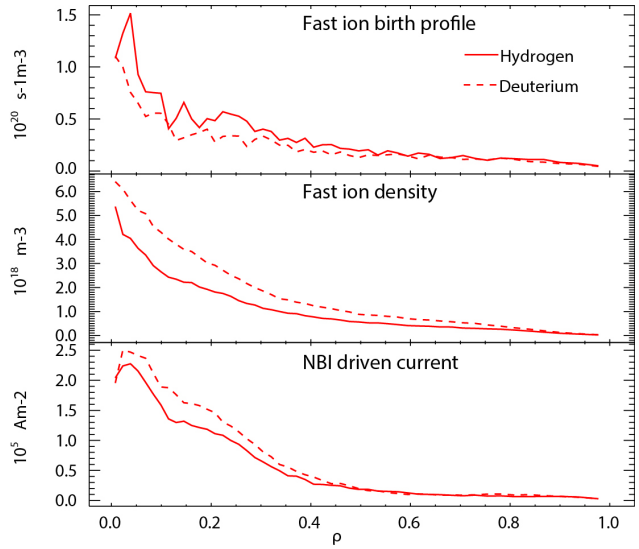

Figure 21.: Fast ion birth profile, fast ion density and driven current profile (after a time interval longer than fast ion slowing down time).

finement for H fast ions in H case. A worse NB absorption with H plasma and H NBI is evident by the comparison of shine-through power losses for H and D cases, which is shown in figure 22. From this figure we can observe that shine through losses in H are approximately double than in D: since the density profile is equal for both cases this means that the isotopic change is the reason of the higher losses, although H NB particle source is slightly higher (so we can expect the losses), but definitely not double than D NBI case. From this analysis we can conclude that, in case of identical kinetic profiles, the losses are higher for H case and the confinement of H fast ions in H plasma is worse than in D case. This is shown from fast ion density and driven current profiles, while the final power deposition seems not to depend clearly on the isotope. The fast ion confinement degradation in H case is in line with the isotopic studies in JET and JT-60U presented.

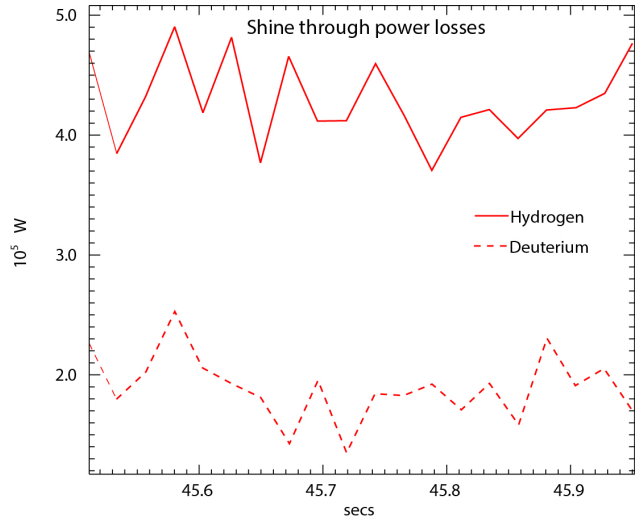

Figure 22.: Shine through power losses in H and D cases.

ASCOT vs PENCIL NBI modelling

The reference JET D pulse 84796, used for the preparation of H14-03 experiments on isotope effect discussed above, has been originally modelled using PENCIL code for NBI-plasma interaction modelling, since PENCIL is the code used routinely for NBI investigations due to its rapidity. This gives the opportunity to compare PENCIL and ASCOT modelling for the same case. Figure 23 compares the power deposition profiles for the reference shot with D plasma and D NBI calculated by PENCIL and ASCOT codes.

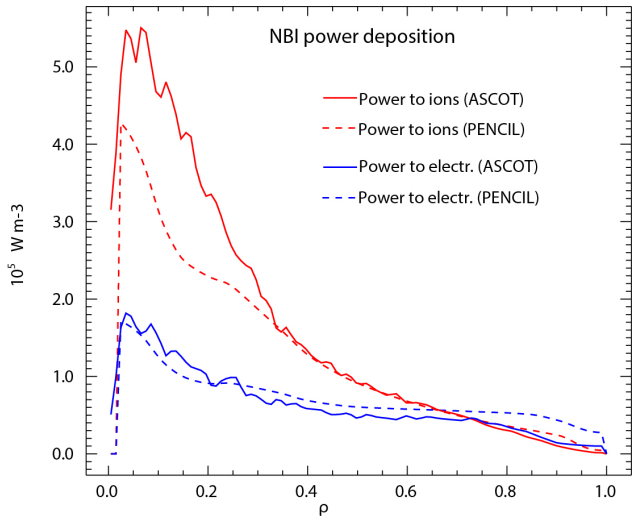

Figure 23.: NB power deposition profiles for reference D pulse 84796 modelled by PENCIL and ASCOT.

We can observe that PENCIL underestimates the power deposition to ions in core plasma, and slightly overestimate the deposition to electrons in outer plasma region. An explanation can be that for NB PINIs with tangential injection, PENCIL is distributing the power only along the NB trajectory (pencil-like) inside the plasma (i.e. off axis), while ASCOT, which is an orbit-following code, considers also the orbit effects which make the power spreading also toward the plasma centre.

As described in section 3.1.2, ASCOT is a Monte Carlo code, and one of the required settings when running a simulation is the number of test particles. This affects the simulation in two ways: with more test particles the simulation is slower, but on the other hand it is also more accurate: the standard deviation of the result (reflected in the "noise" of profiles) of a simulation of N random particles is proportional to $\sqrt{\frac{1}{N}}$. Usually ASCOT is run with 10000 Monte Carlo test particles (as used e.g. for simulations in section 3.1.3), but when the simulation interval is smaller, or when the "noise" in profiles is too high (a typical case is with low plasma density) ASCOT is run with more test particles. In the work presented in this section, since the computational effort was low due to the small simulation interval and the less demanding interpretative simulations, ASCOT was run with 50000 test particles. However an ASCOT simulation with 10000 test particles was run for the reference D pulse, in order to observe the consequence of running faster ASCOT simulations with less test particles. Figure 24 shows a comparison for the NB power deposition profiles between ASCOT runs with 10000 and 50000 test particles for the same simulation. It can be seen that the profiles calculated with 10000 test particles results more noisy than

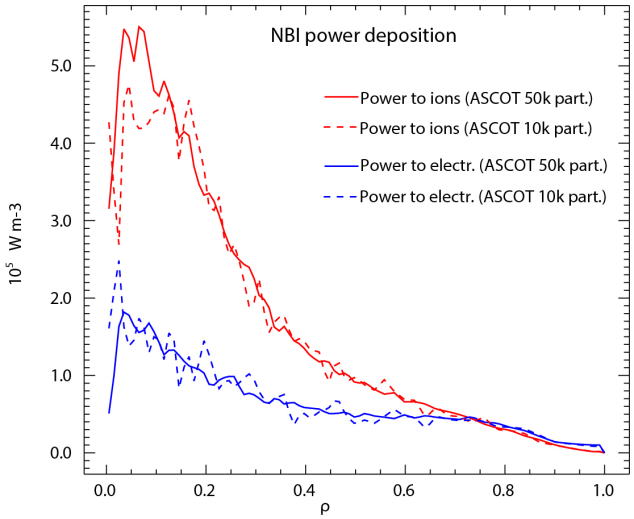

Figure 24.: NB power deposition profiles for reference D pulse 84796 modelled by ASCOT with 10000 and 50000 Monte Carlo test particles.

with 50000 test particles, and the fewer test particles seems also to have in this case an impact on the accuracy of the orbit effect calculations, with a reduced power deposition in plasma centre (which, as discussed before, is linked to power spreading effects due to fast ion orbits). From this analysis we can conclude that depending on modelling needs, NBI modelling can be performed with the faster PENICIL code or the more accurate ASCOT (with more or less test particles). Generally the main trend is followed from both codes, but the accuracy is not the same, especially when orbit effects play an important role.

3.2 NBI-PLASMA INTERACTION AT LHD

3.2.1 LHD device and NB system

LHD (Large Helical Device) [55] is toroidal device for plasma confinement belonging to the family of helical configurations. It is located in Toki-city, Japan, and it is run by NIFS institute. The precise configuration name is "heliotron", and LHD is the largest helical device, together with the recently built W7-X stellarator. It is equipped with superconducting coils which enables long pulses achieving steady state regimes. The peculiarity of this device is the pair of helical coils which, together with 3 poloidal coils, provide the complex non-axisymmetric 3D magnetic field. The magnetic field period is l=2, m=10. LHD started the operations in 1998, and the goal is to study reactor-relevant plasmas in helical configuration, in order to offer an alternative way to tokamaks in the path towards commercial fusion reactors. Main parameters of LHD device are reported in table 3.

JET parameters	
Major plasma radius	3.42-4.1m
Minor plasma radius	0.5-0.65m
Magnetic field	3T at R=3.9m
Plasma volume	$30m^{-3}$
NBI power	up to 28MW
ICRH power	3MW
ECRH power	5.4MW

Table 3.: Parameters of LHD device.

A sketch of LHD and a photo of its internal winding first wall is shown in figure 25.

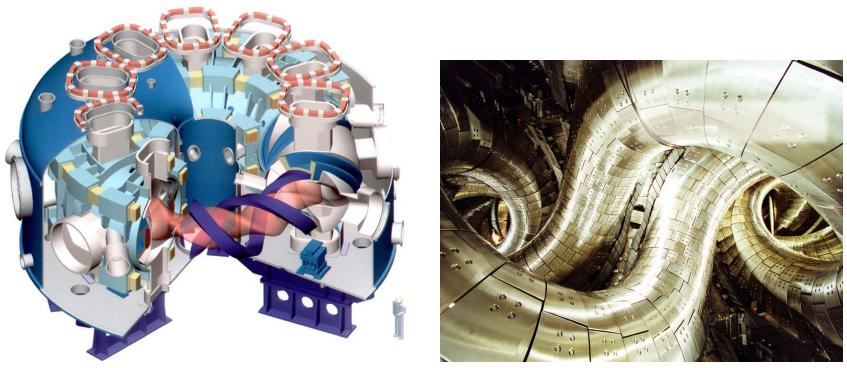

(a) LHD sketch **(b)** LHD internal view

Figure 25.: LHD helical device at NIFS.

High β (5.1%), high density ($1.2 \cdot 10^{21} m^{-3}$), high ion temperature (10keV) and long pulse (3200s) conditions have been separately reached [55]. LHD is usually run with H plasmas (and H NBIs), but a first D campaign is foreseen from 2017 [56]. Currently at NIFS a big effort has been undertaken for the preparation of D experiments. Recently, a study on prediction of plasma performance and fusion reaction production in D LHD experiments has been presented [57], showing an expected increase of ion temperature of more than 20% in D plasmas, assuming an anomalous transport model

based on LHD He plasmas. While in tokamaks the isotope effect is well known (as described in section 3.1.4), for helical configurations it is still discussed, and limited data are available [58]: this is one of the reason that led to the decision of starting a D campaign at LHD . The main objectives of the LHD D campaign are very reactor-oriented and are [59]:

1. to explore high-performance plasmas by confinement improvement relevant for reactor conditions
2. to clarify the mass dependence (isotope effect) of the plasma confinement to establish a model for helical D-T plasmas
3. to demonstrate the confinement capability of high-energy ions, relevant for burning plasmas in helical configurations

The NBI system will be upgraded to D injection. Currently LHD is equipped with 5 hydrogen neutral beam injectors: 2 perpendicular positive-NBIs (40-50 keV, up to 12MW) and 3 tangential (co- and counter-injection) negative NBIs (180-190 keV, up to 16MW). Figure 26 shows a sketch of the NBI system, while NBI parameters are listed in table 4.

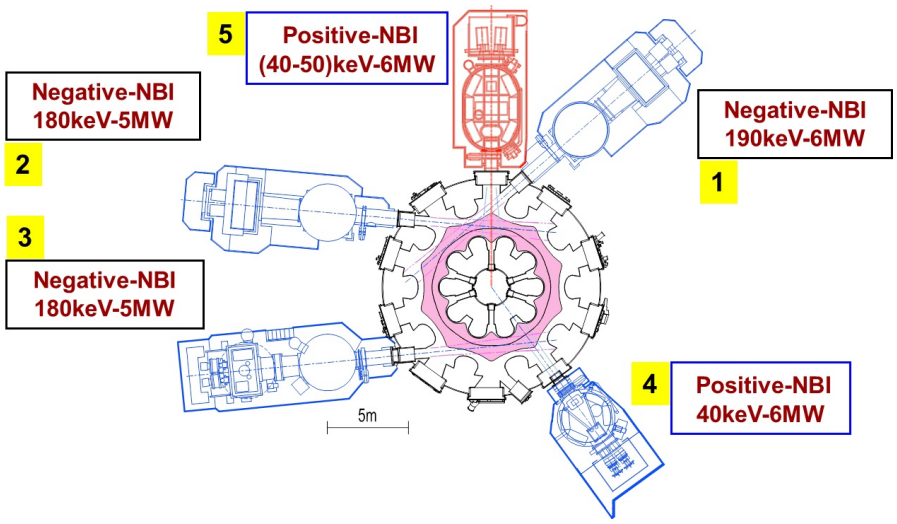

Figure 26.: View of the 5 hydrogen LHD NBIs, with the corresponding line numbers.

Beam line #	Name	Accelerated ions	Injection	E_{NBI} - P_{NBI}
1	Ctr1	H^-	counter	190 keV - 6MW
2	Co2	H^-	co	180 keV - 5MW
3	Ctr3	H^-	counter	180 keV - 5MW
4	Pb4	H^+	perpendicular	40 keV - 6MW
5	Pb5	H^+	perpendicular	40-50 keV - 6MW

Table 4.: Parameters of NB lines in LHD.

Tangential NBIs locally drive current, but thanks to the opposite injection directions, LHD can be run in net current-free regimes. For D injection, NB lines "Pb4" and "Pb5" will be upgraded to 9MW by rising E_{NBI} respectively to 60keV and 80keV. This increase is driven by the idea of providing more ion heating in D operations, in order to reach higher ion temperature for reactor relevant studies. The 3 tangential NBIs will be upgraded to D injection but will keep the current energy and power [60].

3.2.2 TASK3D-a integrated transport suite for LHD experiment analysis

The analyses of LHD discharges are usually performed by TASK3D-a tool [61], which is an integrated transport suite for the analysis of LHD plasmas in 3-D magnetic configurations. TASK3D-a has an interface for reading the LHD data, a routine to calculate the magnetic equilibrium with VMEC code [62] and to transform the coordinate into Boozer system, a routine for the calculation of heating by NBI named "FIT3D" [63] and a transport routine to calculate energy and momentum balance [64, 65]. Other routines can be coupled for additional analyses, e.g. "aurora" for the evaluation of neutral particle distribution [66], "giota" [67, 68] for evaluation of ripple transport in helical configuration and "gsrake" [69] for the evaluation of neoclassical radial diffusion in helical systems. The code is capable of treating hydrogen and multi-ion species plasmas [70]. The physical experimental data are stored in the Kaiseki server [71], and are made available for the analysis. Figure 27 shows the computational flow of TASK3D-a.

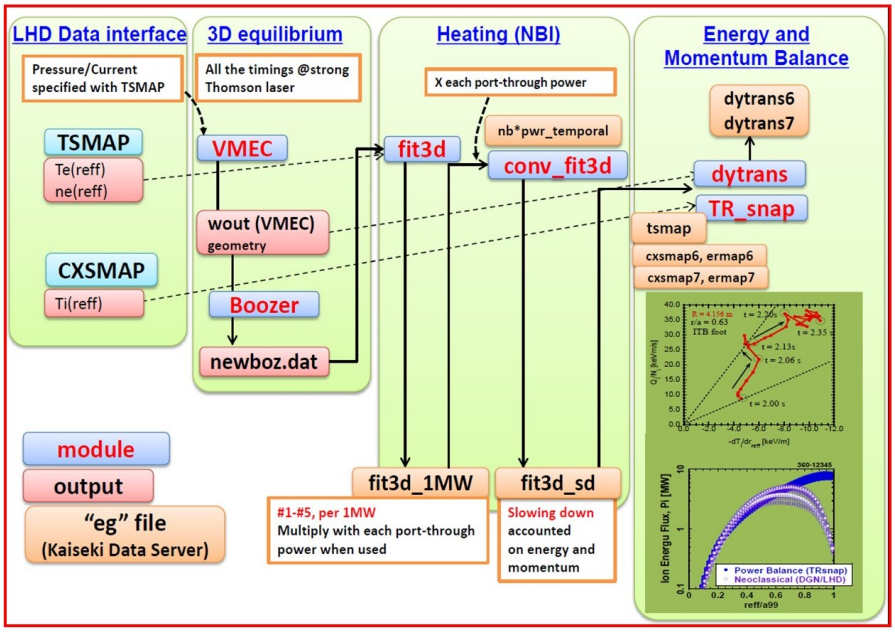

Figure 27.: Computational flow of TASK3D-a transport analysis suite of code for LHD, from [61].

A recent integrated study with TASK3D-a of LHD plasma with NB heating is presented in [72], where 6 different modules have been coupled for the analysis of turbulent particle transport, which has been compared to experimental measurements.

FIT3D and other NB modelling tools for LHD

External heating in LHD is essential since the ohmic power contribution is missing. Among the installed heating systems, NBI is the most powerful, and most of the experiments rely on NB heating. The complex combination of injection trajectories in a non-axysimmetric device and different NB energies makes NBI modelling crucial for the experiment analysis. FIT3D [63] is a routine integrated in TASK3D-a for NBI-plasma interaction modelling and it has been developed to evaluate radial profiles of NB absorbed power,

beam pressure, beam particle source, induced momentum and driven current. It has been developed as a reduced version of GNET code [73] (see below for a short description). The calculations performed by FIT3D consists of three parts [74]:

- HFREYA routine calculates the fast ion birth profile for H NBI taking into account the beam trajectory
- MCNBI routine follows the newly-born fast ions for a time interval shorter than the energy slowing-down time, but longer than the time scales of orbit effects
- FIT3D finally calculates analytically a steady-state solution of the Fokker-Plank equation without taking into account orbit effects

The code mixes Monte Carlo techniques (for HFREYA which calculates the ionization position of each test particle and for MCNBI) and an analytical approach (for steady-state solution of Fokker-Plank equation), and does not consider orbit effects. The set of equations of FIT3D is similar to the model adopted in PROCTR code [75]. In order to follow the dynamics of fast ion slowing down, the code is coupled with a routine named "conv_fit3d" [74] which calculates the power transfer from fast ions to plasma during the slowing down process, taking as input the calculations of FIT3D.

Other codes have been used to analyse LHD NBI-plasma interaction, but they are not integrated in the TASK3D-a suite, and therefore cannot be used routinely. For instance, the above-mentioned GNET Monte Carlo code has been used stand-alone for LHD confinement studies of energetic ions from NBI in order to calculate the steady-state beam distribution function solving drift kinetic equation in five-dimensional phase-space (3-D space, 2-D velocity) using Boozer coordinates in a full 3-D magnetic field [76]. An extended version of GNET named GNET-TD (Time Development) has been used to calculate the NB distribution function with an evolving background plasma [77]. In these studies the boundary has been fixed at the LCFS, and the fast particles were considered lost when passed the LCFS. A Monte Carlo code named MORH [78, 79] has been developed at NIFS to follow fast ion orbits in real space (Cartesian coordinates), giving the possibility to set the particle loss boundary at the vacuum vessel and therefore allowing the inclusion of re-entering fast ions in the calculation of the distribution function.

3.2.3 FIT3D upgrades for LHD D operation: discussion of physics models and implementation in the code

TASK3D-a and FIT3D are routinely used to analyse H plasma with different impurities (e.g. C, He...) with H NBI. Effort has been recently put to upgrade TASK3D-a code in order to extend the analysis capabilities to D plasmas with D NBIs. In this section the upgrades proposed for FIT3D code during the activity performed in order to enable the modelling of D NBI in D plasma are described. Two main modifications have been proposed, and a discussion on the underlying physics models and approximations is presented. The first modification regards the calculation of the ionization of a D neutral beam in D plasma. The second regards the estimation of the neutron production from D-D reactions, both from thermal and beam-plasma reactions. In this work beam-beam fusion reactions are not considered; a first study on beam-beam fusion reaction prediction for LHD D campaign has

recently been presented in [80]. Finally, the implementation of the discussed models in FIT3D code is described.

Beam stopping cross section for NB ionization process

HFREYA routine is one of the three main routines of FIT3D code, and it deals with the calculation of the ionization cross section of the neutral beam in the plasma, which is often called "beam stopping cross section". The beam attenuation process is described by the stopping cross section $\sigma_s = \frac{1}{n_e \lambda}$, where n_e is the plasma density and λ is the beam attenuation length. The original FIT3D code uses an analytical formula for the beam stopping cross section proposed by Janev [81]. The formula takes into account the ionization by hydrogen plasma ions and electrons, charge-exchange process, ionization by impurities (He, C, O, Fe) and a cross section enhancement due to multistep ionization (ionization from excited states). Input for Janev's formula are: atomic mass "u" of the beam particles, beam energy E_{NBI}, plasma density n_e, plasma temperature T_e and the effective charge Z_{eff} together with the chosen representative impurity (if only one impurity species is considered) or in case of more impurities, their concentrations instead of Z_{eff}. The fit used to obtain the analytical formula proposed by Janev is calculated for the following ranges:

- $100 \leqslant E_{NBI}(keV/u) \leqslant 10^4$
- $10^{18} \leqslant n_e(m^{-3}) \leqslant 10^{21}$
- $1 \leqslant T_e(keV) \leqslant 50$
- $1 \leqslant B(T) \leqslant 10$

The formula for one representative impurity using the effective charge value Z_{eff} is the following (from Janev's work [81]):

$$\sigma_s^{(z)}(E, n_e, T_e, Z_{eff}) = \frac{\exp[S_1(E, n_e, T_e)]}{E}\left[1 + (Z_{eff} - 1)\, S_z(E, n_e, T_e)\right] \left(10^{-16} cm^2\right) \tag{46}$$

where:

$$S_1 = \sum_{i=1}^{2}\sum_{j=1}^{3}\sum_{k=1}^{2}\left\{A_{ijk}(\ln E)^{i-1}[\ln(n/n_0)]^{j-1}(\ln T_e)^{k-1}\right\} \tag{47}$$

$$S_z = \sum_{i=1}^{3}\sum_{j=1}^{2}\sum_{k=1}^{2}\left\{B_{ijk}^{(z)}(\ln E)^{i-1}[\ln(n/n_0)]^{j-1}(\ln T_e)^{k-1}\right\} \tag{48}$$

The values of the coefficients A_{ijk} and B_{ijk} are listed in table III and table IV of the paper. In case of multiple impurities with charges Z_q and impurity concentrations n_q, the formula becomes:

$$\sigma_s^{(N)} = \frac{\exp[S_1(E, n_e, T_e)]}{E}\left[1 + \frac{1}{n_e}\sum_q n_q Z_q (Z_q - 1)\, S_{z_q}(E, n_e, T_e)\right] \left(10^{-16} cm^2\right) \tag{49}$$

where E is in keV/u, n_e in cm^{-3}, T_e in keV and $n_0 = 10^{13} cm^{-3}$. In case of $Z_{eff} = 1$ we have the case of pure hydrogen plasma. The formula was originally calculated for neutral hydrogen injection in H plasma; however changing the beam atomic mass u we can obtain the attenuation of a deuterium beam, but still in hydrogen plasma. Janev's formula is obtained, as remarked, for $100 \leqslant E_{NBI}(keV/u) \leqslant 10^4$. Considering LHD hydrogen NBIs,

the two positive NBIs are out of this range. In case of D beams, $E_{NBI}(keV/u)$ for deuterium will be less than 100 keV/u for all the NB lines, being out of the range of Janev's calculation. For this reason a more suitable formula for LHD deuterium injection has been proposed. Suzuki provided a more recent fit for the ionization cross sections [54], which includes more impurities (He, Li, Be, B, C, N, O, Fe) and is calculated for a wider $E_{NBI}(keV/u)$ range. Moreover different fitting coefficients are provided in case of H, D and T background plasmas, while Janev did not distinguish different background plasmas. Suzuki's fit for beam stopping cross section uses a similar formulation to Janev's work, being actually an updated and extended alternative to Janev's formula. Following equation 46, Suzuki presents the beam stopping cross section as the multiplication of two terms, the first representing a term for a pure plasma without impurities, the second the contribution of plasma impurities: $\sigma_s = \sigma_H \cdot \sigma_{imp}$, if $Z_{eff} = 1 \Rightarrow \sigma_{imp} = 1$. With respect to Janev, Suzuki gives a new formula for σ_H while he just updates the coefficients given by Janev for σ_{imp} fit (but including more impurities). With Suzuki formula, σ_H can describe H, D or T plasmas by choosing the related fitting coefficients. Suzuki's coefficients have been calculated in the following ranges:

- $10 \leqslant E_{NBI}(keV/u) \leqslant 10^4$
- $10^{18} \leqslant n_e(m^{-3}) \leqslant 10^{21}$
- $E_{NBI}(keV/u)/100 \leqslant T_e(keV) \leqslant E_{NBI}(keV/u)/2$

Figure 28 shows a comparison between Janev and Suzuki formulas for beam stopping cross sections of a D plasma for different beam energies and different plasma densities. It is possible to see that there are some differences at lower beam energies, which is the interesting region for LHD NBI system.

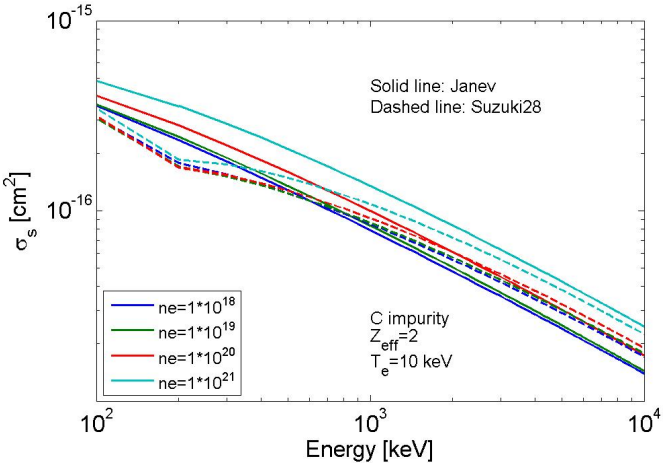

Figure 28.: Comparison between Janev and Suzuki fits for beam stopping cross section in D plasma with Carbon impurities. "Suzuki28" refers to formula 28 in his paper [54], which has been discussed in this section.

A comparison between Janev and Suzuki formulas has been performed for LHD relevant D NB energies, which, as said, are out of the range of Janev's fit. Figure 29 compares the beam stopping cross sections for two beam energies: 80 keV (i.e. 40 keV/u for D injection) and 180 keV (i.e. 90

keV/u for D injection). It is possible to note some discrepancies, especially at higher densities. In these figures carbon is the only representative impurity with an arbitrary input Z_{eff} of 1.5.

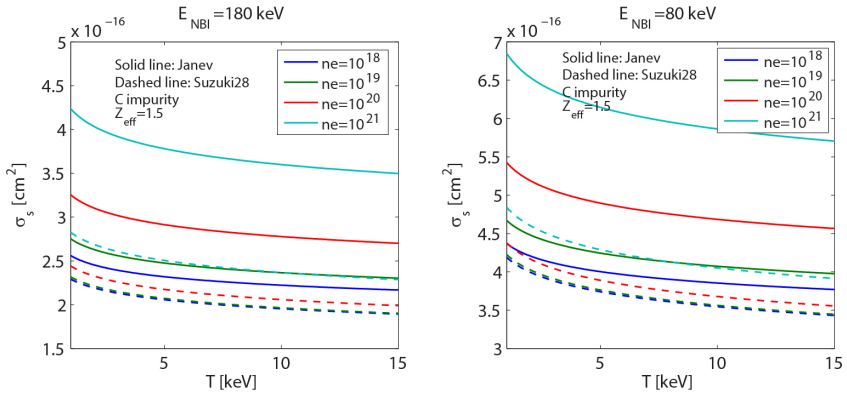

(a) $E_{NBI} = 180keV$ (D Co2 or Ctr3 lines) **(b)** $E_{NBI} = 80keV$ (D Pb5 line)

Figure 29.: Comparison of Janev (solid line) and Suzuki (dashed line) cross sections for D plasma with D NBI.

The parameter ranges of Suzuki's fit, especially E_{NBI}(keV/u), fulfil LHD requirements both for H and D operation. Given the possibility of considering D plasma background and given the wider E_{NBI}(keV/u) range of fit's validity, the use of Suzuki formulation is preferable to treat the modelling of D plasma and D NBI for LHD. Suzuki's formula for σ_s has been implemented in the upgraded version of FIT3D.

Neutron rate and fusion power source estimation for D plasma with D NBIs

The second part of FIT3D modifications has been the implementation of a routine which calculates the neutron rate produced by fusion reactions in case of a deuterium plasma.

D-D fusion reaction has two branches:

$$D + D \rightarrow p(3.02MeV) + T(1.01MeV) \tag{50}$$

$$D + D \rightarrow n(2.45MeV) +^3 He(0.82MeV) \tag{51}$$

Reaction 50 produces a proton and a tritium particle, while reaction 51 produces a neutron and a ^{3}He particle. Fusion reactions arise from background (thermal) plasma, from beam-plasma and beam-beam interactions. In the present work beam-beam fusion reactions are not treated. The fusion power which heats the plasma is carried by charged particles born in the reactions (protons, T, ^{3}He), while neutrons escape from the plasma. The fusion power density source in the plasma from charged particle-only is:

$$P_{DD,tot} = (E_p + E_T) \cdot S_{p,DD,tot} + E_{^3He} \cdot S_{n,DD,tot} \tag{52}$$

where:

$$E_p\,[J] = e \cdot \left(3.02 \cdot 10^6 eV\right) \tag{53}$$

$$E_T\,[J] = e \cdot \left(1.01 \cdot 10^6 eV\right) \tag{54}$$

$$E_{^3He}\,[J] = e \cdot \left(0.82 \cdot 10^6 eV\right) \tag{55}$$

E_x is the energy carried by charged particles, S is the source term (S_p is the proton rate, S_n of neutrons) and e is the electron charge.

THERMAL FUSION REACTIONS In this subsection fusion reactions in thermal D plasma are discussed. The fusion rates per volume are:

- proton rate per volume:
  $S_{p,DD,thermal} = \frac{1}{2} n_D^2 \langle \sigma v \rangle_{D(d,p)T}$
- neutron rate per volume:
  $S_{n,DD,thermal} = \frac{1}{2} n_D^2 \langle \sigma v \rangle_{D(d,n)^3He}$

where the reactivity $\langle \sigma v \rangle$ is defined as:

$$\langle \sigma v \rangle = \iint f\left(\vec{v_i}\right) f\left(\vec{v_j}\right) \sigma(|\overrightarrow{v_{rel}}|) \left|\overrightarrow{v_{rel}}\right| d\vec{v_i} d\vec{v_j} \tag{56}$$

with $\overrightarrow{v_{rel}} = \vec{v_i} - \vec{v_j}$ and f(v) the velocity distribution function. Bosch proposed a parametrization of the fusion reactivity for a Maxwellian plasma [82], starting from Peres [83] functional form:

$$\langle \sigma v \rangle = C_1 \theta \sqrt{\xi / m_r c^2 T^3} e^{-3\xi} \tag{57}$$

where:

$$\theta = T / \left[1 - \frac{T\left(C_2 + T\left(C_4 + TC_6\right)\right)}{1 + T\left(C_3 + T\left(C_5 + TC_7\right)\right)}\right] \tag{58}$$

$$\xi = \left(B_G^2 / \left(4\theta\right)\right)^{1/3} \tag{59}$$

The reactivity $\langle \sigma v \rangle$ is given here in $\frac{cm^3}{s}$ and T is the ion temperature in keV. Bosch listed the coefficients for various fusion reactions; in our case we are interested in the two D-D reactions (last two columns of table VII in the paper [82]). Thanks to this parametrization we do not have to calculate directly the integral of the reactivity. In figure 30, an example of reactivities, neutron/proton rates and fusion power density calculated with formula 57 is shown. Arbitrary n_e and T_i profiles are given as input and are expressed in the parabolic form $f(\rho) = f_0 \cdot \left(1 - \rho^2\right)$, where f_0 represents the value at plasma centre. Figure 30 has been generated with $T_{i,0} = 5keV$ and $n_{e,0} = 10^{20} m^{-3}$.

S. Murakami (Kyoto University) prepared some years ago an independent version of FIT3D code named "FIT3D_DD" [84], originally developed to calculate D-D fusion reactions, but not integrated in TASK3D-a code. In FIT3D_DD code, thermal plasma reactions are calculated using an older formula for the fusion cross section σ_{DD} given by Duane [85] and reported in NRL formulary [86]. In his paper Bosch shows that Duane's fit for fusion cross section is less precise: it gives in fact an inaccurate extrapolation for low energies. A discussion and a comparison between Bosch and Duane formulas is presented in his paper [82]. The upgraded version of FIT3D with the thermal plasma reaction model described above (which uses the reactivity parametrized by Bosch) has been compared with FIT3D_DD. In FIT3D_DD thermal plasma model, the reactivity is directly calculated integrating the Maxwellian distribution function of thermal plasma. As a remind, the usage of Bosch's fit for reactivity calculations of thermal plasma

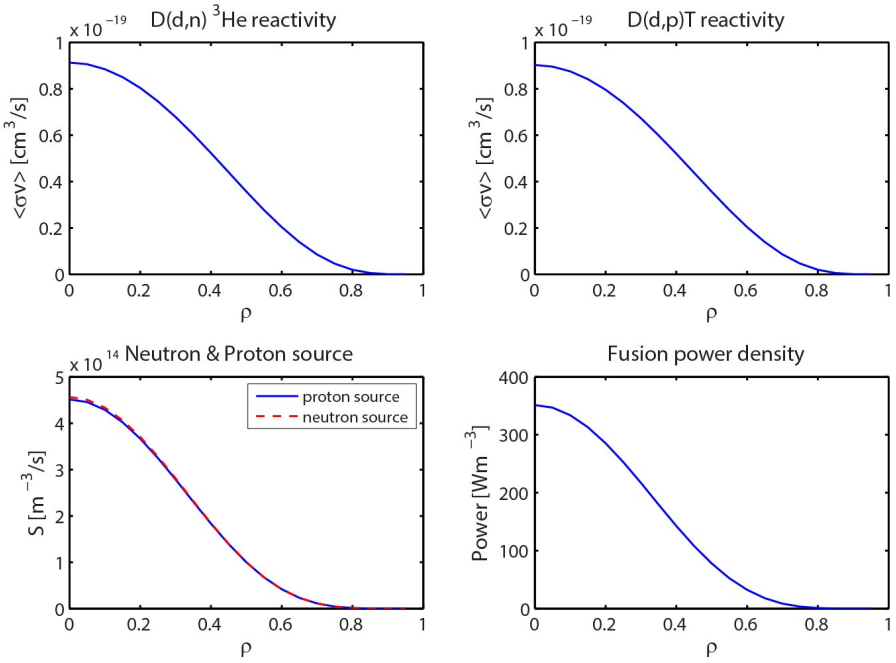

Figure 30.: Profiles of D(d,n)3He and D(d,p)T reactivities, neutron/proton production rates and fusion power density calculated by formula 57 with assumed n_e and T_i profiles of the form $f(\rho) = f_0 \cdot (1 - \rho^2)$, where f_0 with $T_{i,0} = 5\text{keV}$ and $n_{e,0} = 10^{20}\text{m}^{-3}$.

fusion reactions exempts from the complete integral calculation, saving computational time. The input n_e and T_i profiles given to the two compared routines are shown in figure 31.

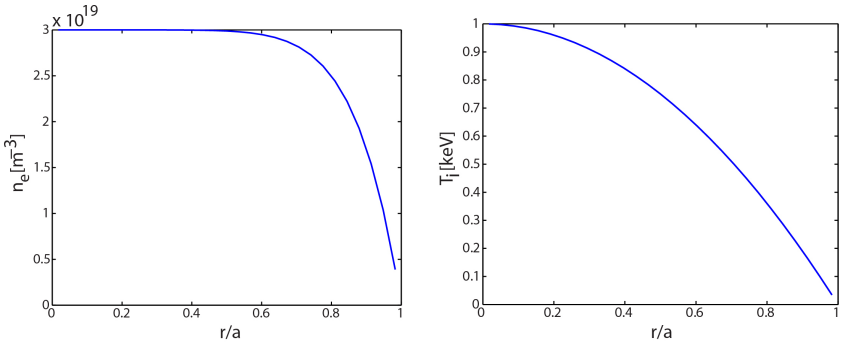

(a) Input electron density **(b)** Input ion temperature

Figure 31.: Input profiles for fusion rate calculations shown in figures 32 (thermal plasma reactions), 37 and 38 (beam-plasma reactions, see next paragraph).

The resulting fusion reactions from thermal plasma contribution are shown in figure 32.

In this example, the upgraded FIT3D model using Bosch's reactivity reported in equation 57 (red curve in figure 32) gives a lower neutron rate estimate for thermal plasma reactions with respect to Duane's fusion cross section fit used in FIT3D_DD. This shows that using the more accurate and recent Bosch's parametrization instead of calculating approximately the in-

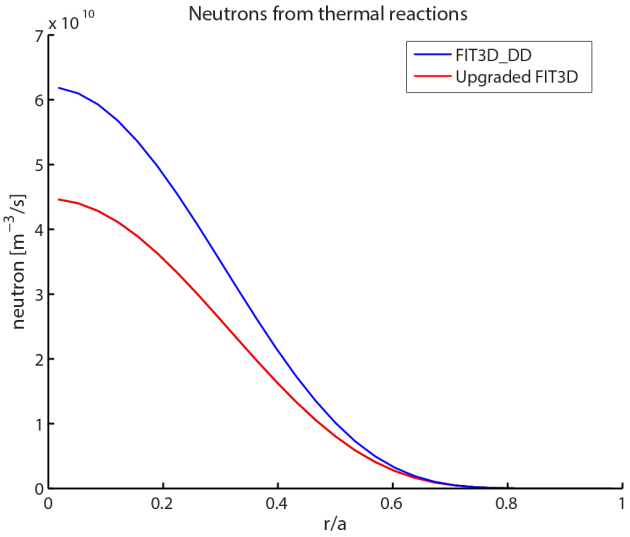

Figure 32.: Neutrons from D-D thermal fusion reactions for input case shown in figure 31. Two models are compared: ″Upgraded FIT3D″ and ″FIT3DD_DD″

tegral using fusion cross sections by Duane has an impact on the final result for thermal plasma reaction rate calculations.

BEAM-PLASMA FUSION REACTIONS Another source of fusion reactions is the interaction between energetic ions from NBI and background plasma. For medium to large sized fusion devices with D plasma heated by D NBI, this source is not negligible; in fact they can be the main contribution to the total fusion power. Reactions among fast D ions from the beams ("beam-beam" reactions) are not considered in this work. A first simplified approach to include beam-plasma reactions in the model has been used, trying to simplify the reactivity calculation. This approximation does not take into account the background plasma temperature, and for this reason it has been called "cold plasma" approximation. In order to treat the beam-plasma source term, the idea is to follow the formalism described for thermal reactions, although including a more complex formulation since we cannot assume a Maxwellian distribution for fast ions (as it is instead for background plasma). The source term must include the deuterium density of the background plasma, the fast ion density and the reactivity term. Proton and neutron source terms become respectively:

- proton rate per volume:
  $S_{p,DD,thermal} = n_D(\rho,t)\langle n_b \sigma v\rangle_{D(d,p)T}(n,T,E_{NBI},P_b)$
- neutron rate per volume:
  $S_{n,DD,thermal} = n_D(\rho,t)\langle n_b \sigma v\rangle_{D(d,n)^3He}(n,T,E_{NBI},P_b)$

where in the formula the dependences of the various factors have been made explicit. P_b is the beam power density (Wm^{-3}), E_{NBI} is the NB energy (eV) and n_b is the fast ion density which has been included directly inside the integral of the reactivity. In order to write the reactivity integral, we start from the definition shown in equation 56, and we include the fast ion density. In this simplified approach, we neglect the thermal plasma velocity in the integral, and we consider only the beam velocity (v_b). Therefore the relative velocity becomes equal to the beam velocity v_b. This approximation is working as good as $E_{NBI} \gg$ plasma kinetic energy. The approximate reactivity becomes:

$$\langle \sigma v\rangle = \int f\left(\vec{v_b}\right)\vec{v_b}\,\sigma\left(\left|\vec{v_b}\right|\right)\mathrm{d}\vec{v_b} \tag{60}$$

For the fast ion velocity distribution function $f(\vec{v})$ we use the analytical formula described in Rome's work [20] in equation 4.17 of the paper:

$$f(v,\xi,t) = U\left[t - \frac{\tau_s}{3}\ln\left(\frac{v_0^3+v_c^3}{v^3+v_c^3}\right)\right]\frac{\tau_s}{2\pi\left(v^3+v_c^3\right)}\left[\frac{v_0^3+v_c^3}{v^3+v_c^3}\right]^{-\frac{\tau_s}{3\tau_{cx}}} \times \sum_{n=0}^{\infty}\left(n+\frac{1}{2}\right)P_n(\xi)P_n(\xi_0)\left[\frac{v_0^3+v_c^3}{v^3+v_c^3}\frac{v^3}{v_0^3}\right]^{m_i\cdot n(n+1)\,Z/6m_f[Z]} U(v_0-v) \tag{61}$$

where U is a step function, P_n are Legendre polynomials, ξ is the pitch angle (ξ_0 the initial pitch angle), τ_s is the slowing down time, v_0 is the initial beam particle velocity with energy E_{NBI}, $v_c = \sqrt{\frac{2E_c}{m_f}}$ is the critical velocity (see section 2.2 for definition of E_c), τ_{cx} is the charge exchange characteristic time and m_f the fast ion mass (please refer anyway to Rome's paper for further details [20]). In order to simplify the equation 61, the following approximations have been considered:

- APPROX. 1: neglect anisotropy in the velocity distribution, taking into account only the term n=0 in the summation ($P_0(x) = 1$), and considering that, being the Legendre polynomials an even function, n=1 term is zero for symmetry reasons (i.e. counting all the pitch angles). We therefore do not consider any dependence on pitch angle ξ.
- APPROX. 2: consider only a stationary solution ($t \gg \tau_s$), therefore we do not consider any dependence on time.
- APPROX. 3: do not consider background neutrals $\Rightarrow \tau_{cx} = \infty$ (background neutrals can be easily taken into account if neutral density is known).

In equation 62 the simplifications related to the discussed approximations are highlighted with different colours corresponding to the colour used above in the text.

$$f(v,\cancel{\xi},\cancel{t}) = U\left[t - \frac{\tau_s}{3}\ln\left(\frac{v_0^3+v_c^3}{v^3+v_c^3}\right)\right]\frac{\tau_s}{2\pi\left(v^3+v_c^3\right)}\left[\frac{v_0^3+v_c^3}{v^3+v_c^3}\right]^{-\frac{\tau_s}{3\tau_{cx}}} \times \sum_{n=0}^{\infty}\left(n+\frac{1}{2}\right)P_n(\xi)P_n(\xi_0)\left[\frac{v_0^3+v_c^3}{v^3+v_c^3}\frac{v^3}{v_0^3}\right]^{1/2}\frac{m_i\cdot n(n+1)Z}{6m_f[Z]}U(v_0-v) \tag{62}$$

The resulting approximation for stationary conditions, neglecting anisotropy and background neutrals depends only on fast ion velocity, and takes into account slowing down of fast ions depending on slowing down time τ_s. In case that neutral density n_0 is known, the charge exchange term can be included. After the simplifications, the velocity distribution functions results:

$$f(v) = \frac{\tau_S}{4\pi\left(v^3+v_c^3\right)}U(v_0-v) \tag{63}$$

This approximation is commonly used in fast NBI modelling tools. For instance it is used in the fast tokamak simulation tool METIS, which is described in section 4.3.2. If we want to consider in a simplified view also the beam density inside the reactivity integration, we can multiply the velocity distribution function by the number of beam particles (i.e. the beam particle source):

$$n_b f(v) = \frac{P_b}{eE_{NBI}}\frac{\tau_S}{4\pi\left(v^3+v_c^3\right)}U(v_0-v) \tag{64}$$

If we use equation 64, which depends on the absolute value of beam velocity, it is simpler to consider the velocity integration of the reactivity in spherical coordinates in order to simply integrate on scalar beam velocities. The Jacobian of this coordinate system transformation is $4\pi v^2 dv$ and the reactivity in spherical coordinates becomes:

$$\langle\sigma v\rangle = \int_{-\infty}^{+\infty} 4\pi v_b^2 f(v_b)\, v_b\, \sigma(v_b)\, dv_b \tag{65}$$

The integration interval is, in principle, $[-\infty, +\infty]$, but it is practically restricted from the thermal plasma velocity v_{th} (instead of v(t) since we consider only stationary solutions) to the velocity of beam particles with

energy E_{NBI} (because of $U(v_0 - v)$ in f(v)). Inserting equation 64 in the integral, we have:

$$\langle n_b \sigma v \rangle = \frac{P_b \tau_s}{e E_b} \int_{v_{th}}^{v_0} \frac{v^3}{\left(v^3 + v_c^3\right)} p_{cx} \sigma_{DD}\left(E_{CM}\right) dv, \quad p_{cx} = \left[\frac{v_0^3 + v_c^3}{v^3 + v_c^3}\right]^{-\frac{\tau_s}{3\tau_{cx}}} \tag{66}$$

where the integration is done in spherical coordinates on the scalar beam velocity v, and we have already multiplied by the fast ion density. p_{cx} is the term in the integral which represents the probability of having no charge exchange interaction between the fast ions during slowing down and a background neutral. This term, as said in the approximation explanations, can be put to 1 if background neutral density is neglected (i.e. $n_0 \sim 0$). Charge exchange characteristic time τ_{cx} is defined as $\tau_{cx} = \frac{1}{n_0 v_0 \sigma_{cx}(v_0)}$. Fusion cross section $\sigma_{DD}\left(E_{CM}\right)$ is taken from Bosch's paper [82] and it is a function of the energy available in the centre of mass:

$$E_{CM} = \frac{\mu v^2}{2}; \ \mu = \frac{m_f m_{pl}}{m_f + m_{pl}} \tag{67}$$

where m_f and m_{pl} are the fast ion mass and plasma ion mass respectively. Reference [82] gives $\sigma_{DD}\left(E_{CM}\right)$ fit for both branches of the D-D fusion reaction, and neutron/proton sources can be estimated.

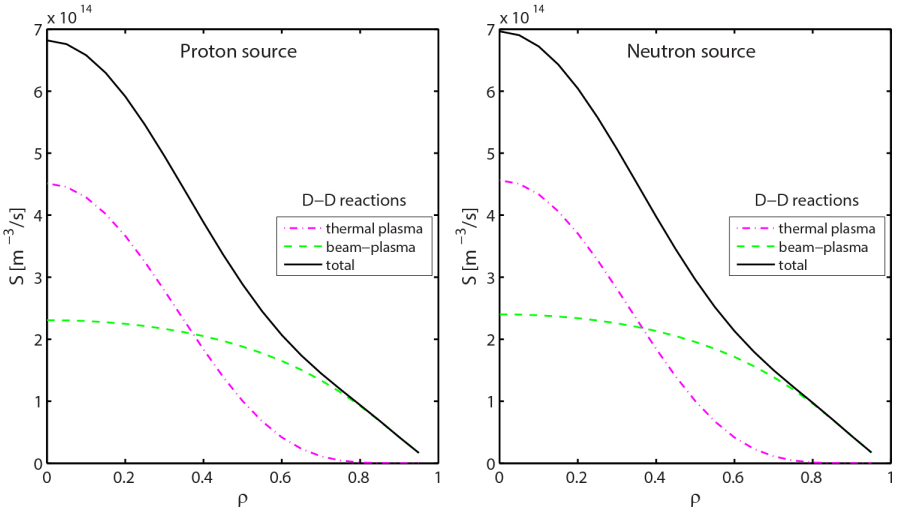

Figure 33.: Proton and neutron sources for $E_{NBI} = 100keV$ and $P_{NBI} = 10MW$, input n_e and T_i profiles are the same as those assumed for figure 30.

Some simple examples of the application of the models described above are now shown. Both thermal plasma and beam-plasma reactions are calculated, the first by the model described in "Thermal fusion reactions" paragraph. n_e and T_i profiles are the same as those assumed for figure 30. For beam-plasma interaction calculations, an injector of $E_{NBI} = 100keV$ and $P_{NBI} = 10MW$ has been considered, assuming an arbitrary uniform NB power deposition. In this case we are not running the complete FIT3D simulation, but only showing an application of the equations just described. For this reason, we do not have an actual power density profile (which depends on beam absorption), but we prescribe an arbitrary profile. The results are shown in figures 33 and 34. In this example plasma density and tempera-

ture are high enough ($T_{i,0} = 5keV$ and $n_{e,0} = 10^{20} m^{-3}$) to make the thermal plasma reactions relevant.

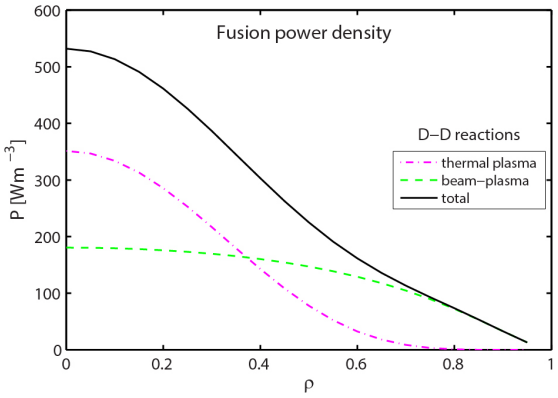

Figure 34.: Fusion power density for $E_{NBI} = 100keV$ and $P_{NBI} = 10MW$, input n_e and T_i profiles are the same as those assumed for figure 30.

The next example shown in figures 35 and 36 demonstrates that, in case of lower plasma density and temperature (values more relevant for LHD - except for the beam power profile shape which is arbitrary), thermal plasma reactions become almost negligible with respect to beam-plasma reactions. In this case, parabolic profiles of n_e and T_i are given as input with $n_{e,0} = 5 \cdot 10^{19} m^{-3}$ and $T_{i,0} = 5keV$. Same NBI parameters as for figures 33 and 34 are given as input.

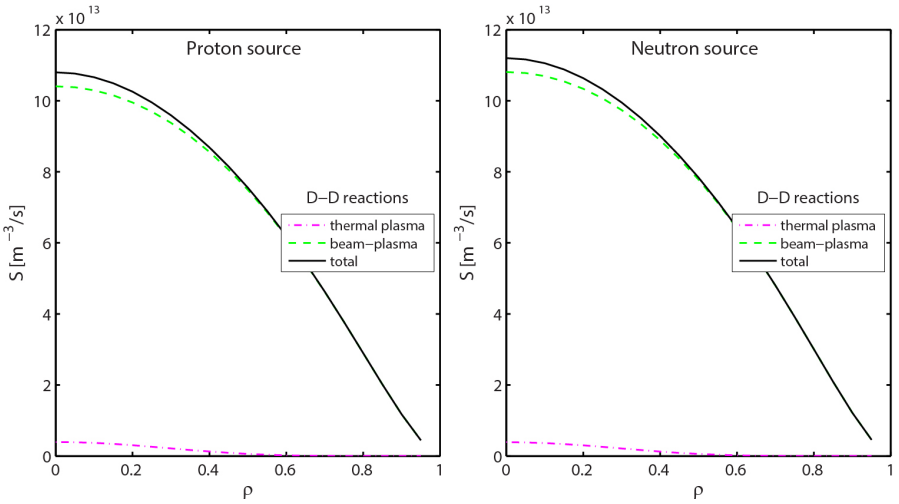

Figure 35.: Proton and neutron sources for $E_{NBI} = 100keV$ and $P_{NBI} = 10MW$ and input parabolic profiles of n_e and T_i with $n_{e,0} = 5 \cdot 10^{19} m^{-3}$ and $T_{i,0} = 5keV$.

In order to have a more accurate estimation of fusion reactions, a refined model for beam-plasma reaction calculations is now illustrated. In this case we take into account the background plasma temperature (i.e. the plasma velocity distribution function), and therefore this model is here called "T effect" model. This amelioration has been possible thanks to the fruitful discussion with S. Murakami (Kyoto University), the author of the above-mentioned code named "FIT3D_DD" [84].

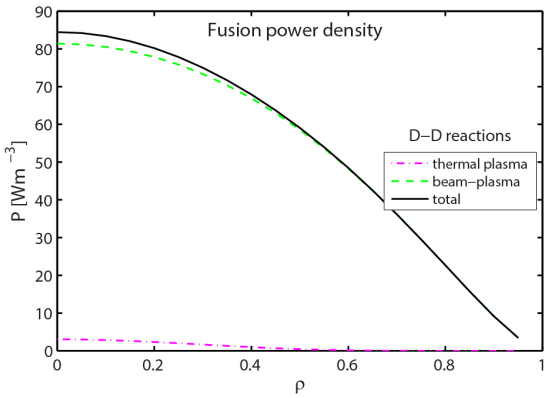

Figure 36.: Fusion power density for $E_{NBI} = 100keV$ and $P_{NBI} = 10MW$ and input parabolic profiles of n_e and T_i with $n_{e,0} = 5 \cdot 10^{19} m^{-3}$ and $T_{i,0} = 5keV$.

The model used in FIT3D_DD, and here recalled for beam-plasma reactions, supposes an isotropic distribution of plasma velocities in the Cartesian space. For convenience, we set a Cartesian reference frame aligned with the beam injection, i.e. we set the z axis parallel to the beam velocity, so that the beam velocity is $\overrightarrow{v_b} = (0, 0, v_b)$. This eases the form of the relative plasma-beam velocity, which can be now written as $\overrightarrow{v_{rel}} = \overrightarrow{v_{pl}} - \overrightarrow{v_b} = (v_{pl,x}, v_{pl,y}, v_{pl,z} - v_b)$. The fast ion velocity distribution function is still the one described in equation 63, while for plasma we assume a Maxwellian distribution function. The overall fusion reaction source (m^{-3}/s) becomes:

$$S_{DD,b-p} = \frac{P_b \tau_S}{E E_b} \int_{-\infty}^{+\infty} dv_{pl,x} \int_{-\infty}^{+\infty} dv_{pl,y} \int_{-\infty}^{+\infty} dv_{pl,z} n_D \left(\frac{m_{pl}}{2\pi KT}\right)^{3/2} e^{\frac{m_{pl}|\overrightarrow{v_{pl}}|^2}{2KT}} \times \int_{v_{th}}^{v_0} dv_b \frac{v_b^2}{(v_b^3 + v_c^3)} p_{cx} \sigma_{DD}(E_{CM}) |\overrightarrow{v_{rel}}| \tag{68}$$

where the integration in v_b variable is done in spherical coordinates (the Jacobian is $4\pi v_b^2 dv_b$). Deuterium plasma density and fast ion density are included in the integral. Bosch's formula [82] for σ_{DD} is used. A comparison between the two beam-plasma interaction models here presented ("cold plasma" and "T effect") is now presented. For completeness, the results of FIT3D_DD routine are also shown in order to have a benchmark with the original routine FIT3D_DD developed by S. Murakami. The compared beam-plasma reaction models are:

1. zero plasma temperature approximation ("cold plasma" approx.)
2. finite plasma temperature model ("T effect" approx.)
3. FIT3D_DD code

Table 5 summarizes the different models for beam-plasma reactions which are now compared.

A comparison among the three models summarized in table 5 has been done directly running three different FIT3D versions, one per each model described in the table. The same input files (containing all information needed

Model	Beam-plasma reaction calculation
Cold Plasma	neglecting background plasma temperature, σ_{DD} by Bosch [82]
T Effect	convolution of plasma Maxw. and fast ion distributions, σ_{DD} by Bosch [82]
FIT3D_DD	convolution of plasma Maxw. and fast ion distributions, σ_{DD} by Duane [85]

Table 5.: Summary of the compared models.

e.g. E_{NBI}, P_{NBI}, n, T profiles etc.) have been used for the comparison. The input n_e and T_i profiles are shown in figure 31. Fusion reactions from beam-plasma interactions are shown in figures 37 and 38 for 2 different LHD beam lines (co2 and pb4 lines).

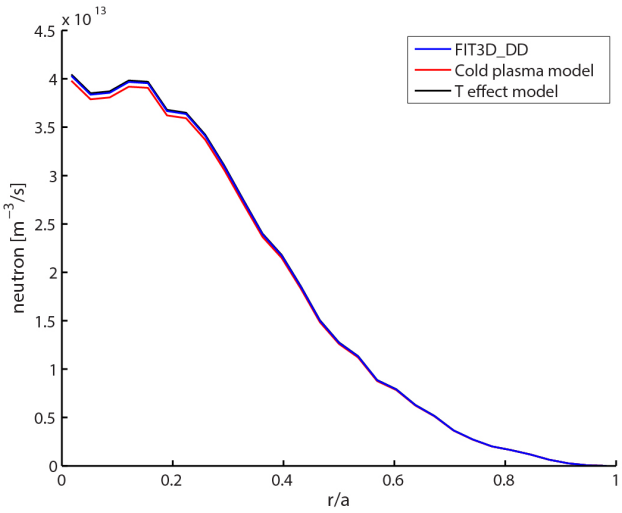

Figure 37.: Neutrons from interaction between D plasma and LHD D NBI co2 (E_{NBI}=180keV). Inputs shown in figure 31.

The three models are in agreement, although "cold plasma" model seems to have slightly lower neutron rate estimation, especially for 40 keV beam line. This inaccuracy can be explained since in this case the beam energy is closer to plasma thermal energy and therefore neglecting thermal plasma energy in the integration has a stronger impact on the final results. Anyway models with time-consuming integrations on plasma velocity ("FIT3D_DD" and "T effect model") exhibit a dependence on the precision of integral calculation: the integration interval and number of iterations to calculate the integral affects the precision and more tests to find the optimum trade-off between precision and computational effort have been suggested before the final implementation of the upgraded FIT3D in TASK3D-a.

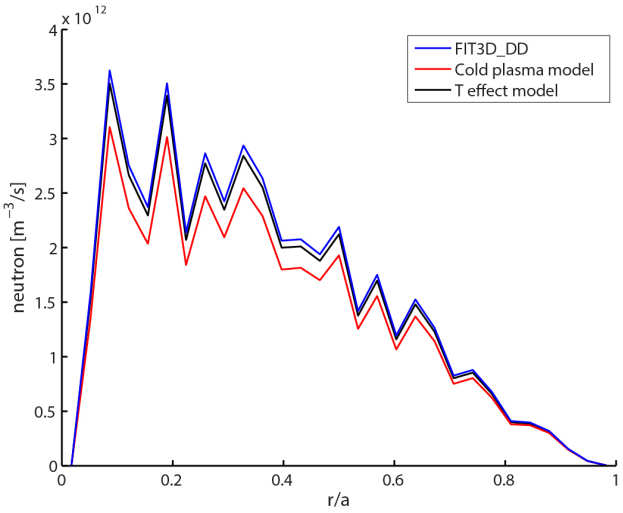

Figure 38.: Neutrons from interaction between D plasma and LHD D NBI pb4 (E_{NBI}=40keV). Inputs shown in figure 31.

Implementation of the discussed modifications in the FIT3D

In the previous section, a discussion on the physics models concerning beam ionization and fusion production estimation for FIT3D has been presented. The discussion focused on these topics since they have been identified as the critical parts of the code which had to be developed in order to enable the analyses of LHD D experiments. After a discussion, the suggested modifications have been presented to NIFS modelling group to be considered for the implementation in FIT3D code integrated in TASK3D-a. The final proposed upgrades for FIT3D code are here summarized:

- The update of beam ionization cross section fit from Janev [81] to Suzuki [54] formulation for a better estimation of beam stopping in case of LHD D NBIs and low energy H NBIs. This allows also to implement more elements for the calculation of the beam ionization due to impurities.
- Implementation of a routine to estimate neutron production and fusion power source from D-D reactions, both from thermal plasma and from beam-plasma reactions. With respect to the previously independently developed FIT3D_DD code, the upgraded FIT3D uses the more accurate and recent Bosch [82] formulas for fusion reaction cross sections. This permit also to calculate easily and rapidly the reactivity for thermal plasma contribution. Regarding beam-plasma reactions, the model "T effect" described above has been proposed for the implementation in the code.

In case of mixed H/D plasmas, or D (H) NBI in H (D) plasma, variables storing the information on beam/plasma composition have been implemented, in order to correctly calculate beam ionization and fusion production. The upgrades of FIT3D code have been presented during EPS conference in 2015 [87] and published in NIFS annual report [88]. A paper on the recent developments of TASK3D-a suite is being written for IAEA-Fusion Energy Conference (Oct. 2016, Kyoto, Japan), including the presented developments for FIT3D code.

3.2.4 Application of the upgraded FIT3D code to NBI-plasma interaction studies for similar H and He discharges

Upgraded FIT3D is capable to analyse H, D and T plasmas with multi-impurity species, calculating also neutron and fusion reaction production in case of D plasma. Since the implementation of the proposed upgrades is on the way, a stand-alone version of the upgraded code has been used for applications to LHD NBI-plasma interactions. In this section the effect of different plasma compositions on beam absorption in the plasma has been investigated with the newly developed code.

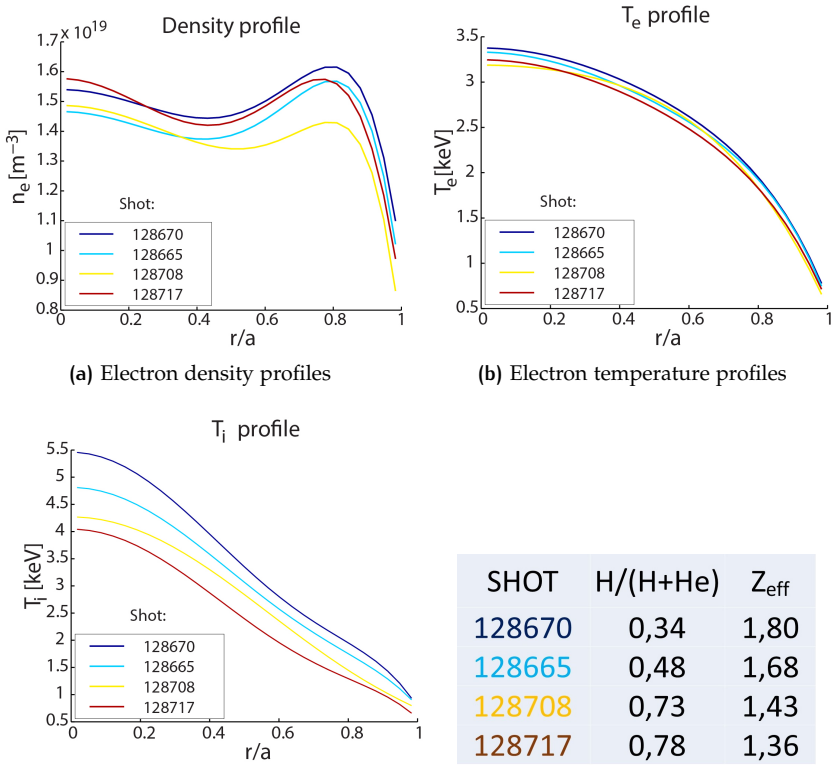

(a) Electron density profiles

(b) Electron temperature profiles

(c) Ion temperature profiles

SHOT	H/(H+He)	Z_{eff}
128670	0,34	1,80
128665	0,48	1,68
128708	0,73	1,43
128717	0,78	1,36

(d) H/(H+He) and Z_{eff}

Figure 39.: Experimental n_e, T_e and T_i profiles for similarity shots with different H/He concentrations, which are reported in figure 39d, together with the calculated Z_{eff} values assuming only H and He as plasma species.

In order to prepare the D campaign in LHD, studies on isotope effect are underway. In TEXT and ASDEX tokamaks, experiments were performed using helium plasma to clarify the origin of the isotope effect, since He discharges showed similar behaviours to D plasmas [89, 90]. For this reason, in the recent 18^{th} LHD experimental campaign, similarity experiments with different concentration of H and He where run, and better ion confinement with He majority was observed. The cause of this behaviour has been investigated during the last year, and first results have been presented in the last International Toki Conference ITC25 (Nov. 2015) [91–94]. An important point was to understand if NB heating (the dominant heating) was directly contributing to the observed better confinement properties with He majority in the plasma. In this work the upgraded FIT3D module has been used to perform stand-alone NBI-plasma interaction investigations for the steady-state analysis of the 4 similar H/He shots (128665, 128670, 128708, 128717)

at time 4.74s, when stationary conditions of the discharges allow a comparison. These shots are characterized by similar n_e and T_e profiles, while higher T_i has been observed with He majority. Fit of experimental data are shown for n_e, T_e and T_i profiles in figure 39. In figure 39d the corresponding value of $\frac{n_H}{(n_H+n_{He})}$ (from now on called H/(H+He)) is reported, together with the calculated Z_{eff} values assuming only H and He in the plasma. The measurement of H/(H+He) is deduced from spectroscopic measurements at the plasma periphery, and then assumed uniform in the whole plasma. Details on H/(H+He) measurement method can be found in [95]. It can be seen from figure 39 that density profiles are quite similar, while electron temperature profiles are almost identical. The above-mentioned better ion confinement with He majority can be seen from figure 39c: the central ion temperature increases of more than 30% passing from 22% to 66% of He concentration. In the analyses with FIT3D, NB power and energy have been read from the actual shot data. The energy of each NB line is almost equal in all the 4 shots at time 4.74s, while NB power is not always equal, especially for shot 128665 where NB line "ctr3" is switched off. Figure 40 shows the NB energy for each line in the 4 analysed shots, while figure 41 shows the NB power for each line and the total NB power.

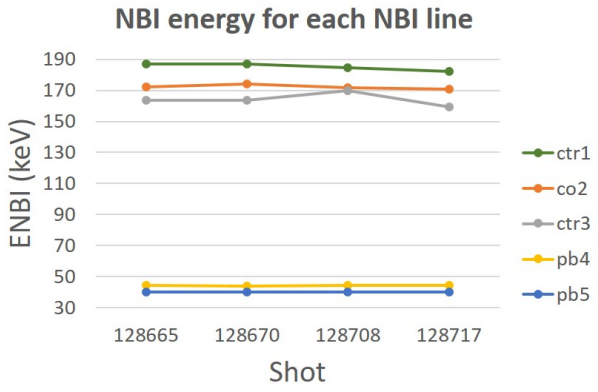

Figure 40.: NB energy for each line in the 4 analysed shots at time 4.74s.

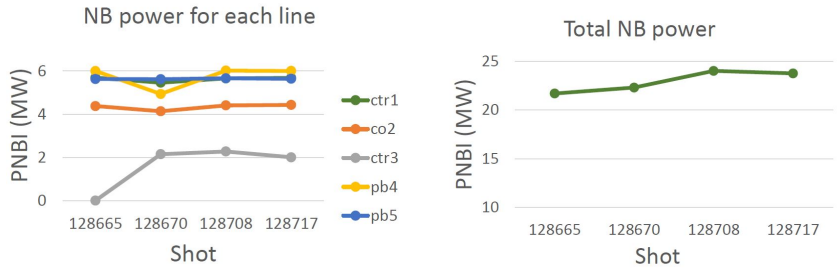

(a) NB power for each line

(b) NB total power

Figure 41.: NB power for each of the 4 analysed shots.

The upgraded FIT3D code has been used stand-alone to analyse NBI-plasma interaction at time 4.74s, in steady state approximation, which means considering the injection of fast particles at time 4.74s and letting the fast ion thermalize. The code takes as input the profiles of n_e and T_e shown in figure 39 and NB energy and power as in figures 40 and 41a. The only species

considered are H and He, since the profile density of C impurity, which is the prevailing impurity, was not available. Anyway, a simulation with an assumed C density profile starting from edge C density measurements has been run, showing no differences with the case with only H and He. For this reason we neglected C presence. Z_{eff} values of figure 39d are given as input. The analysis has been divided in two parts: first the investigation of the beam ionization (ion birth profiles), then the comparison of the fast ion confinement (slowing down process).

In order to understand the beam ionization with different plasma composition, the ion birth profiles have been compared for each beam line, and results for 2 representative beam lines are shown in figure 42.

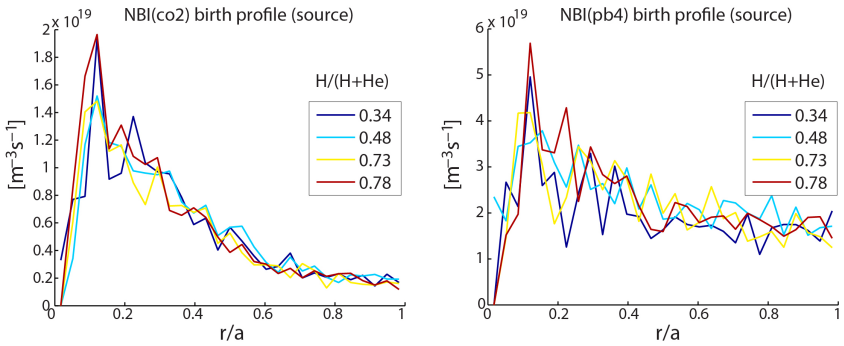

(a) Birth profile of NB line "co2"

(b) Birth profile of NB line "pb4"

Figure 42.: Ion birth profiles of a tangential ("co2") and a perpendicular ("pb4") NB line.

From this analysis it seems clear that in these discharges (considering that the 4 shots have similar but not identical parameters) the beam ionization is not affected by the different plasma composition. This behaviour can be explained from Suzuki's work [54] on beam stopping cross sections: he showed that different plasma composition is not affecting much the beam ionization (see e.g. the similar coefficients for his cross section fit in case of different background plasmas). It must be taken into account, that the NB injection remains in H for all the 4 shots. H. Yamaguchi analysed the NBI-plasma interaction in ideal LHD plasmas with different impurities in [96]: from his analysis on birth rate with different Z_{eff} values in a H/He plasma, it is confirmed that passing from $Z_{eff} = 1.36$ to $Z_{eff} = 1.80$ the difference in ion birth rate is very little ($\lesssim 10\%$).

Fast ion density of newly born ions has been evolved to reach a stationary solution valid for times greater than the slowing down time of fast ions. With this analysis we can understand if the fast ion confinement during the slowing down process is different in the 4 analysed shots. The final NB power deposition for NB lines "co2" (tangential NBI) and "pb4" (perpendicular NBI) is shown in figure 43.

The NB power density results similar for all 4 shots and all beam lines, meaning that in the 4 analysed shots there are no relevant differences in the power deposition from NBI. Also summing the contribution of all the beam lines, we cannot see any dependence on H/He ratio, as it is shown in figure 44.

In figure 44 it is important to remember that the total power injected at time 4.74s is a bit different among the 4 shots. This complicates any conclusion on general behaviour of fast ions with different plasma composition,

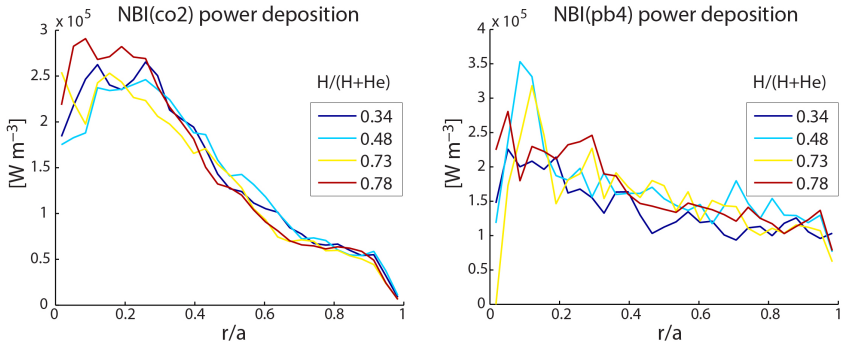

(a) Power deposition for NB line "co2" **(b)** Power deposition for NB line "pb4"

Figure 43.: Power deposition for a tangential ("co2") and a perpendicular ("pb4") NB line.

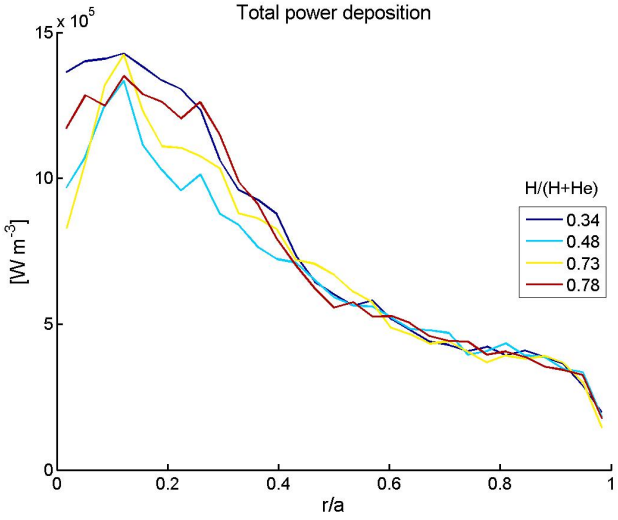

Figure 44.: Total NB power deposition from all NB lines in the 4 analysed shots at time 4.74s.

but can certainly help in the analysis of these shots concluding that no clear differences of NB heat deposition have been observed.

In order to gain some clarification on the effect of plasma composition on the NB absorption, the volume integrated NB power coupled to the plasma has been calculated, and it has been divided by the injected power. The resulting normalized absorbed power is plotted in figure 45, both for each beam line and the total one summing on all the NB lines. In this way the effect of the different injected NB power values in the 4 shots is cancelled out. From this figure, we can see that there is a slight dependence on H/He ratio: the normalized power coupled to the plasma slightly increases with He concentration. A last analysis has been performed to compare the theoretical fast ion confinement with different H/He concentrations. Using the physics model of FIT3D, the fast ion stopping time (corresponding to the time spent in the slowing process to completely thermalize) has been calculated including the different plasma compositions of the 4 shots. Figure 46 shows the prediction of the fast ion stopping time for the 4 shots.

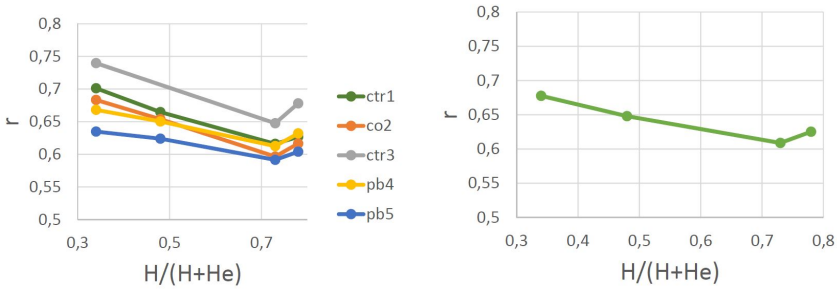

(a) Ratio $P_{coupl.}/P_{inj.}$ for each NB line.

(b) Ratio $P_{coupl.}/P_{inj.}$ summing on all NB lines.

Figure 45.: Ratio between volume integrated NB power coupled to plasma and injected NB power.

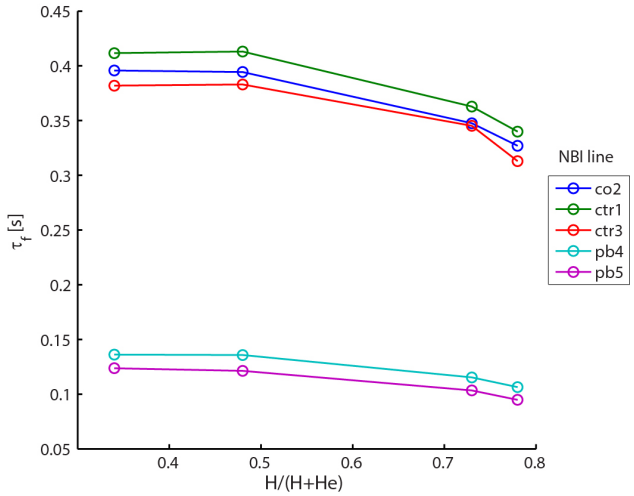

Figure 46.: Fast ion stopping time at $r/a \approx 0$.

The fast ion stopping time decreases with the increase of H concentration, and this behaviour is more pronounced for the 3 high energy tangential beams. Anyway, the different thermalization times have not a clear effect on NB heat deposition in these 4 shots as described above. It can be concluded that although some indication of better NB absorption and longer thermalization time with He majority, the 4 shots have similar NB power deposition profiles, and therefore the observed increased ion temperature is not due to different NB heat deposition. With these results, it is possible to make a comparison with JET isotope studies, assuming that D plasmas can be equated with He plasmas. In figure 20b of subsection 3.1.4 we can note that assuming equal kinetic profiles (as is it the case here for LHD similarity shots) the NB power deposition is similar for H and D cases, as it is similar here for H and He cases. For JET studies, we have seen that in H case the expected shine through losses are larger than in D case (figure 22). Similarly, for LHD we have some indication of better coupling and consequent NB absorption with He instead of H, although the difference is less pronounced (figure 45). It seems that some NBI isotope effects observed for tokamaks are seen also for LHD device, although further studies are needed before drawing any conclusion.

A hypothesis to explain the better ion confinement with He majority in LHD similarity experiments has been proposed by S. Maeta and S. Murakami and presented at the last Toki Conference [94]: this behaviour seems not to be due to the change of heat deposition and neoclassical transport, but it seems due to a different turbulent transport. A modified turbulent transport code tuned on these H/He experiments have then been used to predict the performances expected in D LHD experiments [93]. The work presented in this section, which includes the analysis of NBI-plasma interaction in the 4 similar shots with different H/He concentration, has been presented in [92].

4 INTEGRATED NBI-PLASMA SIMULATIONS

In this chapter the NBI is modelled within complex scenario simulations, where the plasma is consistently evolved taking into account all particle, current and energy sources/sinks in a dynamic transport simulation. If in the previous chapter the focus has been on detailed NB studies, the focus is here on the scenario performances and the role of NBI in plasma evolution. The work here presented consists of DEMO simulations carried out within the EU DEMO group. Since the aim is to investigate an unknown scenario, fully predictive simulations are run. The presented work on integrated DEMO simulations followed a first part on stand-alone NBI-plasma interaction studies previously carried-out within PPPT WP-PMI activities [97]. In that work the NB power deposition and driven current profiles have been studied for different injection geometries in stationary conditions of DEMO1 flattop phase, with an assessment of current drive efficiency by the NBI Monte Carlo code SPOT [98] coupled to NEMO [99] and RISK of the CRONOS transport suite of codes [100]. The following work carried out and here presented focused therefore on scenario simulations, integrating and evolving the work already performed. NBI role has been investigated in the last 3 years for DEMO pulsed and steady-state scenarios, both in stationary and transient phases. It has also been compared to other heating systems, in order to have a complete overview of the possible heating mixes.

This chapter is organized as follows. An introduction on EU DEMO studies is presented in section 4.1, while section 4.2 describes fusion power plant and DEMO studies outside Europe. One of the activity carried on from EU DEMO group is scenario modelling, which is described in section 4.3. Various EU DEMO designs have been released in the last 3 years and are illustrated in subsection 4.3.1. The work performed within EU DEMO scenario modelling group is described in subsection 4.3.2, where first of all simulation tools used are presented. The investigations performed on DEMO scenarios are divided in flattop studies (subsection 4.3.3) and transient phase studies (including ramp-up and ramp-down, subsection 4.3.4). A summary of the work completed, and a discussion on the role of NBI in DEMO scenarios is finally given in subsection 4.3.5.

4.1 EU DEMO STUDIES

Fusion research in Europe is undoubtedly reactor oriented, as it is clearly stated in the document "Fusion Electricity-A roadmap to the realisation of fusion energy" from EFDA, dated 2012 [101]. The last step foreseen before the commercial exploitation of fusion power plants is DEMO, which is meant to be a basis for the extrapolation to a commercial reactor, and which will follow the construction and operation of ITER. This strategy foresees a single step (DEMO) between ITER and a fusion power plant. DEMO must demonstrate the viability of fusion as an energy source. DEMO final mission is to:

1. Demonstrate reliable plasma operation

2. Demonstrate full power operation for several years (and tritium self-sufficiency)
3. Demonstrate conversion of heat into electricity
4. Minimize activation waste, no long-term storage
5. Obtain license for construction and operation from nuclear authority
6. Allow extrapolation of DEMO solutions to a fusion power plant

Top requirements for EU DEMO studies are safety, environmental sustainability and high plant performances. In parallel, the proposed concept must be assessed in terms of the economic viability. DEMO must be not only self-sufficient in tritium breeding, but also produce enough tritium to provide adequate back-up storage to compensate the natural decay in case of unforeseen long shut-down periods and to provide tritium for the start-up of another fusion power plant. Tritium availability could be in fact an issue, especially in case of the construction of D-T fusion test facilities not tritium self-sufficient (e.g. ITER simultaneously with other D-T facilities). The development of a conceptual design for DEMO is one of the main priorities in the coming years as reported in the European fusion roadmap. DEMO studies are now in the pre-conceptual phase and they have already started in parallel with ITER construction. After the present pre-conceptual design phase, the plan foresees a conceptual design activity (~7 years), an engineering design activity (~11 years), the site preparation and construction (~10 years) and finally the commissioning phase (~5 years). According to EFDA document, in order to achieve the goal of fusion electricity production by 2050, DEMO should be built in 2030s and operated in 2040s, although due to the delays of ITER, the present schedule will be likely delayed. The design and construction of DEMO will indeed benefit from the realization and operation of ITER, and from all the other facilities (e.g. IFMIF) and dedicated studies carried out in parallel. Differently to ITER which is still an experiment, the philosophy of the European DEMO is to have a prototype reactor, i.e. a robust and reliable machine with a reduced set of diagnostics working in an established scenario to produce a large amount of electric power (~hundreds of MW). A close interaction with industries is essential for the design of DEMO, and this is clearly stated in the EFDA document. An artistic view of a fusion power plant is shown in figure 47.

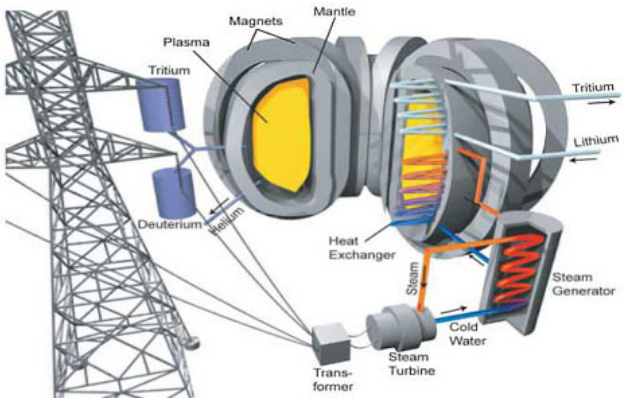

Figure 47.: Artistic view of a fusion power plant from http://fusionforenergy.europa.eu/understandingfusion/demo.aspx.

DEMO studies in Europe have been carried on starting from early 1990s, in parallel with US, Japanese and Russian fusion communities. A first program towards a fusion reactor was published in 1991 [102]. Under EFDA, Power Plant Physics and Technology (PPPT) department studies started in early 2000s with the "Power Plant Conceptual Study" (PPCS) which had the overall objectives of assessing the fusion energy status and establishing coherence and priorities in the EU fusion programme. Within these studies, 5 plant models were developed, all steady-state tokamaks with different levels of extrapolation from the physics and technology knowledge at that time (from near term solutions to more advanced models, respectively PPCS A, B, AB, C and D). Figure 48 shows sizes and plasma shapes of the 5 different PPCS concepts. A summary of PPCS concepts is reported in [103] while an

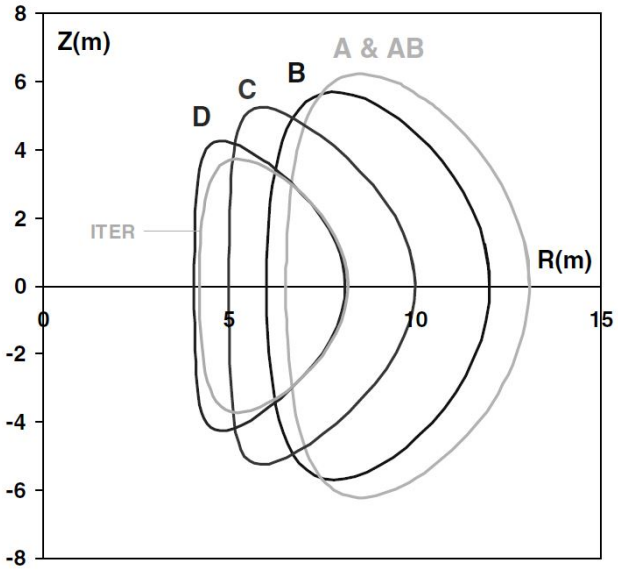

Figure 48.: Size and plasma shapes of the 5 PPCS concepts, compared to ITER from [103].

economic analysis of the proposed PPCS power plants is illustrated in [104].

Since 2011 EFDA first and EUROfusion then started a systematic revision of reactor studies within the Power Plant Physics and Technology (PPPT) department. Currently the PPPT activities are organized in work packages (WPs) and two reactor options are being investigated: a pulsed reactor named DEMO1 and a steady-state reactor named DEMO2. Since the goal is to realize and operate DEMO in the central part of this century, both DEMO1 and DEMO2 concepts are tokamaks, which at the moment seems to be the most advanced concept, although it is not a priori excluded a stellarator DEMO (currently a "backup option"). DEMO1 is a conservative near-term solution which employs the present physics and technology knowledge, or it requires at most "low extrapolation" from the current knowledge. DEMO1 is a H-mode baseline reactor concept, with most of the plasma current induced by the central solenoid. DEMO2 is an advanced tokamak, able to operate in steady-state conditions therefore relying on non-inductive currents for plasma sustainment. Safety factor profile (q) is mildly reversed thanks to bootstrap and non-inductive currents, and auxiliary heating systems are direct actuators for current profile shaping. At the moment advanced scenarios are being studied, and DEMO2 design is therefore based on moderately optimistic assumptions on future developments. The 2 design options are

in constant evolution, and being now in the pre-conceptual phase, they are often modified and updated. After discussions and proposals from all the groups working on EU DEMO, new designs of DEMO1 and DEMO2 are released, usually every ~1-2 years. The concepts are then again assessed and modified in an optimization cycle. An overview of DEMO R&D activities of the last years is presented in [105]. PPPT DEMO activities are organized in the following work packages (WPs):

- PMI-Plant Level System Engineering, Design Integration and Physics Integration
- MAG-Magnet System
- CS-Containment Structures
- BB-Breeding Blanket
- DIV-Divertor
- HCD-Heating and Current Drive Systems
- TFV-Tritium, Fuelling and Vacuum Systems
- BOP-Heat Transfer, Balance of Plant and Site
- DC-Diagnostics and Control
- RM-Remote Maintenance Systems
- MAT-Materials
- ENS-Early Neutron Source
- SAE-Safety and Environment

PPPT guidelines for EU DEMO envisages a power production from 300MW to 500MW of electricity and in case of a pulsed reactor (DEMO1), the discharge duration shall be $\gtrsim$ 2 hours. Physics knowledge for DEMO (DEMO Physics Basis) is being currently assessed within PPPT activities, having as reference the work done for ITER (ITER Physics Basis [106]). In a paper of 2013 [107], the status of the physics basis for DEMO has been analysed. On the basis of this work, the area where major progresses are needed is the power exhaust. This area is an example where there is a strong interlink between physics and technology, since power exhaust capabilities rely on material characteristics, but at the same time influences the operational scenario which has to rely on an unprecedented high level of radiation losses [108]. Other areas where progresses are needed are MHD stability, particle and energy balance and disruptions. Recent results on the progress made in the last years on these topics are reported in [109].

4.2 NOT ONLY EU DEMO: OTHER DEMO CONCEPTS

Other countries might decide to build a DEMO, and this would be beneficial, providing different ideas in a "healthy competition". Within the "Broader Approach" agreement between EU and Japan, some interaction for the realization of DEMO is foreseen [110]. However, even if the different DEMOs are not build exploiting international collaborations, the exchange

of scientific and technological information would be beneficial. In the international fusion community, various DEMO concepts have been proposed and many are currently under investigation, not only tokamaks but also stellarators and RFPs. DEMO and power plant concepts are driven from the different needs of the various countries. In countries as USA, Japan and Europe the electric supply needs are mainly for the replacement of the existing infrastructures, aiming at more sustainable and publicly accepted solutions. In other countries as China and India (and in some sense Russia and South Korea), the electric supply needs are to sustain the economic growth and usually the government actively follows policies to expand the energy supplies.

Sometimes there is a sort of confusion between the role of DEMO and a fusion power plant: in the European view the aim of DEMO is to demonstrate the technological and economic viability of fusion while the goal of a first fusion power plant is to sell energy in the market. DEMO is often meant to be the last step before the commercial exploitation of fusion reactors. Following, an overview of some of DEMO and fusion power plant concepts developed in the international fusion community is presented. An historic summary of reactor concepts until 2008 can be found in [111], where a timeline with the main reactor concepts is presented. The same timeline, but updated, is maintained by the University of Wisconsin-Madison and is reported in the appendix A: it can be observed that only EU, Japan, Korea and China are currently developing fusion reactor concepts.

ARIES STUDIES IN USA During the last 25 years, a broad study on fusion power plant has been carried out in USA within the ARIES program, giving birth to many reactor concepts (all the information are published in http://aries.ucsd.edu/ARIES/). The ARIES Program is a US multi-institutional research activity aiming to "perform advanced integrated design studies of the long-term fusion energy embodiments to identify key R&D directions and to provide visions for the fusion program". The ARIES designs tend to be very advanced since US reactor concepts aim to a competitive cost of electricity. Some of the various power plant concepts proposed by US ARIES group are: a reversed field pinch reactor (TITAN 1988), a D-^{3}He tokamak (ARIES III, 1991), a pulsed tokamak (PULSAR 1993), a reversed-shear tokamak (ARIES-RS 1996), a spherical torus tokamak (ARIES-ST 1999) , an "advanced technology" tokamak (ARIES-AT 2000) and finally a compact stellarator (ARIES-CS late 2000s). The solutions proposed aim to be economically competitive, and exploit high power density, high thermal conversion efficiency (using e.g. He at 550°C) and using less-expensive systems. Public acceptance has been guaranteed by excellent safety and environmental characteristics, achieved using low-activation and low toxicity materials. Particular care to reliability and availability resulted in the design of e.g. ARIES-RS which exhibited an ease maintenance. As mentioned in the list above, ARIES group considered all the main magnetic configurations (tokamak, stellarator, RFP). All the references to the above mentioned concepts and to ARIES group studies are linked at http://aries.ucsd.edu/ARIES/DOCS/bib.shtml. Recently a new reactor concept has been developed by MIT, named "ARC" reactor (affordable, robust compact reactor) [112]. ARC is expected to produce the same amount of power of ITER, at only half the size. It aims to reduce size, cost and complexity of fusion reactors. At the moment there are no plans to build any of these concepts.

REACTOR STUDIES IN JAPAN The Japanese fusion community was not organized in a comprehensive strategy for a unique fusion power plant, although a sort of roadmap illustrating the strategy towards a fusion power plant was released in 2005 (HP of the Atomic Energy Commission of Japan http://www.aec.go.jp/jicst/NC/senmon/kakuyugo2/siryo/kettei/houkoku051026_e/index.htm). It is possible to count 3 different Japanese lines for a DEMO concept: 2 tokamak DEMOs (as reported e.g. in [113]) and a stellarator DEMO. The 3 different studies were supported by different partners: "CREST" reactor by CRIEPI (Central Research Institute of Electric Power Industry) and some universities, "SSTR" concept later replaced by "CS-less" reactor by JAEA (Japan Atomic Energy Agency) and "FFHR" helical reactor by NIFS (National Institute of Fusion Science). All Japanese concepts tended to be fairly advanced (e.g. all steady-state reactors, including tokamak DEMOs), but the designs converged in the last years to more realistic technical solutions. This fact is due also to the interaction within the Broader Approach agreement with Europe (which is developing a near-term DEMO concept), and the different European and Japanese views are slowly merging. Similarly to Europe, Japanese fusion community is thinking to have only one step between ITER and a fusion power plant. CREST strategy by CRIEPI proposed a fast track to commercial fusion power, with a DEMO-CREST before the first fusion power plant CREST. The idea was to have a tokamak DEMO with similar performances of ITER, but with more reliable, optimized operations and higher efficiency [114]. Reactor studies at JAEA started in early 1990s, with the study of a steady-state tokamak reactor named SSTR [115]. This project was then replaced by the CS-less DEMO line, whose underlying idea is to minimize the cost of electricity with a compact tokamak. The aim of this project is to have a fusion power plant without the central solenoid (CS-less), preceded by a CS-slim DEMO. A summary of this strategy is reported in [116], and design progress and issues of a CS-slim DEMO are described in [117]. FFHR (Force Free Helical Reactor) is studied at NIFS, and since the great experience in heliotron devices gained with LHD facility, it is a helical DEMO concept. This concept has been investigated in parallel with the exploitation of LHD experiment, and it is currently being developed. The idea behind FFHR is to have a LHD-type fusion reactor, bigger in size with higher performances. Different options have been presented, and the work has been performed in different rounds, each of them providing more and more detailed insights of the reactor. Many papers describing the different investigations and design options for FFHR are available, and a recent overview of the proposed concept is reported in [118]. Early power plant concepts of Japanese and US fusion communities have been compared in 2005 by K. Tobita at the IEA/LT Workshop (W59) [119]. The comparison was done in terms of cost of electricity scaled to 1992 price basis. Figure 49, re-elaborated from the original presentation, shows the comparison of SSTR, CREST and two ARIES concepts. It is interesting to note not the absolute value of the cost of electricity (COE) but the relative values for COE of Japanese and US concepts, and also the comparison to the COE from fission and coal sources: ARIES-AT in particular showed a very low expected COE, in line with the US strategy of a very competitive COE. In the same presentation, a comparison of early Japanese, US and European fusion power plant concepts was performed in terms of aspect ratio and β_N parameter, and it is shown in figure 50a. From this figure it is possible to see that among conventional tokamak concepts PPCS reactors have the lowest aspect ratio, while CREST and ARIES-AT have the highest β_N. ARIES-ST has a very low aspect

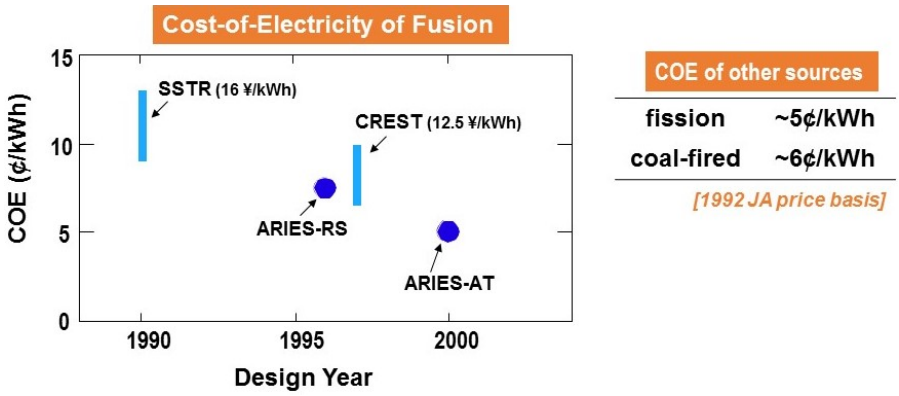

Figure 49.: Comparison of different Japanese and US early fusion power plant concepts in terms of electricity cost (COE), re-elaborated from [119].

ratio, being a spherical tokamak. It is interesting to note that the aspect ratio of the conventional tokamak reactors presented in the figure corresponds to the values considered in the ongoing studies for the EU DEMO. The fusion power divided by the reactor weight has been also compared for the different reactor concepts, including ITER as reference. Figure 50b shows how the CS-less Japanese concepts aim to reduce the reactor weight in order to make the solution more economical.

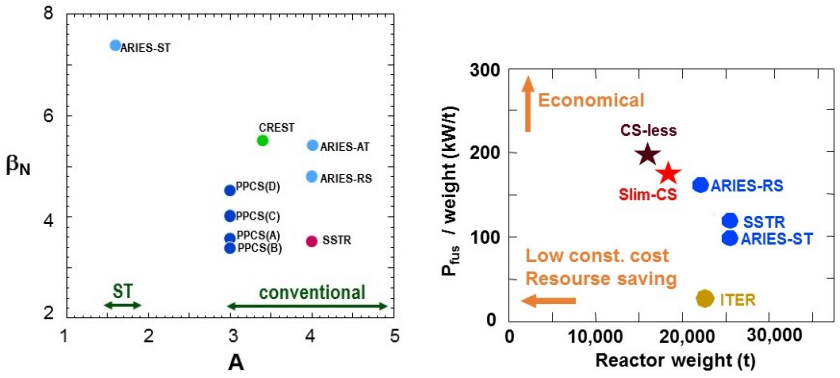

(a) Aspect ratio and β_N comparison

(b) Fusion power and reactor weight comparison

Figure 50.: Comparison among different reactor concepts done in 2005. Images re-elaborated from the original presentation [119].

FISSION–FUSION HYBRID REACTORS AND OTHER CONCEPTS IN CHINA Due to the rapid expansion of the Chinese economy in the last decade, the first reactor studies in the Chinese fusion community were driven by the more and more impelling need of energy. For this reason, the main trend in China was to have an early production of fusion energy, and one of the first proposed concepts (2002) was a fission-fusion hybrid reactor named Fusion Experimental Breeder (FEB) [120]. In 2006, 4 different reactor concepts were presented in "FDS series", a Chinese fusion power plants study [121]. The aim of FDS studies was "the examination of the feasibility and the safety, environmental and economical potential of fusion with emphasizing the blanket design optimization on neutronics, thermal-hydraulics, electro-magnetics, material, structural performance analyses" (from the original paper [121]).

One of the options recalls the hybrid fission-fusion concept and it is named FDS-EM. It consists of a fusion plasma core with fission blanket [122]. In the following years China developed a strategy to achieve fusion power plants, and a roadmap was presented in 2008 [123]. China focused more and more on "pure" fusion power plants. In that years, at SWIP (Southwestern Institute of Physics, Chengdu) another DEMO concept called HCSB-DEMO was developed. Its aim is to produce a fusion power of 2550MW, with a He-cooled blanket system [124]. Recently a new Chinese study proposed an intermediate fusion reactor named CFETR (China Fusion Engineering Test Reactor), which is meant to be a step between ITER and DEMO, since there is the belief that many fundamental aspects of DEMO design may not be clarified only by ITER exploitation. This concept which should be built in parallel or just after ITER is a tokamak device producing 50-200MW, and it includes a blanket, which would guarantee also the tritium supply thanks to a breeding ratio of at least 1.2. The description of this device can be found in [125]. A preliminary cost assessment of CFETR is reported in [126].

K-DEMO: THE KOREAN REACTOR In the recent years South Korea developed a strategy to achieve fusion energy production after ITER exploitation [127]. This step was strongly supported by the government who established a special law to support fusion research (fusion energy development promotion law -FEDPL- 2007). In 2013 South Korea proposed a preliminary conceptual design for a steady-state tokamak named K-DEMO [128]; the conceptual design has been finalized in 2015 and presented in [129]. K-DEMO has a near-term development plan, which is divided in 2 stages: the first will demonstrate a net electricity production, but at the same time acting as a test facility, the second, after a major upgrade replacing in-vessel components, will demonstrate the production of hundreds of MW of electric power at a competitive cost of electricity. Figure 51 compares the two stages of K-DEMO with other reactor concepts and ITER.

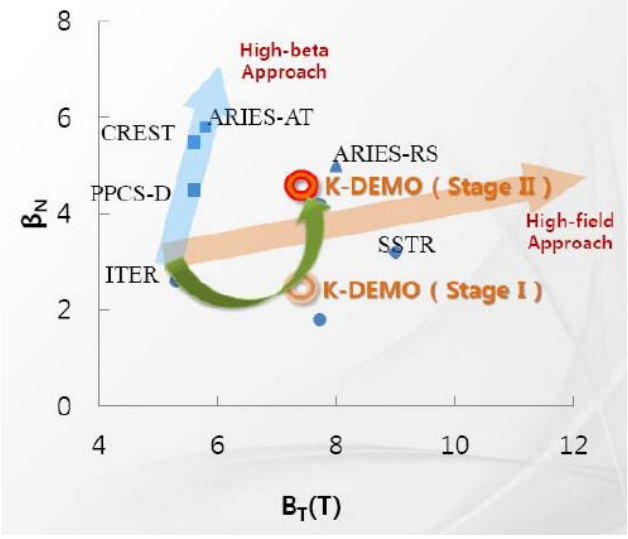

Figure 51.: Comparison of the two stages of K-DEMO with other reactor concepts and ITER (courtesy of G.S. Lee).

HISTORICAL DEMO STUDIES IN RUSSIA AND RECENT HYBRID CONCEPT Studies on a Russian DEMO machine started in 1991, almost in parallel with the

first studies on fusion power plants carried out in the international fusion community. A first overview of Russian DEMO concepts was presented in 1995 [130]. Two tokamak concepts were described: a pulsed reactor (DEMO-P) and a steady-state reactor (DEMO-S). In the following years, the main efforts were concentrated to the steady-state concept DEMO-S which was designed to operate in an advanced scenario with high bootstrap current. The concept was very advanced considering that it was presented in 1998: it operated with open liquid lithium as plasma facing material, allowing heat fluxes from 100 to 150 MW m^{-2} [131]. In this case, "DEMO" meant already a fusion power plant and not a intermediate step. Later, DEMO-S study was refined, and a conceptual study was presented in 2000 [132]. In 2008 an overview of DEMO-S concept with the last progresses was published, with particular care on the blanket choice and on radioactive waste management [133]. In the last years, a roadmap to build a pilot hybrid power plant (PHP) exploiting fission-fusion concept has been proposed. A key milestone to achieve the construction of PHP is the realization by 2023 of DEMO-FNS tokamak for fusion and hybrid technologies studies, whose conceptual design is ongoing [134, 135]. The tokamak is expected to produces some tens of MW of fusion power, with Q~1.

DEMO 2-STEP PROJECT IN INDIA India at the moment does not have a fully developed DEMO or fusion power plant project, although some preliminary studies have been carried out. In India a national fusion program started in late 2008 and it pushed the development of a strategy to achieve fusion energy production. The Indian idea is to have an intermediate test facility before DEMO. SST-2 would be in fact an intermediate size superconducting tokamak, capable of steady-state operation with modest fusion power. This project shall be followed by an Indian DEMO machine, bigger and with higher fusion energy production. Details on the Indian project can be found in [136].

EXOTIC D-^{3}HE REACTORS An attractive reactor concept foresees the use of D-^3He as fuel, since it has the advantage of avoiding the production of neutrons in fusion reactions and of working at very high β. The exploited reaction would be $D +^3 He \rightarrow^4 He + p$, which produces only charged particles. The drawback is the necessity of having a very hot plasma, in the order of hundred keV. Before bumping into the reality of technology and material limitations clearly appeared in the ITER era, a number of studies proposing D-^3He reactors appeared in scientific literature. In 1991 "RUBY" reactor was proposed from a collaboration among USA, Japan and Austria [137]. The objective was to update the previous concept called "SAFFIRE", appeared in 1978 [138]. These concepts relied on field reversed configuration (FRC), a kind of theta pinch exploiting mirror coils. The plasma of RUBY has an ion temperature of 100 keV, and the average $\beta(\%)$ is close to 90. The concept was designed to generate electricity directly from the charged particle component coming from fusion reactions. Almost in parallel, a similar field reversed reactor "ARTEMIS" (1992 [139]) was proposed from NIFS Japanese institute. In the same years two D-^3He tokamak reactors were proposed in US: "ARIES-III" from the US ARIES group (1991 [140]) and "APOLLO" (1992 [141]). An issue highlighted in these works is the very high synchrotron radiation produced in these concepts. Plasma current achieves values much higher than current D-T concepts, up to 53MA (APOLLO). Last in order of appearance is the D-^3He reactor proposed by F.

Romanelli and G. Giruzzi in 1998 (at the time at ENEA-Frascati). They proposed a working scenario with an edge radiating layer in order to avoid too high power loads to plasma facing components [142]. These concepts were almost completely abandoned in 2000s, because of the demanding conditions required to ignite D-^{3}He reactors. The (un-)feasibility of using D-^{3}He as fuel in a fusion reactor with the present physics and technology knowledge is discussed in [143].

4.3 EU DEMO SCENARIO MODELLING

Within European DEMO studies described in section 4.1, PPPT WP-PMI effort on DEMO scenario modelling is a crucial activity which is beneficial for two aspects: it firstly validates with physics based models the proposed pre-conceptual designs and secondly it proposes updates and modifications for the next engineering design release. This optimization cycle is performed in collaboration with the group working on plant level system engineering, who takes inputs from all PPPT groups to elaborate an optimized reactor design. The engineering design is prepared by the system engineering group using the system code PROCESS [144]. This code assesses the engineering and economic viability of a proposed fusion power station, by means of simple models of all parts of the reactor. PROCESS combines 0-D plasma description and technology constraints performing an automatic search for an optimum working point. Due to the basic physics assumptions of the code, PROCESS concepts must then be validated by scenario modelling, which includes more sophisticated physics codes. Figure 52 shows the DEMO concept optimization cycle. As mentioned before, new DEMO

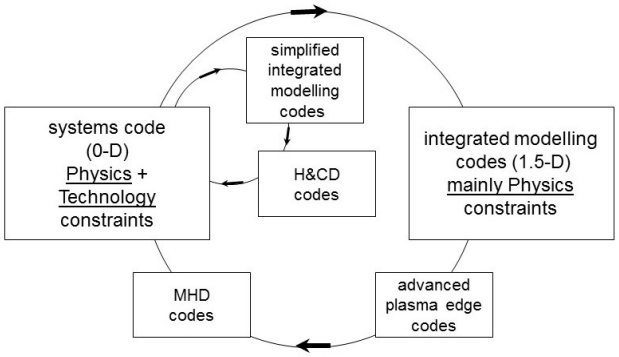

Figure 52.: Optimization cycle for DEMO concept design in PPPT activities, from [145].

designs have been often released in the last years as a consequence of the collaborative effort of all PPPT groups. A summary of the modelling activities of PPPT regarding DEMO 2013 version has been recently published in [146]. Scenario modelling group uses a variety of simulation codes, depending on the modelling needs (see [146]). Usual areas investigated are plasma MHD stability and control, coil limits, core and edge transport properties, pedestal physics, fuelling, impurities and radiation, heating and current drive, bootstrap currents, transient phases etc.

The modelling activity here presented concerns mainly integrated scenario simulations with dominant NBI and comparison with other heating systems. The next subsections are organized as follows. First the different

DEMO design options analysed in the presented work are described in section 4.3.1. After this, DEMO scenario modelling activities carried out are introduced in section 4.3.2, and the modelling codes used are described in section 4.3.2. Flattop studies are presented in section 4.3.3. The work is split in 2 parts: one for pulsed DEMO1 concept and one for steady-state DEMO2 concept. Finally the work on transient phases (plasma ramp-up and ramp-down) is presented in section 4.3.4. The work done is always divided by the DEMO release analysed: during the 3 years' activity 2012, 2013 and 2015 releases have been investigated.

4.3.1 DEMO designs analysed: 2012, 2013 and 2015 releases

EU DEMO tokamak concept is organized as shown in figure 53. Starting from the interior to the exterior, DEMO is composed by the magnet coil for induction of the plasma current, main field coils for toroidal magnetic field, plasma vessel, blanket, divertor, auxiliary coils for control magnetic field, cryostat and finally neutron shielding. The engineering design of DEMO is

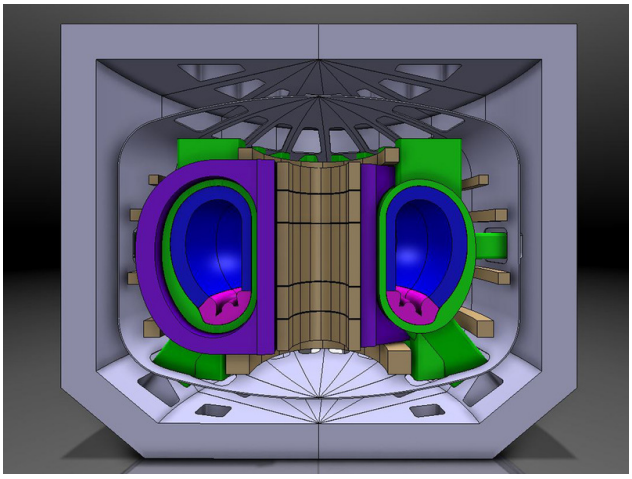

Figure 53.: Sketch of a tokamak demonstration power plant. From the interior to the exterior: magnet coil for induction of the plasma current (brown), main field coils (lilac), plasma vessel (green), blanket (blue), divertor (magenta), auxiliary coils (brown), cryostat (grey), shielding (grey), ©EFDA from https://www.ipp.mpg.de/16427/stand.

optimized by means of PROCESS code (see section 4.3), which gives as output the main "optimum" reactor parameters for given constraints. DEMO design options vary during the years, following an "evolution" process in which the various DEMO groups tries to find a convergence on an optimized DEMO concept. Figure 54 shows the main PROCESS parameters of DEMO designs from 2012 to 2015, corresponding to the concepts investigated in sections 4.3.3 and 4.3.4. Regarding DEMO1 concepts, during the last years the major radius has been kept almost constant, while minor radius a has increased. This affected the plasma volume, which has in the last version considerably increased. The decision to decrease the aspect ratio A to the last value 3.1 has been taken for various reasons. First of all, in the engineering design, while considering a high number of constraints, the aspect ratio still had some degree of freedom. Therefore an aspect ratio sensitivity study for values A=2.6, 3.1 and 3.6 has been carried out, highlighting advantages

Main parameters	DEMO1			DEMO2		
	2012	2013	2015	2012	2013	2015
R_0 (m)	9	9,25	9,07	8,5	8,15	7,5
a (m)	2,25	2,64	2,93	2,83	2,98	2,885
A	4	3,5	3,1	3	2,73	2,6
Elongation	1,66	1,52	1,59	1,65	1,61	1,8
Triangularity	0,33	0,33	0,33	0,33	0,33	0,33
Plasma vol. (m^3)	1527	2009	2502	2275	2363	2217
I_p (MA)	16	18,56	19,6	19	19,85	21,63
B_T (T)	7,1	6,8	5,7	4,7	5	5,6
H	1	1,1	1,1	1,3	1,3	1,4
Z_{eff}	1,98	2,82	2,6	3,23	3,28	4,7
P_{aux} (MW)	50	50	50	122	135	133
β_N %	2,4	2,47	2,59	3,7	3,4	3,8
$<n_e>$ (10^{19} m^{-3})	8,5	9,1	8	6,4	7,7	8,7
$<T_e>$ (keV)	12,8	14	13,1	16,3	15,5	18
P_{fus} (MW)	1943	2119	2037	1819	2104	3225
Burn time (h)	2,44	1,9	2	∞	∞	∞
COE ($/MWh)	276,43	210,98	355,8	244,92	212,85	128,1

Figure 54.: PROCESS parameters for DEMO designs from 2012 to 2015.

and disadvantages of the various options. Comparing the options, the result was:

- Significant advantage on plasma vertical stability for low A
- Significant advantage on wall and divertor loads in case of fast disruptions for low A
- Significant advantage on tritium breeding ratio (TBR) for low A
- Some advantage on toroidal field ripple for high A

From this analysis, the major advantages are for low A, but an important consideration pushed the final decision to A=3.1: ITER has an aspect ratio of 3.1. It was therefore preferred to adopt an intermediate solution (A=3.1) for which the physics basis is almost fully established, in line with a "conservative" line matching the near-term philosophy of DEMO1. Anyway, comparing the various DEMO1 concepts presented in the last years, A=3.1 represents a low A option, with main advantages with respect to the previous designs at higher A. In this evolution process plasma current I_P increased up to almost 20MA, while toroidal magnetic field at the axis B_T decreased. The burn time has been kept around 2 hours, with a fusion power in the order of 2GW.

Regarding DEMO2, the design options are more advanced, driven from the requests of accessing to fully non inductive scenarios with reversed q profiles (advanced scenario). β_N is higher with respect to DEMO1, and the aspect ratio is smaller (2.6). Aspect ratio A followed the same reduction trend as in DEMO1 in 2012-2015 versions. H factor is quite optimistic, reaching in the last design release 1.4. Also Z_{eff} reaches very high values, which can pose some issues on radiation and impurity accumulation. Plasma current in DEMO2 is sustained inductively by bootstrap currents and auxiliary

current drive systems: for this reason we have more than 100MW of auxiliary heating power. A lower major radius permits to reduce the overall plant costs, which is mirrored in a reduced cost of electricity (COE) in 2015 design. COE has been shown in figure 54 just to give an idea of the effect of design changes on the economic assessment. For DEMO2, the proposed designs are still in an earlier phase than for DEMO1, and a convergence among all the physics codes is hardly reached.

4.3.2 Integrated DEMO scenario simulations: effect of NBI and auxiliary heating systems

During the last 3 years, tasks within WP-PMI regarding DEMO scenario modelling with dominant NB injection have been carried out and are now presented. Both DEMO1 (releases 2012, 2013 and 2015) and DEMO2 (release 2013) have been investigated. Sensitivity studies on NB injection in the reference DEMO flattop plasma have been carried out with the fast tool METIS (a description of the tool will soon follow). METIS has been used also to perform a sensitivity study on NBI and auxiliary heating systems in DEMO1 ramp-up phase. In order to assess issues and optimization possibilities for DEMO1 ramp-down, fully predictive integrated transport simulations with given boundaries using 1.5-D JINTRAC code have been performed. In this study the role of NBI and ECRH has been assessed, highlighting the different but complementary capabilities of the two systems. The investigation of the effects of different heating systems during DEMO flattop and transient phases, in addition to selected NBI sensitivity scans, helped in the definition of the potential role of NBI in a DEMO device.

DEMO NBI DEMO1 requests for NB system is to provide a power of 50MW, mainly for central plasma heating, with lower interest on current-drive capabilities. In order to guarantee the desired power deposition profile, given the machine dimension and plasma density, the NB energy has been fixed to 1MeV, which is a realistic option equal to the ITER NB injector. In order to reduce shine-through losses, the NBI is tangential, and this have the beneficial by-product of driving some plasma current, which can help in the discharge duration extension. Different requests are demanded from DEMO2 NB system. Since DEMO2 is designed for advanced scenario operations, with reversed q profile, NBI is an essential scenario actuator. In addition to plasma heating, the NB tangential trajectory is set to drive off-axis currents, which, with the contribution of bootstrap currents, helps in keeping the desired current density profile. In order to reach fully non-inductive plasma current, the total NB driven current is considerable, and therefore higher NB power (>100MW) is required. In the reference design, NB energy for DEMO2 is 1MeV, as in DEMO1.

Discussions whether to increase DEMO NB energy (for plasma performance amelioration) or to decrease it (to improve the NB system efficiency) has been tackled and are still occurring. Papers on DEMO NBI optimization describing different NB system solutions have been published and animate the H&CD community [147–149].

Modelling tools used for DEMO simulations

Two different approaches have been used to perform integrated DEMO simulations. For transport validations and detailed investigations, JINTRAC

1.5-D transport suite of codes (described in section 3.1.2) has been used. This is the case of integrated ramp-down simulations (see section 4.3.4 for details) with plasma boundaries consistently calculated by CREATE code, where the focus has been put on detailed analyses on scenario evolution in consistent transport simulations. The output of this work has usually been a unique complex plasma simulations of tens/hundreds of seconds. CREATE code [150], run by CREATE group, has been coupled to JINTRAC simulation. It produced boundary calculations for JINTRAC input, and it has been then used for post-analysis of the transport simulations. CREATE is a free boundary code solving plasma equilibrium code, i.e. "the MHD time evolution of 2D axysimmetric plasmas in toroidal fusion devices, including eddy currents in the passive structures, and feedback control laws for current, position and shape control" [150]. The code is able to produce the plasma boundary from estimation of plasma parameters and coil design. It can then be used to assess plasma vertical stability and plasma controllability issues starting from the allowed coil currents, given the main plasma kinetic parameters.

In case of sensitivity studies, the fast tool METIS has been used. This tool permitted to run complete tokamak discharges very rapidly, allowing many parameter scans. METIS tool is now briefly described.

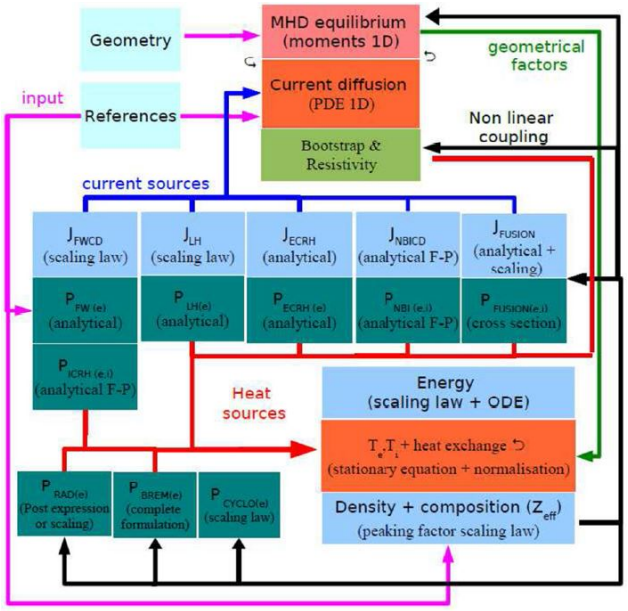

Figure 55.: Computational flow of METIS, from [151]

METIS (Minute Embedded Tokamak Integrated Simulator) is a fast tokamak simulator [151], developed and maintained at CEA (France). METIS, initially developed as a part of CRONOS suite [100], is a 0.5-D integrated modelling code which can evolve plasma global quantities for given input control parameters using simplified models and scaling laws. The code can simulate a complete plasma discharge for various machine geometries in a CPU time of the order of minutes using an almost always convergent scheme. The code includes a full fast current diffusion solver on a 21 points radial grid and uses a mix of 0-D laws and 1.5-D equations. It takes into account various non-linear couplings between physical quantities. Plasma shape is described by means of geometrical parameters, as triangularity and elongation. Current sources are described by simple analytical formulations,

and in case of NBI and ICRH an analytical solution of the Fokker-Planck equation is used to assess the fast ion slowing down related quantities (similar to the analytical solution adopted in FIT3D model described in section 3.2.3). In METIS, NBI is described by a decay equation in a simplified geometry. The NB ionization in the plasma is calculated for 3 sub-beams and then averaged, in order to consider the beam spreading. Ionization cross sections are taken from Janev's work [81], including the cross section enhancement due to fast ions [152]. The tangency radius of the beam trajectory is prescribed, and the injection is calculated in the equatorial plan. After this, thanks to a remapping, the beam vertical tilt (described by "zext" input parameter) is considered. METIS zext parameter can vary from 0 to 0.5, and it is defined as the vertical normalized coordinate on a vertical axis passing from the plasma magnetic axis, where 0 is the plasma centre and 1 is the the plasma boundary. Figure 56 exemplifies zext parameter definition. The

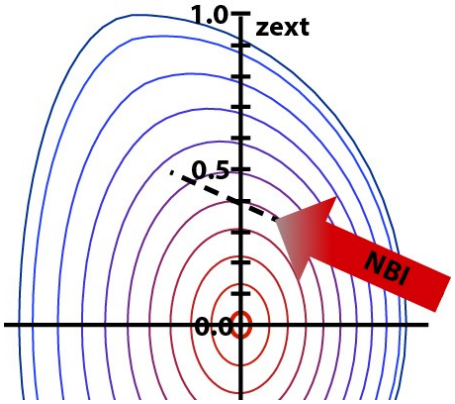

Figure 56.: METIS zext parameter definition, in this example zext=0.4.

vertical and horizontal width of the beam are internally fixed, depending on the analysed tokamak. From power deposition, orbit losses, which are calculated by a simplified model, are subtracted. Power deposition to electrons and ions is calculated following Wesson formulation [4]. The NB current drive source is estimated by an approximated analytical solution of the Fokker-Planck equation. Current drive efficiencies for other H&CD systems are either prescribed (LHCD), deduced from scaling laws (Fast Wave CD) or simply calculated (ECCD). Density is controlled by a prescribed value of the line-averaged density, and by a density peaking factor which can be prescribed or deduced from a scaling law. Edge density is calculated from a scaling law. The energy content of the plasma is calculated by means of a scaling law, which depends on the selected scenario (prescribed H-factor). Simple analytical transport coefficients are used, and the temperature profile is calculated consistently. The ratio between ion and electron heat diffusivities is prescribed. Fusion power from D-D and D-T reactions is calculated, and the produced He ashes are included in the plasma composition, which is deduced from a prescribed line-averaged Z_{eff} value. Radiation is consistently calculated assuming coronal equilibrium, and bremsstrahlung radiation is corrected for relativistic effects. Figure 55 shows the computational flow of METIS.

The purposes of this codes are various. One is a fast shot analysis using the first available experimental data. Another is plasma scenario studies, both for shot preparation in existing tokamaks and for non existing tokamak scenario projections and validation. METIS is widely used in the fu-

sion community, and different METIS works have been published in the last years [153–156]. In the recent work already mentioned on PPPT scenario modelling activities [146], METIS tool is described together with some DEMO applications. METIS, in addition to DEMO sensitivity studies, has been used within PPPT WP-PMI for a first validation of PROCESS engineering DEMO designs.

In the work here presented, DEMO design is integrated in METIS, and in particular DEMO NB systems is defined by METIS parameters. METIS has the possibility to run 2 NBI systems, and in the following sections, the total NB power is divided equally in the two systems. For DEMO1, the tangency radius of both NB injectors is fixed to 7.69m, with a vertical tilt described by a zext parameter equal to 0.10 and 0.26 for the two beam lines. For DEMO2, the tangency radius is the same of DEMO1, and zext is equal to 0.20 and 0.41 for the two different lines. The beam horizontal and vertical dimension is fixed internally in METIS and it is scaled from ITER beam dimension.

4.3.3 Flattop studies

In this section DEMO flattop studies are presented. DEMO1 flattop simulations have been performed for 2012, 2013 and 2015 releases with different aims: transport validation and reference scenario creation as starting point for ramp-up and ramp-down studies for 2012 and 2015 designs, and investigations on flattop duration and NBI characteristics for DEMO1 2013. As spin-off activity born within PPPT WP-PMI activities, a study on fuelling and density control has been carried out for DEMO1, and it has been recently published [157]. This work in part analysed also the fuelling impact of DEMO NBI, and this part is here reported. Regarding DEMO2 flattop modelling, an NBI sensitivity study has been carried out for 2013 version.

DEMO1

2012 DESIGN: FLATTOP ASSESSMENT A complete engineering design of 2012 DEMO1 concept was produced, and this allowed a deep investigation of DEMO1 scenario with JINTRAC code coupled to CREATE tool, which uses the coil design to assess plasma controllability issues related to scenario performances. This was particularly interesting for ramp-down, when plasma might be difficultly controlled by magnetic coils. This work is presented in 4.3.4. In order to perform this study, DEMO1 2012 flattop has been simulated with the aim of providing a starting point for ramp-down JINTRAC+CREATE studies. The fully predictive simulation tried to match the overall PROCESS parameters, listed in figure 54. Following, JINTRAC DEMO1 flattop simulation is presented.

First of all, CREATE group provided the flattop plasma shape consistently calculated by realistic assumptions on plasma stability and allowed coil currents. The plasma boundary for the reference flattop is shown in figure 57. The fully predictive JINTRAC transport simulation has been performed using GLF23 and NCLASS for anomalous and neoclassical transport models respectively, ESCO code for equilibrium (calculated every 1s) and PENCIL for NBI (50MW, 1MeV) modelling. Transport coefficients of the edge transport barrier (ETB) have been scaled down to neoclassical values, except during an ELMs. Input prescribed quantities have been: average Z_{eff} (with Ar as representative impurity), plasma shape, plasma current (16MA) and toroidal magnetic field (7.1T at the magnetic axis). Density has been con-

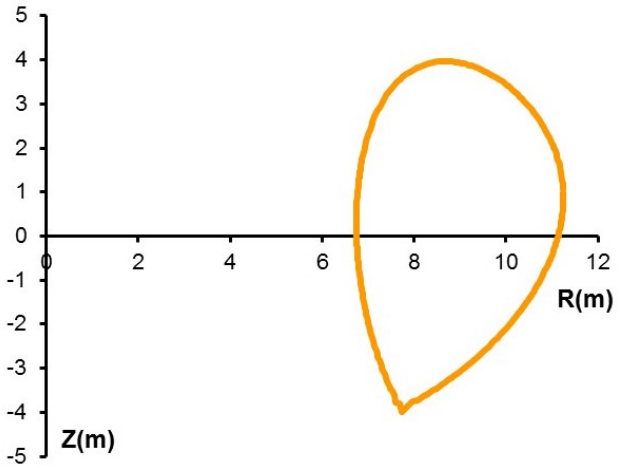

Figure 57.: Reference flattop plasma boundary for DEMO1 2012 calculated by CREATE.

trolled by pellets injected from the high field side of the machine. Neutrals have been modelled by FRANTIC code. Fusion products have been consistently taken into account, considering also a delay in alpha particle heating. The JINTRAC flattop reference scenario created has been tuned to match the kinetic profiles of PROCESS DEMO1 2012 scenario. Not all the parameters could be matched, and PROCESS seemed to give more optimistic values than JINTRAC. A total of 25s of flattop phase have been run, reaching almost stationary condition. The following plasma parameters have been reached: $\langle n_e \rangle = 9 \times 10^{19} m^{-3}$, $\langle T_e \rangle = 11.1 keV$, $q_0 = 1.1$ and $q_{95} = 3.5$. The resulting H-factor (0.9) is lower than PROCESS estimation, and fusion power (1350MW) could not be matched with the PROCESS reference. This highlights some inconsistency of PROCESS estimations due to the different approach of the physics models used. Figure 58 shows the stationary density and temperature profiles.

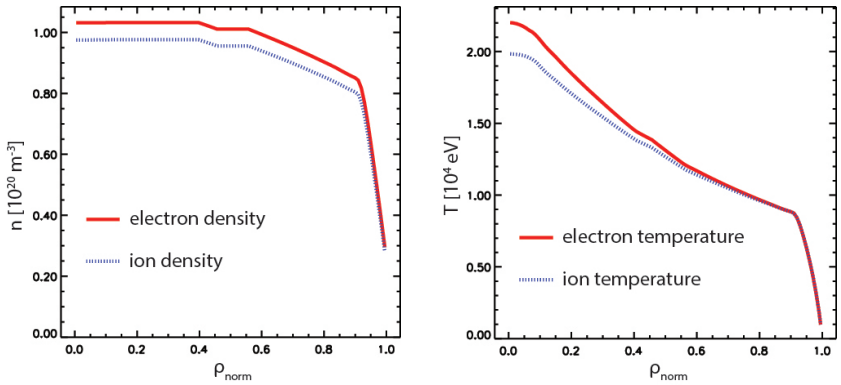

(a) Density profiles

(b) Temperature profiles

Figure 58.: Stationary density and temperature profiles in flattop phase of DEMO1 2012 by JINTRAC modelling.

In this simulation the role of NBI is manly for central plasma heating, giving an essential contribution to the energy balance. Current-drive is not a main request for pulsed scenarios. The decision of using PENCIL for NBI-

plasma interaction modelling, and not e.g. ASCOT, has been taken in order to speed up the very time-demanding simulation.

DEMO1 2012 flattop scenario has also been simulated by METIS, in order to create a reference simulation useful as starting point for ramp-up sensitivity studies presented in section 4.3.4. The modelled scenario is the same just described for JINTRAC, but with a small difference in plasma current (14MA instead of 16MA): due to the different timing of JINTRAC and METIS analyses, slightly different design versions have been used, although, except I_P, main plasma and geometrical parameters are almost equal. A complete reference DEMO1 discharge has been simulated, reaching ~1GW of fusion power with H=1. Pedestal has been modelled following the guidelines emerged from PPPT discussions, with $n_{e,ped} \approx 85\% n_G$ and $T_{e,ped} \approx 5keV$. NBI has been modelled in METIS and represents the dominant heating system in the flattop phase. Fusion power is smaller than in the reference PROCESS design, but as happened for JNTRAC, the matching with kinetic average parameters came at the cost of a lower fusion power. In figure 59 the main kinetic parameters of the simulation are reported. Some physics inconsistency between PROCESS and METIS/JINTRAC has

METIS DEMO1 2012			
Density		**Temperature**	
$<n_e>$ [10^{19} m^{-3}]	9,48	$<T_e>$ [keV]	10,04
$<n_{e,0}>$ [10^{19} m^{-3}]	12,31	$<T_{e,0}>$ [keV]	22,87
$<n_{e,ped}>$ [10^{19} m^{-3}]	7,31	$<T_{e,ped}>$ [keV]	5,01
$n_{e,ped}/n_G$ %	82,9		
$n_{e,line}/n_G$	1,2		
Pfus=950 MW			

Figure 59.: Reference flattop plasma parameters for DEMO1 2012 calculated by METIS.

been noted, and actually this consideration drove ameliorations in PROCESS code, which has been upgraded several times in the last years.

2013 DESIGN: A SENSITIVITY STUDY During 2013 a new DEMO design has been released (refer to figure 54 for main parameters). The scenario validation has been done by means of METIS within WP-PMI activities, and it is reported in [146]. Starting from this working point, DEMO1 flattop duration has been investigated by a sensitivity scan where NBI parameters have been varied. DEMO NBI-plasma interaction has also been studied by specific sensitivity studies here reported.

The motivation of the flattop duration investigation is that the pulse dropped below 2 hours in PROCESS DEMO1 2013 concept. The value itself may be not so important (e.g METIS estimates a duration of 2.5h for the same scenario), but the interest has been focused on understanding the main actors determining the pulse duration. One of these is certainly the NBI, and dedicated scans have been performed. First of all, the NB power has been varied, observing the effect on flattop duration and total Q factor (P_{fus}/P_{aux}). The results are shown in figure 60. It can be seen that increasing the NB power leads to an increase of the flattop duration. This can be explained by two facts. The first is that NB injection drives non inductive currents, and we can expect an increase of the driven current with more NB power. This im-

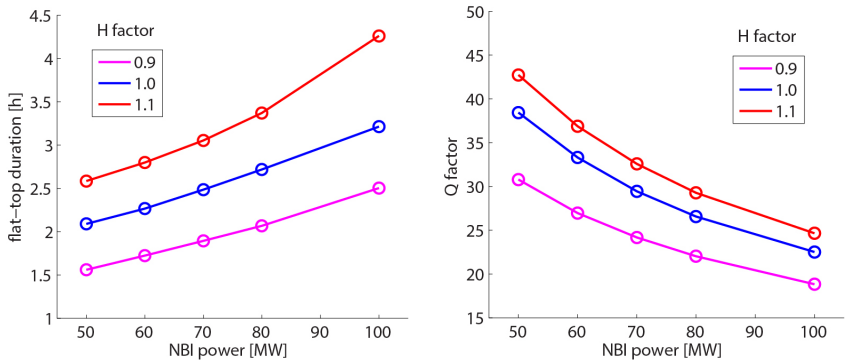

(a) Density profiles **(b)** Temperature profiles

Figure 60.: NB power scan at different H-factors: effect on DEMO1 flattop duration and total Q.

plies less requests on the central solenoid, extending the pulse duration. In addition to this, the increase of central heating leads to higher plasma temperature and steeper gradients: we can then expect higher bootstrap current fraction, which increase the ratio of non-inductive currents and therefore the pulse length. A drawback of an increase of the auxiliary heating power is the loss of the reactor efficiency, observed with a decrease of Q (figure 60b). Anyway, assuming the expected H=1.1 scenario, even doubling the NB power to 100MW, Q does not drop below 25, which can still be considered an acceptable value. From figure 60 it is clear that reaching the expected H-factor (1.1) is essential to guarantee high performances. We can conclude that although the reference 50MW of NB power during flattop is mainly for plasma heating, the contemporary current-drive is beneficial for a long plasma burn, and an increase of NB power can benefit the duration without strongly compromising the Q factor.

In METIS, DEMO NB system is composed by two NB injectors, each of them scaled from the ITER injectors and having the same power. The reference METIS NBI parameters for DEMO1 are a tangency radius of 7.69m, and zext values of 0.10 for the first NBI line and 0.26 for the second line (see section 4.3.2 for parameter descriptions). A tangency radius scan was previously performed within PPPT WP-PMI activities in 2012 [97], so it has been decided to see the effect of changing the METIS parameter zext, which roughly correspond to give a vertical tilt to the NBI line. This permits to produce a more off-axis beam, which can be useful to drive off-axis currents. For this reason this study has been done also for DEMO2, where q profile control is an essential request. In this case, the scan has been performed to have comprehensive information on the sensitivity of the NBI parameters on the scenario. For the sake of simplicity an equal value of zext parameter has been given to both DEMO NBIs in this scan. In addition, two energy values (1 and 1.5MeV) have been studied. Figure 61 shows the NB driven current density profiles for different values of NB vertical tilt and energy. As already mentioned, CD is not the main driving request for DEMO1 optimization, but it can help in extending the flattop duration. Therefore it is interesting to investigate the dependence of the driven current on NB vertical tilt also for DEMO1. Less the vertical tilt, more central is the driven current, as it can be expected. Reference NB vertical tilts for METIS DEMO1 simulations (included between 1 and 2.6) provide in fact a broad core heating, differently from DEMO2 case where higher vertical tilts are necessary

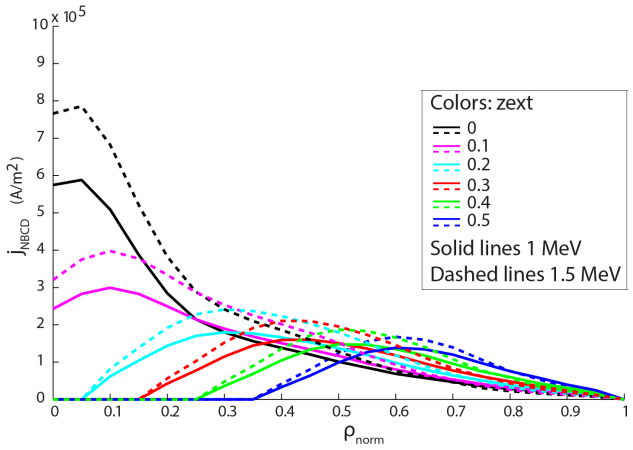

Figure 61.: Scan in NB vertical tilt and energy and resulting NB driven current density profiles for DEMO1 2013.

for more off-axis current drive (see following paragraphs). Although NB energy for DEMO1 will be unlikely increased, we can observe that in principle higher NB energy leads to higher driven current, for all the vertical tilts scanned in this study. The current drive efficiency is shown in figure 62a. Current drive efficiency is calculated as in [148]: $\eta_{CD} = R_0 n_e \frac{I_{CD}}{P_{NBI}} \left[\frac{10^{20} A}{W m^2}\right]$. The NBCD efficiency slightly decreases with higher zext (more accentuated for 1.5MeV). Higher CD efficiency is observed with 1.5MeV, although METIS η_{CD} values seem to be too optimistic compared to the assessment done by means of PENCIL code in [148]. Increasing the vertical tilt of the beam could

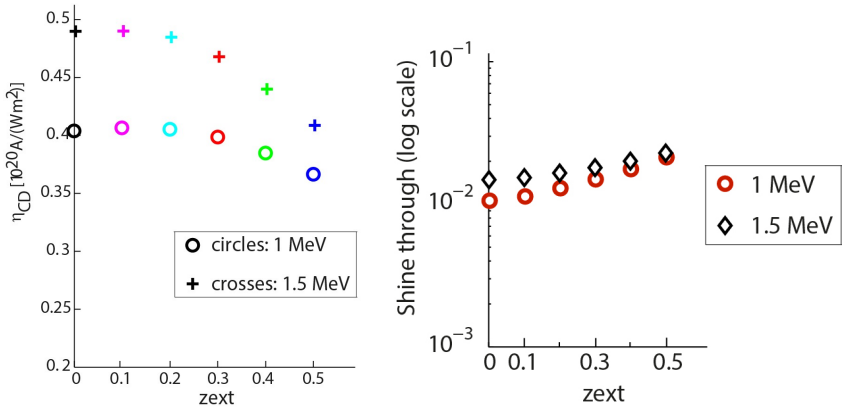

(a) NBCD efficiency

(b) NB shine through

Figure 62.: Scan in NB vertical tilt and energy and resulting NBCD efficiency and shine through losses for DEMO1 2013.

affect the beam absorption, resulting in enhanced thermal loads on the first wall due to higher shine through losses. This is indeed observed in figure 62, since more off-axis NB injection lines experience lower density plasma zones. Therefore, with higher vertical tilt, the beam is less efficiently ionized by the plasma. As the beam penetration depends on the injection energy, with higher NB energy we can observe slightly higher shine through losses. In general, from METIS evaluation, we can conclude that NB shine through is not an in issue for DEMO1 flattop phase, at all zext values scanned: it represents a few percent of the beam particles, resulting in less than 0.5MW of

losses (per beam line) spread on the beam perpendicular cross section area. Considering the beam divergence, this estimation is far below the material limitations for wall thermal loads. The flattop duration is not affected by the vertical tilt, and the same is for q profile: this is explained by the fact that in DEMO1 most of the plasma current is induced by the central solenoid, and unless increasing the NB power, the NBCD contribution is very low with the present configuration of the beam lines.

As spin-off activity of WP-PMI 2013 activities performed, a work on DEMO fuelling and density control has been published [157], born from the collaboration with CCFE experts. In this work JINTRAC DEMO1 simulations have been run, reaching stationary conditions (flattop phase). Starting from this working point, considerations on particle fuelling and control of the plasma density are presented, highlighting the probable unfeasibility of gas puffing in favour of pellet injection. Beside all these results, an interesting conclusion on NB particle source for DEMO1 has been drawn. Comparing the different particle sources, NBI is at least two orders of magnitude lower. This means that, differently from current experiments, NBI is not a relevant actuator for plasma fuelling due to the large plasma volume at the considered NB power. In DEMO2 the NB power is roughly doubled: likely, also for DEMO2, NBI will not play an important role in fuelling and density control.

2015 DESIGN: FLATTOP ASSESSMENT DEMO1 2015 concept has been accompanied by a complete engineering design, including all the information needed by CREATE for assessing plasma control capabilities from coil currents. The task within WP-PMI activities for 2015 has been to run JINTRAC+CREATE simulations for DEMO1 ramp-down (ramp-down work is described in section 4.3.4). In order to generate a ramp-down starting point, DEMO1 2015 flattop has been modelled by means of JINTRAC transport suite, in a similar procedure as done for 2012 design described in this section. CREATE group provided the plasma boundary for the flattop phase, which is illustrated in figure 63. The fully predictive transport simulation

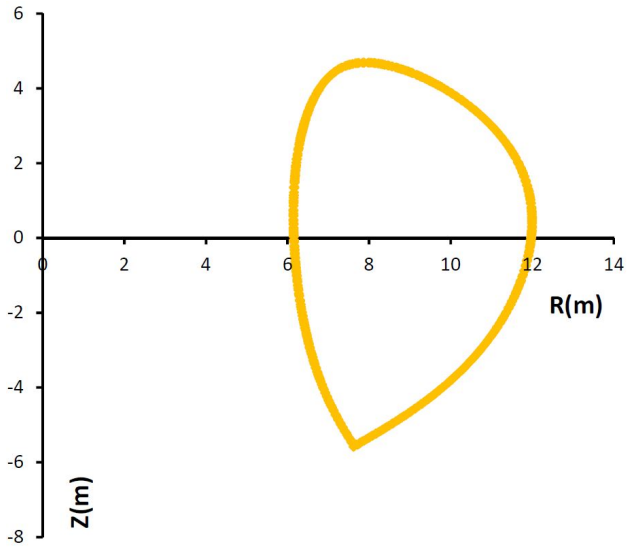

Figure 63.: Reference flattop plasma boundary for DEMO1 2012 calculated by CREATE.

with JINTRAC has been performed in collaboration with CCFE laboratory.

NCLASS has been used for neoclassical transport and analytical expressions have been used for transport coefficients (particle diffusivity D and heat conductivity χ), set in order to retrieve the desired scenario (as done also in [146]). ESCO code has been used for equilibrium calculation. NBI for a total of 50MW at 1MeV energy has been modelled with the fast analytical code PENCIL. As already mentioned, the main role of the NBI in this scenario is plasma central heating, essential for the sustainment of the discharge. Anyway PENCIL consistently calculated also the NB driven current which has been included as current source in the simulation. Plasma boundary has been prescribed to CREATE inputs, and Z_{eff} has been set to 2.6 (matching PROCESS value) assuming a radially constant distribution with Xe as representative impurity. Plasma current has been prescribed to 19.6MA, and the toroidal magnetic field to 5.7T at the magnetic axis. Neutrals have been modelled by FRANTIC code, and fusion products have been taken into account. Line radiation has been also prescribed to PROCESS values, in order to simplify the convergence of the simulation. The tuning of the flattop parameters has been done in order to match the overall PROCESS parameters, although, as happened for 2013 analysis, not all the parameters could be matched. A comparison between PROCESS and JINTRAC parameters for DEMO1 2015 is reported in figure 64, where also the reference METIS simulation carried out by WP-PMI CEA experts is included. The overall match-

DEMO1 2015 flattop	PROCESS	METIS	JINTRAC
I_p (MA)	19,60	19,60	19,60
B (T)	5,67	5,67	5,67
q95	3,25	3,81	3,69
R (m)	9,07	9,07	9,07
Vol (m3)	2502	2407	2417
$<n_e>$ (10^{19} m^3)	7,98	7,93	8,54
$<T_e>$ keV	13,07	12,84	12,99
$n_{e,0}$ (10^{19} m^3)	10,14	10,09	9,44
$T_{e,0}$ keV	27,36	28,54	31,31
Z_{eff}	2,58	2,00	2,60
H	1,10	1,10	1,20
P_{NBI} (MW)	50	50	50
P_{fus} (MW)	2037	2004	2455
β_p	1,11	1,39	1,33

Figure 64.: Comparison among PROCESS reference design, METIS and JINTRAC simulations for DEMO1 2015.

ing is fairly good, although some discrepancies can be noted. In particular, the high Z_{eff} value resulted in high radiation losses, which has been compensated in JINTRAC by a higher H-factor, in order to obtain the desired temperature profile and fusion performances. METIS simulation, in order to retrieve the desired scenario performances, has been run with a lower Z_{eff} value of 2, keeping the H-factor to the reference value of 1.1. Since the aim of 2015's work was focused on ramp-down, further flattop optimizations have not been attempted, since this simulation has been needed mainly as ramp-down starting point. Optimized JINTRAC flattop simulations reaching stationary conditions are a considerable task, far beyond the requests of this task.

DEMO2, 2013 design: a sensitivity study

The METIS investigations for DEMO1 2013 flattop illustrated in this section have been repeated also for DEMO2 2013 release. The aim has been to study the flattop scenario sensitivity on NB parameters. The NBI role in DEMO2 is double: certainly plasma heating, but also a relevant current drive. NBCD is indeed an essential contribution for the advanced scenario sustainment. It is fundamental for q profile control and to contribute to a fully non-inductive plasma current. For this reason the NB reference power for DEMO2 is 135MW and the reference METIS zext parameters for the two beam lines are 0.2 and 0.4. This reflects the strong need of a more off-axis current drive, with a considerable contribution of NBCD to the total plasma current. The DEMO2 2013 scenario validation has been done by means of METIS within WP-PMI activities [146]. Starting from this working point, the NBI parameter zext corresponding to the beam vertical tilt (see section 4.3.2 for the definition) has been varied, and the effects on NBI-plasma interaction has been investigated. Figure 65 shows the NB driven current density profiles, where zext parameter has been varied from 0 to 0.5 with two NB energies (1 and 1.5MeV). The zext values reported are applied to both in-

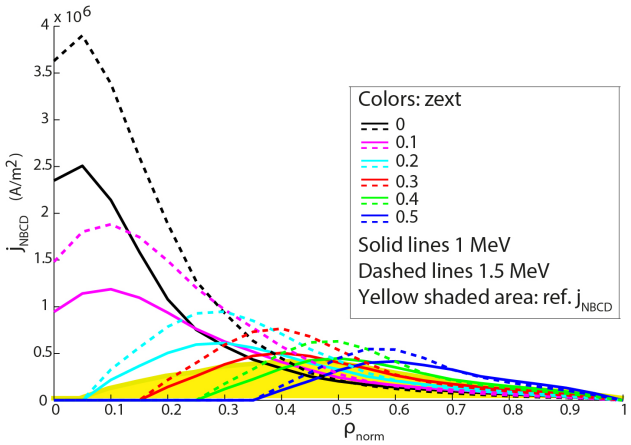

Figure 65.: Scan in NB vertical tilt and energy and resulting NB driven current density profiles for DEMO2 2013.

jectors in METIS code. The modification of the vertical tilt is a method to induce current centred at different radial position. In particular with zero vertical tilt the driven current density is peaked at the centre, while for a tilt of 0.5 the maximum of the curve moves to almost 0.6 in normalized poloidal flux coordinate. The reference scenario (yellow shaded area in the plot) has a broad profile and helps in maintaining the mildly reversed q profile characterizing DEMO2 flattop scenario. As highlighted for DEMO1, an increase of NB energy leads to higher driven current, as it can be seen from figure 66a. The total driven current I_{NBCD} for 1MeV NBI does not change significantly with the tilt of the beam lines, therefore the effect of the vertical tilt is negligible on the current drive efficiency. This is shown in figure 66a. A bit different is the case for 1.5MeV NBI: the NBCD efficiency decreases of ~10% passing from zext=0 to 0.5. Efficiency absolute values are probably overestimated by METIS predictions, therefore we comment only their relative values. The shine through losses increase with the beam vertical tilt (figure 66b). This can be explained by the more off-axis beam trajectory and the consequent lower plasma density encountered. With the increase of NB energy,

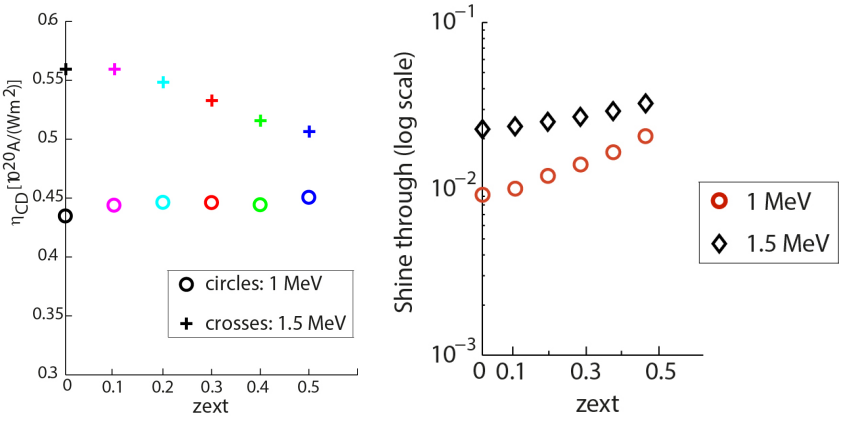

(a) NBCD efficiency **(b)** NB shine through

Figure 66.: Scan in NB vertical tilt and energy and resulting NBCD efficiency and shine through losses for DEMO2 2013.

the beam penetration increases, leading to higher losses. As mentioned, the importance of NBI in DEMO2 is connected also to q profile control, essential to access to advanced scenarios with reversed q profiles. The high NB power makes the scenario very sensitive to NB vertical tilt, and this is shown in figure 67 where the q profile is plotted for different zext values. High NB vertical tilt solutions give non realistic q profiles, while for middle tilting it is possible to obtain the desired scenario. From this analysis it seems clear

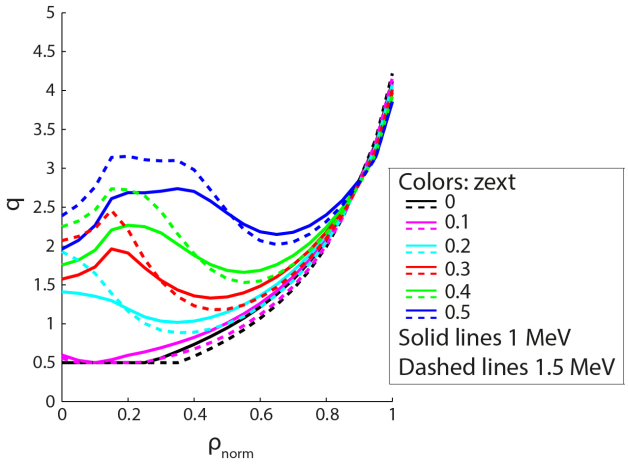

Figure 67.: Scan in NB vertical tilt and energy and resulting q profiles for DEMO2 2013.

that NBI is playing a central role not only for plasma heating but also for current drive and q profile control. The requirement on NB system is to have a very high power on off-axis trajectories, in order to produce very a effective NB injection in terms of driven current and scenario control. Part of the work on DEMO2 here presented has been published in [146].

4.3.4 Investigation of transient phases for DEMO1: ramp-up and ramp-down

In this section the work on DEMO1 transient phases is presented, with investigations of both ramp-up and ramp-down phases. This work exploited the reference flattop simulations described in section 4.3.3. The work is here divided in two parts: sensitivity studies on DEMO1 ramp-up by METIS and transport analysis of DEMO1 ramp-down by JINTRAC+CREATE simulations. It has been chosen to use different tools because of the aim of the work: a parametric scan of DEMO1 ramp-up (METIS) and a detailed transport assessment of DEMO1 ramp-down (JINTRAC).

DEMO1 2012 ramp-up: heating mix assessment

The motivations to study DEMO ramp-up are different. It is a crucial phase where optimizations can save swing flux, helping in this way to extend flattop duration. Ramp-up should also give a fast and robust access to the desired scenario. The ramp-up trajectory must fulfil at the same time the machine constraints, such as avoiding high NB shine-through losses and allowing the plasma controllability by PF coil currents.

The work here presented consists of a parametric study of the ramp-up heating mix for DEMO1 2012 by means of METIS simulations, which is particularly suited for scenario sensitivity studies due to its rapidity. The results have been then analysed by FREEBIE free boundary equilibrium code [158] by CEA experts. The aim of FREEBIE analysis has been to perform a consistency check on plasma controllability from coil system point of view for the proposed ramp-up trajectories (this part is described in CEA WP-PMI 2014 report [159]). This procedure is similar to the one used for ramp-down studies with JINTRAC+CREATE (see next sections). DEMO1 2012 version has been used since at that time (2014) it was the last version for which an engineering design was available, which was needed for FREEBIE PF coil current calculations. All this work has been done in collaboration with PPPT WP-HCD, the PPPT group studying DEMO heating systems. This has been an essential collaboration for both sides: on one hand the discussions on heating system parameters helped scenario modelling activities, on the other hand these simulations helped in the assessment of DEMO heating mix and auxiliary system requirements. Part of this work has been presented in [17]. The starting point for the sensitivity study is DEMO1 2012 METIS simulation presented in section 4.3.3 and summarized in figure 59. The ramp-up in DEMO1 2012 reference METIS discharge foresees the use of 40MW of ECRH power, which is gradually switched-off when the 50MW flattop NBI is switched-on (after ~120s). Plasma current and density are set to linear increase during this phase. The NBI 1MeV system is switched-on in this work considering the density constraints due to shine-through issues: as first approximation, a line averaged density of $3 \times 10^{19} m^{-3}$ is taken as minimum density which allows the NBI switch-on scaling this value from the ITER estimations [160]. A detailed calculation of shine-through limitations for NBI switch-on would require a the complete description of DEMO first wall and a description of beam dimensions, which are still not defined and only scaled from ITER. A discussion on DEMO NBI shine-through issues for a 1.5MeV beam is presented in [147]. Since the estimation of ECRH power deposition in the plasma would need a complex ray tracing code, in METIS the ECRH power deposition is prescribed by the position ("xECRH" parameter) of the maximum of the power deposition profile. The deposition

is prescribed to have a Gaussian shape with the FWHM automatically determined by the code. In all the simulations presented in this section (except when differently stated) ECRH during ramp-up has been prescribed to have xECRH=0.7 in normalized coordinates. This value has been set in the reference simulation of DEMO 2012 by CEA team, but further optimizations in terms of scenario performance might be possible. As mentioned in section 4.3.3, METIS simulations for 2012 design present a flattop plasma current of 14MA. The reference ramp-up used as starting point of the sensitivity study is described in terms of density and current evolution in figure 68a, and in terms of auxiliary heating systems in figure 68b. In figure 68b the

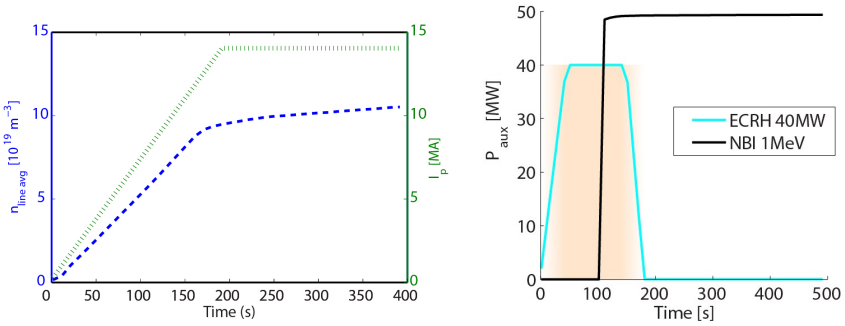

(a) Line averaged density [$10^{19}\,m^{-3}$] and plasma current [MA]

(b) Auxiliary power

Figure 68.: Reference ramp-up for DEMO1 2012 by METIS.

background orange colour intensity has been set to be proportional to the ECRH ramp-up power: this colour scheme is maintained in the following figures in order to include the heating information in the plots.

Starting from reference ramp-up, sensitivity studies on heating systems have been carried out. NBI is the reference flattop heating system, but a solution with an additional low energy NBI for ramp-up phase has been discussed. The comparison criteria have been the successful achievement of the reference flattop, the robustness and rapidity of scenario build-up, evolution of parameters β_p and $li(3)$ and L-H transition time. When available, $li(3)$ values from CREATE calculations are shown for comparison.

DIFFERENT HEATING SYSTEMS DURING RAMP-UP: ECRH, ICRH AND NBI 100 KEV The heating power during ramp-up has been varied, using not only the reference ECRH system, but also an ICRH system and a NB with 100keV. The ramp-up NBI energy has been set in order to avoid shine-through issues. 100keV NBI is presented in order to have a complete overview of heating systems during ramp-up, although we do not enter in discussions about the possibility of the implementation of another NB system in DEMO design. For each of these systems 20MW, 40MW, 60MW and 80MW options have been simulated, and the results are now shown.

ECRH POWER SCAN ECRH system is used in the reference simulation to support and drive the plasma in the initial ramp-up phase. Reference ECRH power is 40MW, and in this scan 20MW, 40MW, 60MW and 80MW values are compared, keeping ECRH timing unchanged. Figure 69a illustrates the different power options studied, together with the reference 50MW NBI system used for flattop. Figure 69a can help in the understanding of the heating requirements for an ECRH system during ramp-up (dashed line=L-

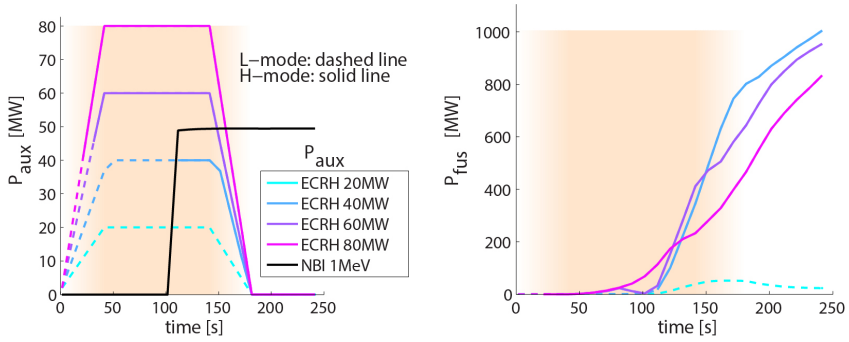

(a) ECRH power **(b)** Fusion power evolution

Figure 69.: Scan in ECRH power during ramp-up: different ECRH power evolutions and corresponding fusion power. The background colour intensity of the plots is proportional to the ramp-up ECRH power. Dashed line represents L-mode operation, solid line H-mode.

mode, solid line=H-mode). In general, higher the power, faster is the L-H transition. With 20MW, we do not reach the H-mode, i.e. it is an insufficient power to guarantee the achievement of the desired scenario. L-H transition happens very early for 60MW and 80MW options, while it coincides with the NBI switch-on for 40MW trajectory. In figure 69b the fusion power evolution is illustrated. All the options except 20MW converge to the flattop fusion power, although some little differences can be observed. Figure 70 presents the evolution of β_p and $li(3)$ parameters, together with $li(3)$ estimations by CREATE. 40MW, 60MW and 80MW options succeed

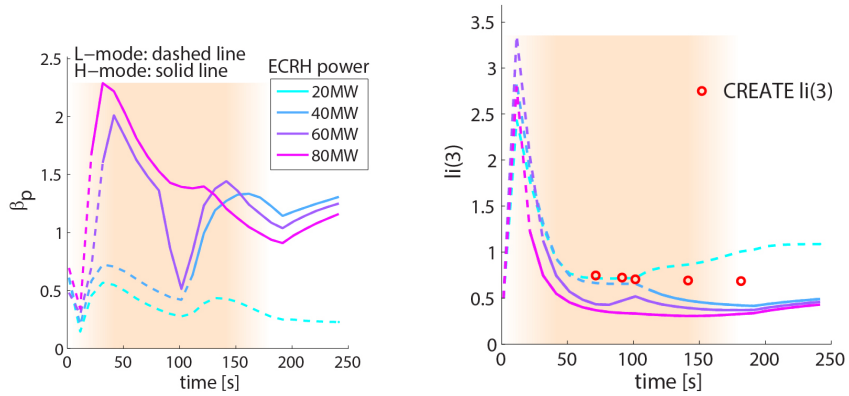

(a) β_p evolution **(b)** $li(3)$ evolution

Figure 70.: Scan in ECRH power during ramp-up: β_p and $li(3)$ evolutions.

in scenario achievement, with li(3) values lower than what calculated by CREATE. The initial li(3) increase shown in figure 70b should not be considered, as it is due to METIS artefacts connected with the initialization of the discharge. 60MW and 80MW options show higher β_p values at the beginning of the discharge, while for 40MW, the increase of β_p is coincident to the NBI switch-on. Generally it is possible to say that increasing ECRH power, li(3) decreases and β_p has an early increase. The decrease of li(3) with higher power likely depend on the current driven by the auxiliary system (off-axis), and on the effect of an earlier and more considerable heating

of the plasma resulting in lower plasma resistivity and higher spreading of the current density profile. We can conclude that ECRH 40MW could be the lower limit for successfully reaching the desired scenario, and L-H timing is determined by NBI switch-on. Higher ECRH power options show instead a faster scenario achievement.

ICRH POWER SCAN In this paragraph the ECRH system needed for ramp-up has been substituted by an ICRH system, and the power has been varied as done for ECRH. According to suggestions of WP-HCD group, an ICRH system with a frequency of 72MHz and a main toroidal number for ICRH launchers of ntor=40 has been used. There parameters are suited for T heating. Figure 71a illustrates the scan performed, together with the reference 50MW NBI system used for flattop. In these figures, the background orange colour has the intensity proportional to the relative ICRH power. Similarly

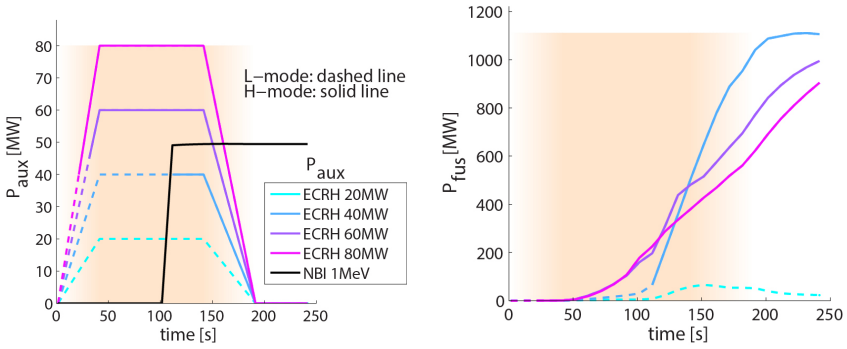

(a) ICRH power

(b) Fusion power evolution

Figure 71.: Scan in ICRH power during ramp-up: different ICRH power evolutions and corresponding fusion power. The background colour intensity of the plots is proportional to the ramp-up ICRH power. Dashed line represents L-mode operation, solid line H-mode.

to ECRH scan, with 20MW H-mode is not reached, while in 40MW simulation the transition to H-mode happens when the NBI is switched on. Faster L-H transitions happen for higher power. We could expect similarities regarding the L-H transition, since, regardless the kind of heating system used, L-H in METIS is sensitive to the power injected. Fusion power (figure 71b) starts growing earlier for higher power options and then, with some differences, 40MW, 60MW and 80MW trajectories converge to stationary flattop values. It seems here, as for ECRH scan, that lower power options overcome the others in fusion power production at the end of the ramp-up phase. Fusion power build-up for 40MW option starts at the end of ramp-up, corresponding to the NBI switch-on. Figure 72 presents the evolution of β_p and $li(3)$ for the described ICRH ramp-up trajectories. In the first half of ramp-up, β_p reaches higher values for higher ICRH power, while for 40MW options it increases to flattop value only with the NBI 1MeV switch-on. li(3) is lower for higher power trajectories, while 20MW and 40MW results in high initial li(3) values, higher than CREATE estimations for the reference ramp-up. Similarly to ECRH, it is possible to say that 40MW ICRH could be the minimum power to access the desired scenario, while increasing the power we have earlier L-H transition, earlier fusion power, lower li(3) and higher β_p in the initial ramp-up phase. Probably with some more gradual increase of injected power, it is possible to lower β_p for high power options.

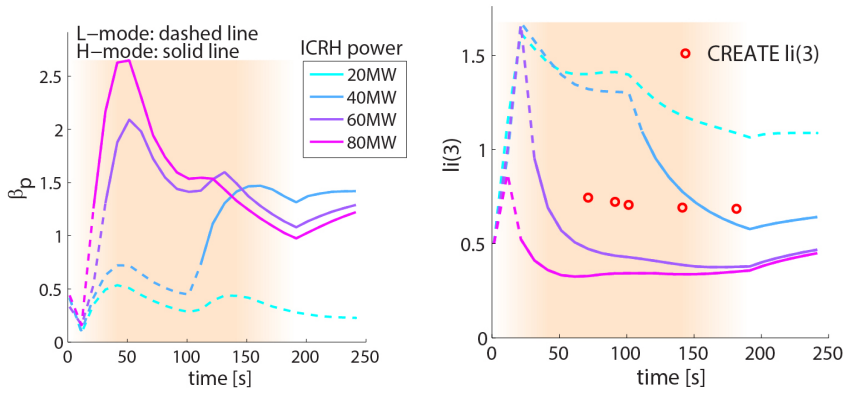

(a) β_p evolution **(b)** $li(3)$ evolution

Figure 72.: Scan in ICRH power during ramp-up: β_p and $li(3)$ evolutions.

NBI 100KEV POWER SCAN The reason preventing an early NBI 1MeV switch-on is the shine-through power losses, which in low density phase could exceed the allowable plasma facing material limitations. There are no other contraindications to use an NBI system during ramp-up. In order to complete the ramp-up heating mix study, a low energy NBI substituting the reference ramp-up ECRH has been simulated. The energy has been set to 100keV, as a conservative choice in order to prevent harmful shine-through losses. This energy allows indeed an early usage of the system according to a rough estimation of the minimum density required to switch-on a 100keV beam [147]. The two METIS NB systems for this simulation has therefore used to have: a 100keV NB source for ramp-up and a 50MW, 1MeV NB source for flattop. Figure 71a summarizes the power options of this scan, and figure 73b the corresponding fusion power. In the following figures, the background orange colour has the intensity proportional to the relative ramp-up NBI power. Fusion power is earlier produced with 60MW

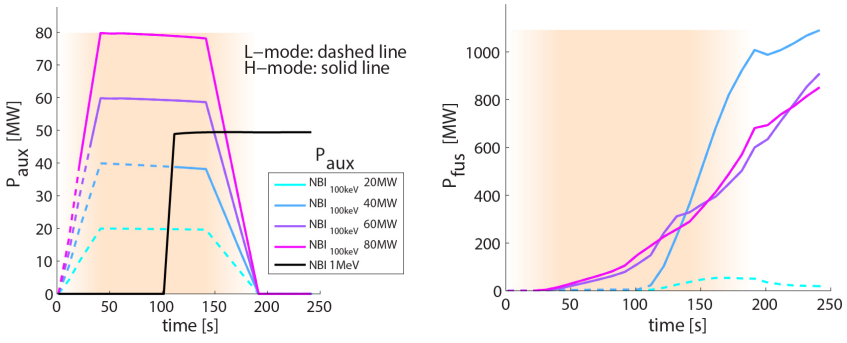

(a) NBI power **(b)** Fusion power evolution

Figure 73.: Power scan for a 100keV NB system during ramp-up: different NBI power evolutions and corresponding fusion power. The background colour intensity of the plots is proportional to the ramp-up NBI power. Dashed line represents L-mode operation, solid line H-mode.

and 80MW, which also present an earlier L-H transition. For 40Mw option, fusion power production and L-H transition happen when more power is available, i.e. when the flattop 1MeV NBI is switched-on. As already seen in

the previous scans, 20MW is not enough for accessing the desired scenario. In figure 74, the evolution of β_p and $li(3)$ is presented. The behaviour is

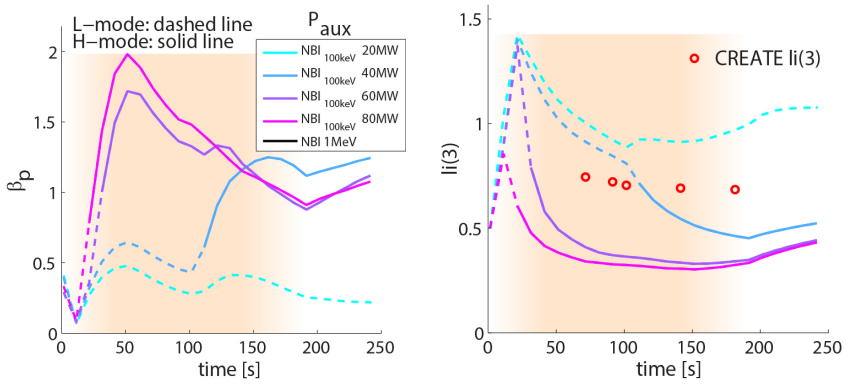

(a) β_p evolution **(b)** $li(3)$ evolution

Figure 74.: Scan in NBI 100keV power during ramp-up: β_p and $li(3)$ evolutions.

similar to the scans presented in previous sections, and no relevant differences are noticed by using a 100keV NB source instead of ECRH or ICRH. A direct comparison of the three analysed systems is presented in the next paragraph.

COMPARISON OF DIFFERENT RAMP-UP SYSTEMS Starting from the work presented in the previous paragraphs, a comparison among the different heating systems for ramp-up is here presented. High power options (60MW and 80MW) have been here used in order to compare scenarios where fusion power production and L-H transition are strongly determined by ramp-up heating systems, and not by the switch-on of the flattop NBI (as it is for 40MW option). The different solutions have been compared in terms of fusion power, and the result for 60MW of heating power is shown in figure 75a. One can notice that for ICRH and NBI 100keV solutions, the fusion

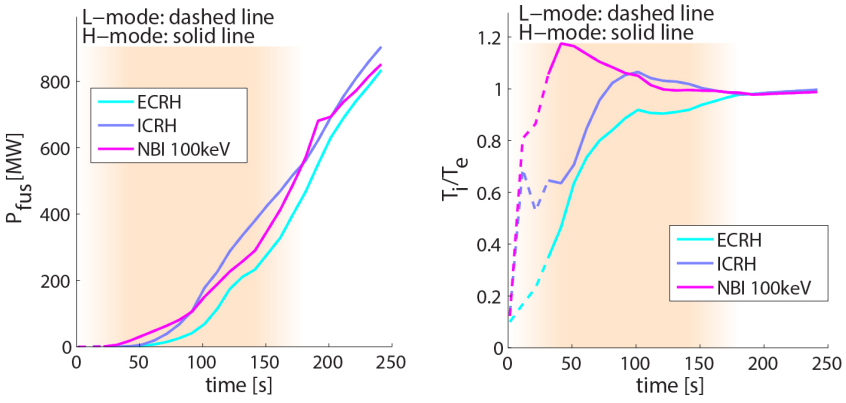

(a) Fusion power **(b)** T_i/T_e evolution

Figure 75.: Comparison among different ramp-up heating systems for DEMO1 2012 by METIS.

power is earlier rising, probably due to the preferential ion heating of these two sources. For NBI, fusion reactions from NBI-plasma interaction can be a relatively high source especially at the beginning of the discharge. For

ECRH ramp-up option, the fusion power rise is delayed, basically to the switch-on of the flattop NBI. At the end of ramp-up, all the simulations converge to the flattop fusion power value. If we consider the time derivative of the fusion power, NBI 100keV shows a slightly slower increase with respect to ICRH, at least until the end of the ramp-up power injection. A possible explanation is that the power deposition profile of the NB 100keV source depends on the plasma density, which is increasing during the ramp-up. This implies that the NB 100keV power is progressively absorbed more and more in the outer plasma, leading to less ion heating in plasma centre and probably progressively less fusion power until the flattop NB source is switched-on. The density ramp-up could also affect ECRH power deposition, which has not been modelled in these simulation but prescribed. Figure 75b helps in the understanding of the preferential heating to ions/-electrons of the 3 different sources. The plot shows the volume averaged ratio between T_i and T_e during the initial phase of the discharge, for 80MW heating power. ECRH is indeed heating preferentially electrons, while ICRH and NBI lead to a stronger ion heating. NBI 100keV in particular leads to high T_i/T_e very early in the discharge, while with ICRH we have higher Ti than Te only when the ICRH source is at full power (most intense orange background). Progressively, thanks to the thermalization process, T_i/T_e approaches 1 when reaching stationary conditions. Observing the L-H transition timing (dashed to solid line in the plot), no differences between heating sources are noted, as it could be expected since the power threshold do not depend in METIS on the heating channel.

From the presented parametric study of DEMO1 2012 ramp-up it is possible to conclude that to have a robust (and fast) access to H-mode, power $> 40MW$ seems to be favourable, while 40 MW could be the lower limit, independently from the heating system used. 20MW is definitely not enough to reach the desired scenario. Generally, increasing the ramp-up auxiliary power, li(3) becomes lower while β_p is higher. Higher temperatures are earlier achieved with higher power, and in general earlier fusion power production is observed with high auxiliary ramp-up power. NBI 100 keV and ICRH show many similarities, probably because they both preferentially heat ions. With these two systems we have a major ion heating in the early phase, leading to early fusion power production.

Two other simulations have been carried out and compared: an ECRH-only scenario and NBI-only scenario. In these simulations the full DEMO discharge has been run using only one type of heating system: ECRH or NBI. Two systems of the same type have been implemented for each of the two simulations: one system for ramp-up and one for flattop. In case of ECRH-only, the maximum position of the power deposition has been prescribed to 0.7 during ramp-up, and to 0.2 during flattop. Regarding the NBI-only scenario, the ramp-up system has been set to have 100keV of injection energy, while the flattop system is the usual 1MeV NB. The auxiliary power for flattop has been set to the reference value 50MW, while the ramp-up value has been varied (40, 50, 60 and 70MW). ICRH could not be simulated, since in the METIS version used only one ICRH system could be implemented. A comparison among NBI-only and ECRH-only simulations on discharge duration is shown in figure 76. NBI-only scenario duration is longer than ECRH-only, for all the ramp-up power options scanned (figure 76a). A possible explanation is that NBI has a higher current drive efficiency than ECRH (at least for flattop) and this is shown for 60MW ramp-up power case in figure 76b. An higher NBCD efficiency than ECCD has also been observed in

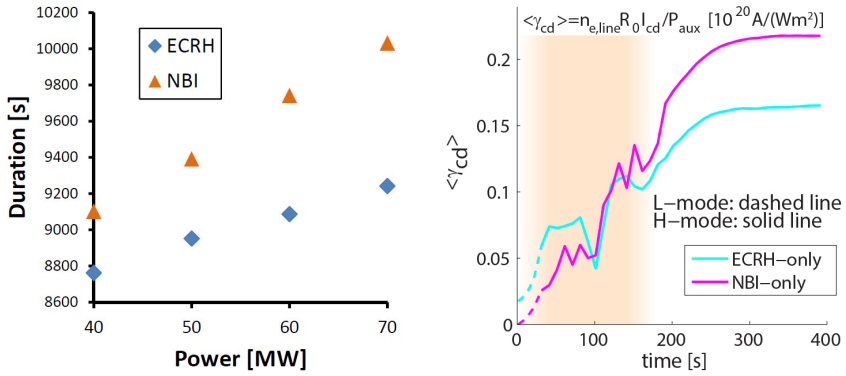

(a) Discharge duration vs ramp-up power **(b)** CD efficiency (ramp-up power:60MW)

Figure 76.: METIS simulations of DEMO1 2012 with one heating system only (ramp-up power scan + flattop 50MW): full ECRH vs full NBI discharges.

other studies (e.g. [148]). If these results will be confirmed by more detailed studies, a NB system for flattop could be preferable in terms of discharge duration.

The work on DEMO1 2012 here presented has been reported in [161].

DEMO1 ramp-down

DEMO ramp-down phase must ensure a robust and safe discharge termination, considering that NBI switch-off and H to L transition are very critical steps. The plasma position is difficult to be controlled, and coils might not be able to provide the necessary field if plasma termination is not well controlled. The possibility of controlling plasma vertical stability depends directly on plasma kinetic and current profile evolution. The aim of the activity presented in this section has been to perform JINTRAC transport simulations of DEMO1 ramp-down coupled with CREATE code, in order to produce a validated ramp-down transport simulation. CREATE team in particular provided the plasma shapes during the ramp-down phases and then performed a post-analysis of the ramp-down trajectories in order to validate the solution in terms of plasma stability and controllability. In this work, the role of the heating systems, the corresponding effect on kinetic profiles, radiation issues and H-L transition have been discussed. This work can build a basis for future detailed analysis of the ramp-down phase of DEMO. Fruitful discussions with CCFE (for JINTRAC modelling), CEA (for ramp-down options) and IPLM (for impurity and radiation) in addition to CREATE colleagues enlivened this work. DEMO1 2012 and DEMO1 2015 ramp-down phases have been studied.

2012 DESIGN The starting point for ramp-down studies for DEMO1 2012 has been the flattop simulation performed by JINTRAC with the prescribed plasma boundary provided by CREATE. This simulation has been described in section 4.3.3. CREATE provided then the plasma boundaries for ramp-down phase at 5 plasma current values (16, 13, 10, 7.5 and 5MA), based on a preliminary estimation of kinetic quantities and H-L timing for ramp-down. The final goal of JINTRAC simulations have been therefore to reach 5MA, when the last plasma boundary was available. Lower currents have not been investigated since this analysis has been done only for diverted plasma configurations. The correspondence between plasma current (and

therefore CREATE plasma shapes) and time has been a free parameter of JNTRAC simulations (determining the current ramp rate). The shapes have been implemented in JINTRAC, interpolating the plasma boundary between the available CREATE inputs. In JINTRAC, plasma current has been set to linearly decrease during the ramp-down, and the density too (controlled by pellet injection) in order to work at constant Greenwald fraction below destabilizing limits. Plasma volume decreased according to the plasma boundaries provided by CREATE. NBI switch-off has been set when reaching a plasma density of $\sim 3 \times 10^{19} m^{-3}$ in order to avoid shine-through issues (same limitations as in METIS simulations previously presented, scaled from [160]). Main JINTRAC settings are the same used for the JINTRAC DEMO1 2012 flattop simulation presented in section 4.3.3. The plasma ramp-down boundaries provided by CREATE are illustrated in figure 77. The full

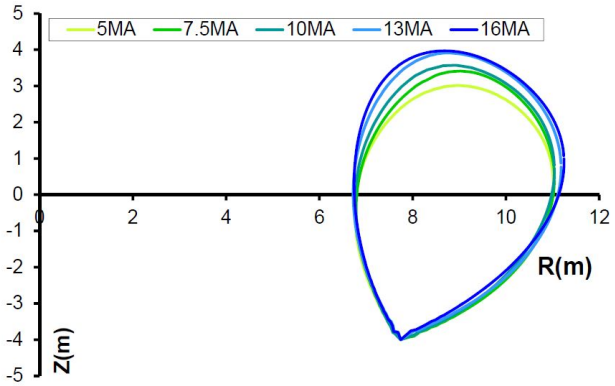

Figure 77.: Ramp-down plasma boundaries for DEMO1 2012 calculated by CREATE.

ramp-down duration has been set to 300s (as first guess, scaled from ITER), which, with hindsight, correspond to a maybe too low current ramp-rate. Since the last available shape is at current of 5MA, we could simulate the first ~200s of the ramp-down phase. In JINTRAC simulation, ramp-down started at time 5000s (which is an arbitrary value, but helpful to interpret the following figures). Figure 78 shows the time evolution of different parameters during ramp-down until t=5100s. It is possible to notice a decrease in plasma volume, density, current, temperature and β_p, whereas an increase of li(3) can be seen. Fusion power is considerably decreasing, and the net power is approaching the L-H threshold (calculated by Martin scaling [162]). The net power approaches the L-H threshold at t=~5120s as a consequence of the continuous alpha power drop. From t=5145s the plasma is permanently in L-mode, with the edge plasma temperature approaching the separatrix value. When the NBI is switched off after 150s of ramp-down, the plasma experiences a radiative collapse. This is due to the lack of enough heating power (alpha power + NB power), which causes low temperatures which in turn lead to enhanced impurity radiation. In this picture, ohmic heating is increasing due to the temperature drop and consequent plasma resistivity increase, but it is not enough to sustain the plasma. The increasing radiation due to cold plasma edge finally lead to an acceleration of the decrease of plasma temperature. The consequence is an abrupt plasma termination due to a radiative collapse. Figure 79 illustrates the evolution of density and temperature during the H to L transition and the successive radiative collapse happening at $t \cong 5150s$. In this simulation the NB source has been switched-off passing from 50MW to 0MW: a milder NB switch-off

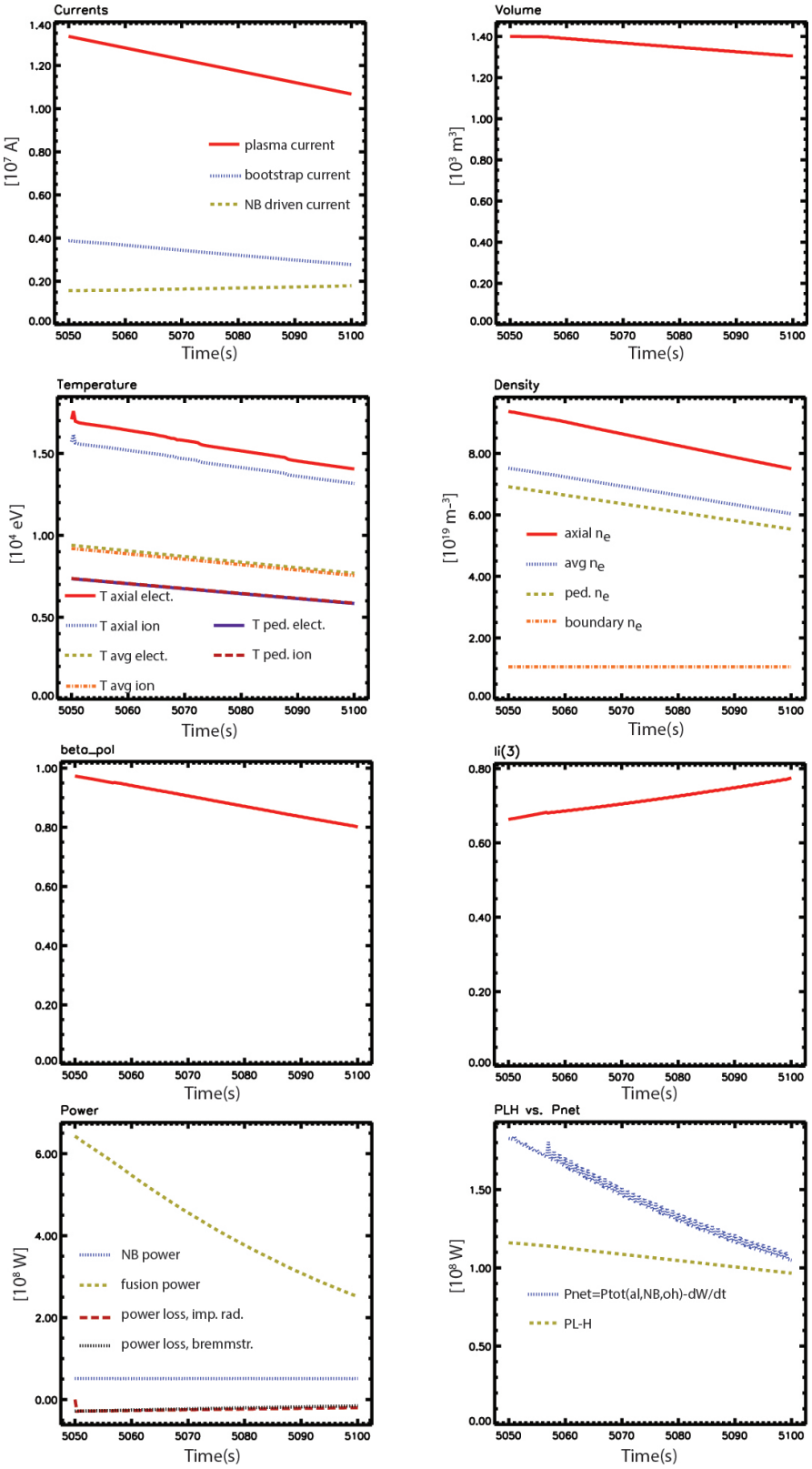

Figure 78.: Summary of the first part of JINTRAC ramp-down simulation (5000s-5300s) of DEMO1 2012.

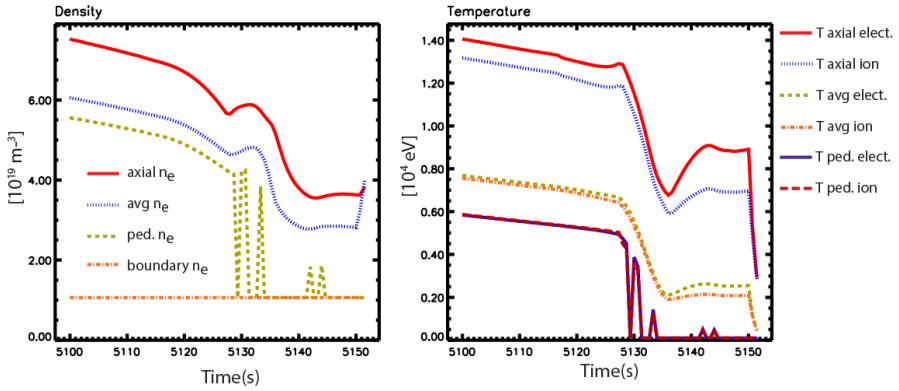

Figure 79.: Plasma density and temperature during H-L transition and NB switch off (5150s). The plasma cannot survive to strong radiation resulting in a collapse.

could help to have a smoother passage. Since it seems that heating power is lacking causing the radiative collapse, an extra power source consisting in a ERCH system has been implemented. In this new simulation, NBI is switched-off starting from 5100s in two steps of 25MW, and the lacking NB power is substituted by an ECRH source reaching 50MW as soon as the NBI is switched off. 50MW of ECRH seems to be the minimum power to sustain the plasma, since other simulations with lower ECRH power failed. ECRH power heat deposition in JINTRAC is prescribed to central heating (Gaussian profile centred at ρ=0, with FWHM=0.15). For this simulation, current drive from EC has not been taken into account. In figure 80a the auxiliary heating power from t=5100s is shown, with the ECRH system gradually substituting the NB system. The plasma density and temperature is presented

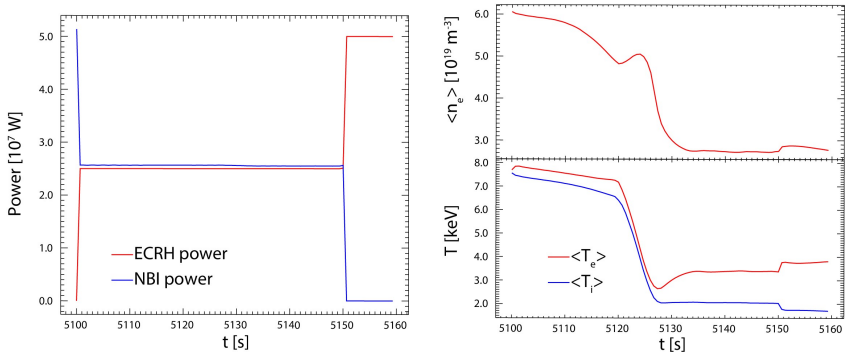

(a) Auxiliary power **(b)** Density and temperature

Figure 80.: Heating mix to solve radiation issues in the final part of the ramp-down phase and corresponding plasma parameters simulated by JINTRAC.

in figure 80b. Thanks to this heating system mix, it has been possible to successfully complete the ramp-down simulation until reaching 5MA, when the last available CREATE boundary has been reached. ECRH helps indeed to keep higher temperatures, avoiding any radiative collapse. The successful ramp-down trajectory has been passed to CREATE group for a stability validation. From this analysis [163], li(3) has been identified as a critical parameter which should be kept below 2 for the analysed ramp-up simula-

tion. The current ramp rate can be increased, to values of ~100kA/s. These considerations have been taken into account in 2015 work, now presented.

2015 DESIGN An assessment of DEMO1 2015 ramp-down by means of JINTRAC transport code is here presented. This activity is similar to what has been performed for 2012 design (previous paragraph), consisting in coupled transport simulation with CREATE code. The starting point of the ramp-down simulation is the JINTRAC flattop simulation of DEMO1 2015 presented in section 4.3.3, where the main JINTRAC settings have been described. As for 2012 design, the ramp-down plasma shapes have been generated by CREATE from a preliminary estimation of ramp-down kinetic profiles and H-L timing. These estimations have been proposed on the basis of 2012 design work consisting of: a current ramp-rate of 100kA/s (resulting in ~200s of full ramp-down from 19.6 to 0MA), β_p and li(3) of 2012 design work and an estimated H-L transition happening after ~100s from the beginning of the ramp-down. CREATE prepared plasma boundaries for diverted plasma configuration for 19.6, 17.5, 15, 12.5, 10, 7.5 and 5MA values of plasma current. Figure 81 shows the plasma boundaries calculated by CREATE. The correspondence between plasma current and time is a free

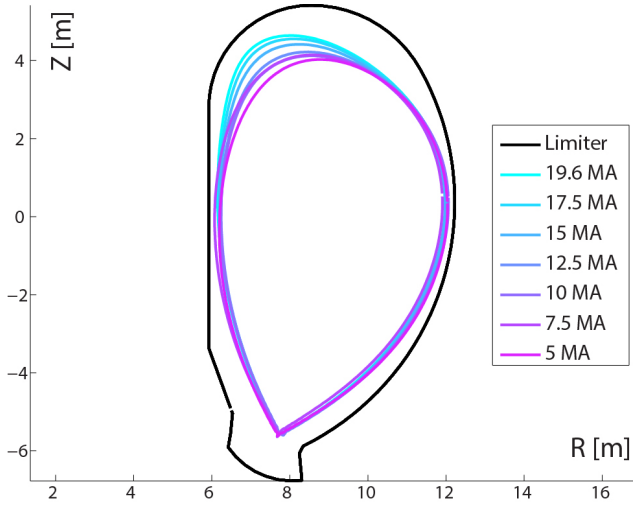

Figure 81.: Ramp-down plasma boundaries for DEMO1 2015 calculated by CREATE.

parameter and has been fixed during the transport simulations in order to have the chosen current ramp-rate. Fully predictive JINTRAC simulations of ramp-down with given boundaries have been run, with the aim of finding a successful trajectory from 19.6MA to 5MA. JINTRAC simulation setting has been performed in collaboration with CCFE and in this simulation gas puff has been used for particle fuelling. This is anyway irrelevant in terms of the aim of this work. Plasma current has been set to linearly decrease, together with the target density value for gas puff feedback: this has been done in order to keep a constant Greenwald ratio below destabilizing limits. Also boundary plasma density has been set to linearly decrease. The code interpolates the plasma boundaries between the shapes given by CREATE. NBI has been switched-off when reaching the lower density limit due to shine through losses (density limit of $\sim 3 \times 10^{19} m^{-3}$ scaled from ITER, conservative estimate [160]). L-H threshold power has been calculated using Martin scaling [162]. Two trajectories with different current ramp rates have been simulated: 100kA/s for a total of 196s of complete ramp-down and 80kA/s

for a total of 245s of full ramp-down (simulations stopped anyway when reaching 5MA). Figure 82 shows the two plasma current trajectories. In the

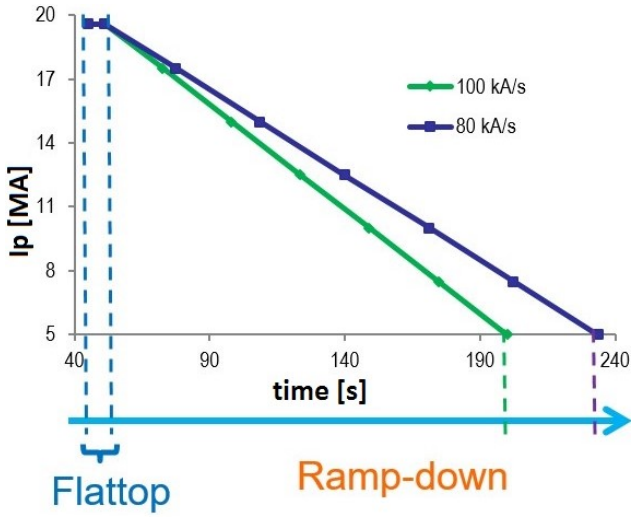

Figure 82.: Plasma current in the two ramp-down trajectories simulated.

following simulations, ramp-down starts at 51s (arbitrary time, but useful for the understanding of the next figures).

A first trajectory has been simulated with 100kA/s, which is the value suggested by CREATE group during 2012 design analysis. This scenario presents very high radiation resulting from a (too) high Z_{eff} value and high temperature. As discussed in section 4.3.3, PROCESS parameters for DEMO1 2015 could not be validated by transport simulations, unless acting e.g. on H factor (as done for JINTRAC flattop DEMO1 2015 simulations). Keeping PROCESS Z_{eff} value came at the cost of higher temperature, and this combination, as said, resulted in high radiation losses. Density is set to decrease during ramp-down, and this, together with the temperature decrease in the ramp-down phase, causes a decrease of alpha heating power. As a result, this scenario presents high power losses, not sustained by enough heating power. In order to avoid a radiative collapse, high auxiliary power up to a total of 100MW has been used, trying to find a (difficult) balance. Central heating by 1MeV NBI and on-axis ECRH are the auxiliary power systems used. ECRH (only heating, no current drive has been modelled) has been prescribed to a Gaussian profile peaked on ρ=0 with FWHM=0.25. The heating mix for this trajectory is shown in figure 83. Analysing the simulation results, a high central heating coming from NBI and ECRH is present, while too strong edge cooling due to high radiation threats the discharge. Due to a very hot plasma in the centre, and therefore locally low resistivity, the current density profile is very peaked. This results in a high value of li(3) which, according to CREATE post-analysis, makes difficult or even impossible to control the plasma. Due to the high radiation and the too hot plasma centre, the discharge finally collapses before reaching 5MA (our ramp-down target). Figure 84 shows the plasma parameter evolution of this unsuccessful trajectory. It can be noted first an increase of temperature: this can be explained by the high plasma heating derived by a considerable energy kept in the plasma due to the a energy confinement (H-factor=1.2) and still strong alpha heating (delayed by the slowing down of fast alphas). All this energy is also redistributed among less particles since the density is decreasing. After this initial part, alpha power decreases more

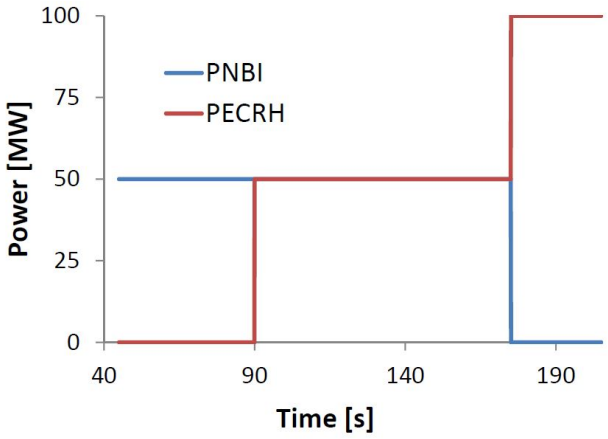

Figure 83.: Ramp-down heating power during 100kA/s trajectory.

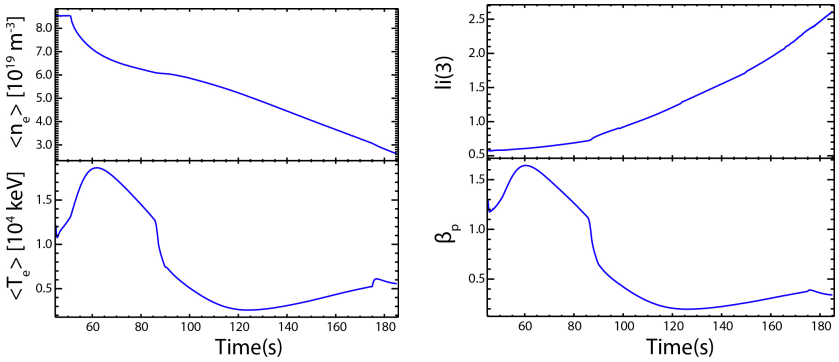

(a) Density and temperature

(b) li(3) and β_p

Figure 84.: Parameter evolution during 100kA/s ramp-down trajectory (started at 51s): due to high radiation the simulation fails at ~185s.

and more due to the decreasing density (fusion power $\propto n^2$), and plasma undergoes to a strong decrease of temperature, reflecting an uncontrolled plasma evolution where power losses are not balanced by enough heating power. A progressive edge cooling makes the current density profile shrinking, resulting in li(3) grater than 2. Beside the radiative collapse, also from a stability point of view (CREATE analysis), the plasma is not controllable.

A different strategy has been therefore adopted in order to succeed in completing the ramp-down simulation. After a discussion with CREATE group on their post-analysis of the 100kA/s trajectory, the current ramp-rate has been lowered, which may help to reduce li(3). The current ramp rate has been hence reduced to 80kA/s (245s full ramp down). Z_{eff} has been gradually reduced in order to lower bremsstrahlung radiation, and the prescribed line radiation has been decreased in order to reduce the edge cooling. Instead of switching-off abruptly the NBI from 50MW to 0, it has been gradually switched-off to help in gradually lowering the central plasma temperature. We used also mildly off-axis ECRH in the final part of the simulation (with a Gaussian profile peaked on ρ=0.3 and FWHM=0.25) to avoid too strong edge cooling and to widen the current profile. The evolution of the input trajectories for auxiliary heating systems and Z_{eff} is shown in figure 85. With these settings, the simulation successfully completed the ramp-down trajectory until 5MA. Reducing the radiation acting

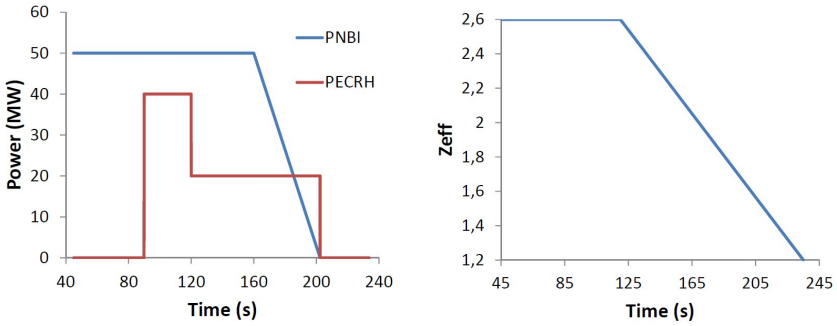

(a) Auxiliary power (b) Z_{eff} evolution

Figure 85.: Auxiliary power and Z_{eff} evolution for the input of DEMO1 2015 80kA/s ramp-down trajectory by JINTRAC modelling.

on the prescribed line radiation and Z_{eff} value allowed to reduce the required auxiliary power with respect to 100kA/s trajectory. Plasma parameters are shown in figure 86. It is possible to see that the temperature is now more gradually decreasing, although some oscillations due to the still not fully optimized trajectory. An important outcome of this simulation is the control of li(3) parameter, which is now kept below 2. CREATE post-

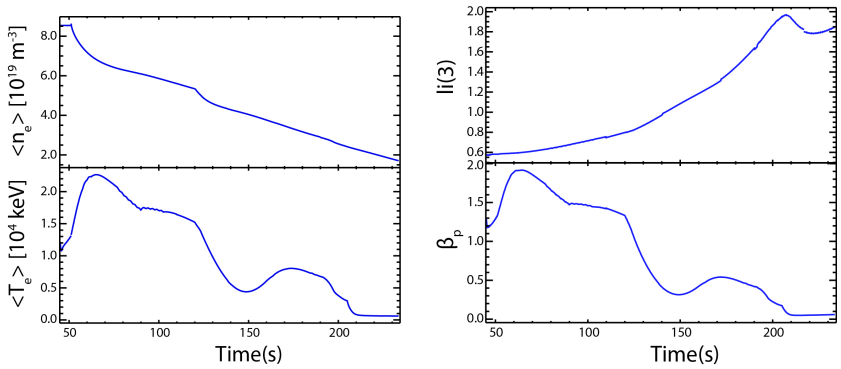

(a) Density and temperature (b) li(3) and β_p

Figure 86.: Parameter evolution during 80kA/s ramp-down trajectory (started at 51s).

analysis of this ramp-down trajectory is ongoing, and it will be described in WP-PMI final report on 2015 activities. This trajectory, although further optimizations can be applied, should be easier to control in terms of plasma vertical stability, due to lower li(3) values. Also the auxiliary heating power could be decreased with further investigations, and in this case METIS sensitivity studies could help to explore the various possibilities. H-L transition happens in this simulation around 195s at 7.5 MA, which is less than half of the initial plasma current. From discussions with CREATE, it seems preferable to have the transition at low plasma current in order to ease plasma control. Figure 87 compares P_{L-H} (from Martin scaling [162]) against $P_{comp} := P_{AUX} + P_{ohm} + P_{\alpha} - dW_{tot}/dt$, which is the critical parameter that rules in JINTRAC the H-L transition. The time derivative of energy content is taken into account since it can provide a substantial heat flux through the separatrix. The two ramp-down trajectories (100 and 80kA/s) have been compared in terms of li(3) (figure 88). It is possible to see that for

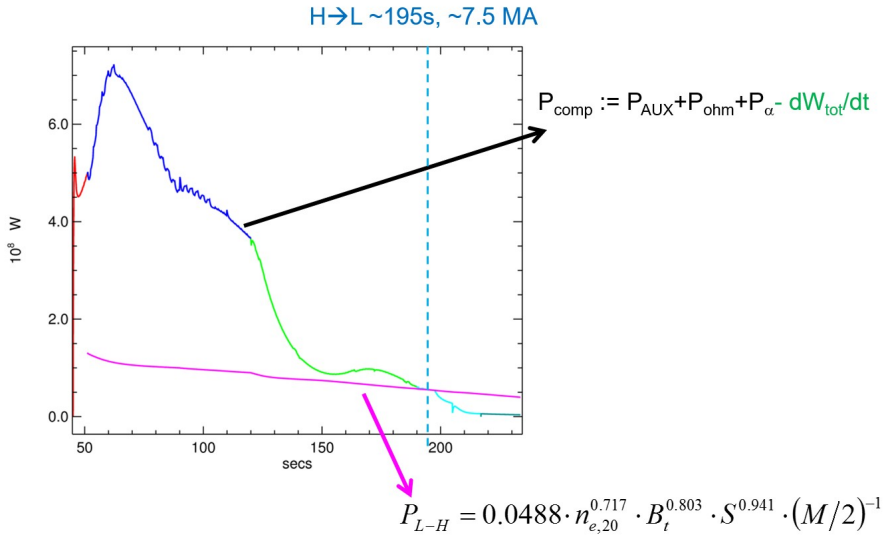

Figure 87.: H-L transition in 80kA/s trajectory.

the given plasma currents, li(3) is lower for 80kA/s, as a result also of the different strategy adopted. A slower current ramp-rate, a decreasing Z_{eff}, a gradual NB switch-off and an off-axis ECRH system in the final part of the ramp-down trajectory enabled the successful completion of the ramp-down simulation. From controllability point of view, avoiding a hot plasma centre

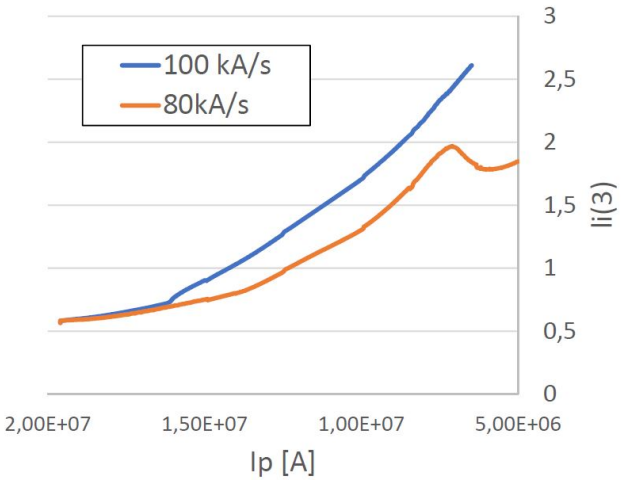

Figure 88.: Comparison of 100 and 80kA/s trajectories: li(3) vs plasma current.

and a cool edge is essential to spread the current density profile. In particular, a gradual switch-off of the NB source seems favourable to help in this process. Radiation has been here not fully consistently modelled, but it is clear that it is strongly dominating the ramp-down phase. This work (for both 2012 and 2015 DEMO designs) helped in the identifications of issues and actors dominating DEMO1 ramp-down.

4.3.5 The role of NBI in DEMO scenarios

This section summarizes the main outcomes related to NBI of the work presented in the previous sections on DEMO scenario modelling both for

DEMO1 and DEMO2. For DEMO1 pulsed concept, the role of NBI is mainly central plasma heating. As a by-product of the tangential injection, we have a current drive action, which is favourable in order to extend the discharge duration. It has been observed that NBI has a better efficiency in driving currents that a same power ECRH flattop system. The injection line and NB energy has been set to fulfil heating requirements, and with this on-axis injection, shine-through losses are negligible. 50MW of NBI at 1MeV guarantees the permanence in the H-mode, high fusion power scenario, and for low ramp-up power options, enables the scenario access. A beneficial properties of a NB system for DEMO would be the capability of a gradual switch-off in order to help in the plasma control during ramp-down. A NB source of 100keV has been discussed for ramp-up phase, showing similar capabilities to ICRH. In particular, an earlier fusion power production than ECRH system has been observed, probably due to the preferable ion heating.

Regarding a steady-state DEMO2 concept, the requirements for a NB system are more demanding. In addition to plasma heating, and scenario permanence, NBI becomes a direct actuator of the advanced scenario by driving a considerable part of the plasma current. In order to do this, more NB power is needed ($> 100MW$), and the NBI is set to drive off-axis currents which are essential to keep a reversed q profile. The beam vertical tilt has been identified as one of the possible parameter for determining the beam deposition. More off-axis depositions come at the cost of higher shine-through losses, although still within the limits for the flattop phase. An increase of NB energy would bring higher CD efficiency, but also higher beam penetration and shine-through losses. In general, at the NB power discussed and considering the remarkable DEMO plasma volume, NB particle fuelling is negligible with respect to the other sources. For the same reasons, it seems probable that DEMO NBI will have a negligible momentum injection.

Summarizing, DEMO NBI is a good actuator in terms of plasma heating and current drive (especially for DEMO2), but it has a negligible effect on fuelling and momentum.

5 CONCLUSIONS AND LIST OF PUBLICATIONS

This thesis deeply investigated the NBI-plasma interaction in magnetically confined fusion experiments. Neutral beam (NB) ionization in the plasma and the slowing down process are usually tackled by NBI modelling, which, depending on the modelling needs, can exploit fast analytical solvers or detailed Monte Carlo methods. The role of NBI has been studied for devices where it represents the dominant heating system, crucial for scenario access and plasma sustainment. NBI, thanks to its robustness and effectiveness, is not only one of the most used heating systems nowadays, but it is also considered for next step reactors. The physics basis of NBI-plasma interaction constitutes the common ground for the investigations carried out in this thesis: beam absorption, heat transfer and preferential heat channel (to ions or to electrons) and current drive have been in fact characterized for both leading experiments (JET and LHD), and for the European demonstration power plant DEMO. This permitted to cover a wide range of NBI and plasma parameters, to make comparisons e.g. on isotope effects for JET tokamak and LHD heliotron and finally to extrapolate and give shape to the role of NBI for DEMO.

Regarding JET tokamak, the first work presented in this thesis deals with detailed NBI modelling by ASCOT code. Starting from a validated simulation, JINTRAC predictive simulations have been run in order to reconstruct the ion temperature profile of a discharge when the experimental measurement was not available. Since at JET typical beam energies NB fast ions transfer heat mainly to plasma ions, a detailed NBI modelling with the Monte Carlo code ASCOT has been the appropriate tool. The ion temperature has been reconstructed, showing some differences with the reconstruction done with simpler models. This modelling scheme, which enabled a detailed and reliable reconstruction, has been then adopted within JET integrated modelling group for similar analyses of shots without a reliable ion temperature measurement.

Within JET isotope studies in support of ITER preparation, NBI modelling has been provided for the preparation of hydrogen experiments H14-03 of C34 campaign. The aim of these experiments was to study the isotopic dependence of transport, pedestal and confinement. Starting from a reference D discharge with D NBI, H NBI-plasma interaction has been predicted. The final power deposition resulted to be unaffected by the isotopic change, although a general fast ion confinement degradation has been observed in H. This lead also to higher shine through losses in H plasma with respect to D plasma.

Isotope effect has been studied also for LHD helical device, where D experiments are planned for the first time in the next future instead of the usual H discharges. The 5 NB systems (with up to 28MW, and energy up to 190keV) will be upgraded for D injection. The work carried out and presented in this thesis is part of the general purpose of upgrading TASK3D-a LHD transport analysis suite to enable D plasma analyses. Upgrades for FIT3D NBI code have been proposed, and a discussion on the underlying physics models have been presented. Two main modifications have been

proposed: the implementation of an updated and more reliable formula for the beam ionization cross section, and the implementation of a module which estimates the neutron production from fusion reactions from thermal plasma and beam-plasma interaction. The modifications of FIT3D are essential for the preparation of the analysis of NBI-plasma interaction for D LHD experiments, and have been reported in [87, 88]. The upgraded FIT3D code has been then applied to analyse LHD experiments: similar shots have been run changing the plasma composition from H to He majority. An increased ion temperature with He majority has been observed, and investigations started to understand the reason of this effect. One of the most impelling question was to understand the role of NBI in the observed ion temperature increase in He plasmas. From the work performed resulted that, although an increase of fast ion confinement with He plasmas, the final power deposition seemed to be unaffected by the plasma composition [92] and causes of the ion temperature increase are not related with NBI. If He and D discharges can be compared (as it seems from previous experiments in TEXT and ASDEX tokamaks), the behaviour seen here is similar to JET: the plasma composition seems to have negligible effects on NB power deposition, although some hints on better fast ion confinement and NB absorption with D or He are visible.

EU DEMO studies are in the pre-conceptual phase, and scenario modelling is an essential activity within EUROfusion Power Plant Physics and Technology (PPPT) department in support of DEMO design. At the moment, NBI is being considered for the main flattop auxiliary power system, and it represents the scenario actuator in terms of plasma heating and current drive. DEMO scenarios with dominant NBI have been hence investigated both for pulsed DEMO1 and steady-state DEMO2 concepts. The effect of NBI in DEMO1 flattop performance has been evaluated, showing that NB power is a sensitive tool to extend DEMO1 flattop duration, because of the increase of NB driven currents. NBI showed higher current drive efficiency with respect to ECRH system during flattop resulting in longer discharges at all the scanned powers. The resulting shine through losses seem to be not an issue for the reference DEMO NBI. In a brief discussion on NBI fuelling contribution to DEMO, it has been highlighted that for current DEMO plasma volume and injected NB power, NBI source of particle is negligible [157].

The switch-on and switch-off of DEMO NBI are delicate steps, and DEMO transient phases have been studied. Moreover the heating mix for ramp-up and ramp-down phase, and main requirements on heating systems are driving discussions in DEMO H&CD group. From the investigation of DEMO1 ramp-up performed, it resulted that, regardless to the heating systems employed (ECRH, ICRH and NBI 100keV have been compared), a minimum of 40MW is necessary for scenario access. Higher power options enable an earlier H-mode transition which does not rely any more to the switch-on of the flattop NBI heating (1MeV, 50MW). A beneficial effect on plasma controllability has also been noted with higher power due to the current profile spreading and the consequent lower values of li(3) during the current ramp-up. In case of ICRH and NBI 100keV systems during ramp-up, it is possible to observe an earlier fusion power production with respect to ECRH, likely due to the preferential ion heating. DEMO1 ramp-down has also been investigated, with the aim of assessing and validating ramp-down trajectories by means of detailed transport simulations. This study highlighted the criticality of the H-L transition and NBI switch-off, which should be done by

steps in order to better control the plasma. An additional ECRH source has been used to overcome the possible radiative collapse of the plasma at the NBI switch-off. In general, the plasma is more controllable with lower li(3), and this can be achieved with a careful mix of on-axis and off-axis heatings and by a reduction of the plasma current ramp-rate.

The role of NBI for DEMO2 is even more central, since this scenario relies on non-inductive currents to achieve mildly reversed q profiles. NB current drive in DEMO2 flattop has been investigated, as NBI is expected to provide the main contribution to non-inductive currents. The effect of different positions of off-axis driven current profiles have been investigated, with the consequent effect on q profile. Part of this work has been published in [146].

The work on DEMO investigated the role of NBI in DEMO scenarios, as a necessary actuator for plasma heating and, in case of DEMO2, for current drive. The ability of driving current is anyway beneficial also for DEMO1 flattop duration extension. DEMO heating mix is a crucial topic and this work gave an important contribution to the discussion. Part of the presented work on DEMO heating mix has been published in [17]. All the work presented on DEMO has been reported or is currently being included in EUROfusion PPPT final reports (e.g. [161]).

5.1 LIST OF MY PUBLICATIONS

- P. Vincenzi, S. Murakami, M. Osakabe, R. Seki, M. Yokoyama, T. Bolzonella, *Modification of FIT3D code for the analyses of LHD deuterium experiments*, NIFS-MEMO-74, Nov. 19, 2015

- P. Vincenzi, S. Murakami, M. Osakabe, R. Seki, M. Yokoyama, T. Bolzonella, *Analysis of LHD NBI-plasma interaction with upgraded FIT3D code of TASK3D-a analysis transport suite*, P1.86 at 25th International Toki Conference (ITC-25), 3-6 Nov. 2015, Toki-city, Gifu, Japan

- M.E. Puiatti, (...), P. Vincenzi et al., *Overview of the RFX-mod contribution to the international Fusion Science Program*, Nucl. Fusion 55 (2015) 104012

- P Vincenzi, F Koechl, L Garzotti, D B King, E Tindale, T Bolzonella, P T Lang, B Pegourié, M Romanelli and R Wenninger, 2015, *Fuelling and density control for DEMO*, Nucl. Fusion 55 (2015) 113028

- T. Franke, K. Avramidis, J. Jelonnek, G. Granucci, M. Kalsey, J.-M. Noterdaeme, A. Simonin, P. Sonato, P. Vincenzi, M. Q. Tran, *On the present status of the EU DEMO H&CD*, 2015, submitted to IEEE journal Transactions on Plasma Science

- P. Vincenzi, T. Bolzonella, *Energetic neutral particle beam interaction with thermonuclear plasmas: from present day experiments to reactor parameters*, FISMAT Italian National Conference on Condensed Matter Physics , Palermo, Italy, Sept 28 - Oct 2, 2015

- P. Vincenzi, S. Murakami, M. Osakabe, R. Seki, M. Yokoyama, T. Bolzonella, *NBI modelling by upgraded TASK3D-a code in preparation of LHD deuterium campaigns*, P1.150 at 42nd EPS European Physical Society Conference on Plasma Physics, 22-26 June 2015, Lisbon, Portugal

- Ronald Wenninger, W. Biel, F. Arbeiter, J. Auber, C. Bachmann, E. Fable, G. Federici, J. Garcia, R. Kemp, A. Loarte, Y. Martin, F. Maviglia, T. Pütterich, C. Reux, F. Ryter, B. Sieglin, P. Vincenzi, H. Zohm, *DEMO: Physics Challenges Beyond ITER*, 42nd EPS European Physical Society Conference on Plasma Physics, 22-26 June 2015, Lisbon, Portugal

- R. Wenninger, R. Kemp, F. Maviglia, H. Zohm, R. Albanese, R. Ambrosino, F. Arbeiter, J. Aubert, C. Bachmann, W. Biel, E. Fable, G. Federici, J. Garcia, A. Loarte, Y. Martin, T. Pütterich, C. Reux, B. Sieglin, P. Vincenzi, *DEMO Exhaust Challenges Beyond ITER*, P4.110 at 42nd EPS European Physical Society Conference on Plasma Physics, 22-26 June 2015, Lisbon, Portugal

- G. Giruzzi, J.F. Artaud, M. Baruzzo, T. Bolzonella, E. Fable, L. Garzotti, I. Ivanova-Stanik, R. Kemp, D. B. King,M. Schneider, R. Stankiewicz, W. Stepniewski, P. Vincenzi, D. Ward, R. Zagórski, *Modelling of pulsed and steady-state DEMO scenarios*, Nucl. Fusion 55 (2015) 073002

- G. Giruzzi, J.-F. Artaud, I. Ivanova-Stanik, R. Kemp, R. Zagórski, M. Baruzzo, T. Bolzonella, E. Fable, L. Garzotti, D. King, R. Stankiewicz, W. Stepniewski, P. Vincenzi, and D. Ward, *Modelling of Pulsed and Steady-State DEMO Scenarios*, TH/P1-14 at 25th IAEA Fusion Energy Conference, 13-18 Oct. 2014, St. Petersburg, Russia

- G. Giruzzi, J.F. Artaud, M. Baruzzo, T. Bolzonella, E. Fable, L. Garzotti, D. King, R. Stankiewicz, I. Ivanova-Stanik, P. Vincenzi, R. Zagórski, *DEMO physics assumptions and scenario modelling*, 2nd IAEA DEMO PROGRAMME WORKSHOP, 17-20 December 2013, IAEA Headquarters, Vienna, Austria

A APPENDIX

In this page: timeline of the main reactor concepts, from http://fti.neep.wisc.edu/ncoe/timeline/mfe/all.

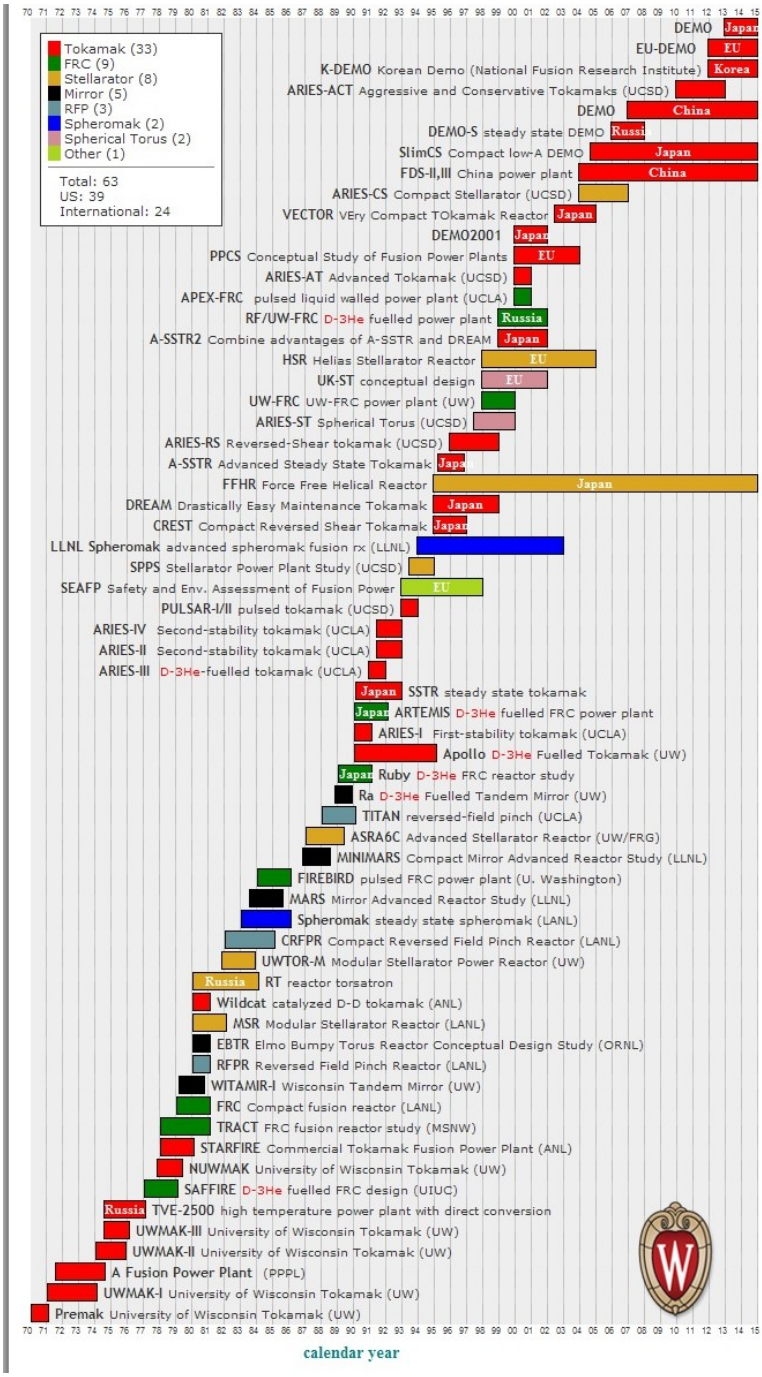

ACKNOWLEDGEMENTS

To conclude my thesis I would like to thank those who gave me help and support during this work.

I start the acknowledgements from my supervisor Tommaso, who guided me through these 3 years, always encouraging me and giving precious advices. I thank him for giving me always interesting opportunities to expand my knowledge and to start new collaborations. I found a very exciting environment in my frequent missions to international laboratories, and this surely helped my work. I wish to thank Osakabe-san, Yokoyama-san, Murakami-san, Seki-san, Kamio-san end Makino-san for the careful tutoring during my visits at LHD, both for work and for free time activities. I found stimulating discussions and guidance also at JET, in particular from Michele Romanelli, Tuomas Koskela and all the core transport modelling group. A particular and special thanks goes to Florian Köchl, who, although his busy life, always found time and energy to help me in the modelling activity, and guided me in the work that I published. DEMO scenario modelling group enlivened my Ph.D. life with stimulating discussions and meetings, and I am glad to say that I will likely continue my work on DEMO also in the future years. If I had a satisfying Ph.D. experience I have also to thank the whole RFX group, who gave me the opportunity of having a very good education. I would like to give a big hug to all the Ph.D. students I encountered at RFX, and in particular to Ondrej, Daniele, Matteo, Nisarg, Vadim e Nicoló: above all, we spent a fantastic period! In the international Ph.D. community I have been lucky to keep in touch with Marco and Hauke: climbing in the free afternoon of the EPS conference is not a common activity! Beside all my colleagues, I have to thank my family, who always supported me in my studies and career: it has been fundamental and I am lucky to have you! The last words are for my girlfriend Giulia: I am immensely happy to still have you near me!

Pietro Vincenzi

BIBLIOGRAPHY

[1] Christopher B Field and Maarten Van Aalst. *Climate change 2014: impacts, adaptation, and vulnerability*. Vol. 1. IPCC, 2014. URL: http://www.ipcc.ch/ (cit. on p. 1).

[2] Maria van der Hoeven. "World Energy Outlook 2013". In: (2013). URL: http://www.iea.org/ (cit. on p. 1).

[3] British Petroleum. "BP energy outlook 2035". In: *BP stats, Feb. 2015* (2015). URL: bp.com/energyoutlook (cit. on p. 1).

[4] Wesson John and Campbell David J. *Tokamaks*. 118. Oxford University Press, 2004 (cit. on pp. 2, 3, 9, 73).

[5] Jeffrey P Freidberg. "Plasma physics and fusion energy". In: Cambridge university press, 2007. Chap. 15 Heating and current drive (cit. on pp. 3, 9).

[6] M.E. Puiatti et al. "Overview of the RFX-mod contribution to the international Fusion Science Program". In: *Nuclear Fusion* 55.10 (2015), p. 104012. URL: http://stacks.iop.org/0029-5515/55/i=10/a=104012 (cit. on pp. 5, 7).

[7] T. Klinger et al. "Towards assembly completion and preparation of experimental campaigns of Wendelstein 7-X in the perspective of a path to a stellarator fusion power plant". In: *Fusion Engineering and Design* 88.6-8 (2013). Proceedings of the 27th Symposium On Fusion Technology (SOFT-27); Liége, Belgium, September 24-28, 2012, pp. 461 –465. ISSN: 0920-3796. DOI: http://dx.doi.org/10.1016/j.fusengdes.2013.02.153. URL: http://www.sciencedirect.com/science/article/pii/S0920379613002688 (cit. on pp. 5, 6).

[8] The ITER project. http://www.iter.org (cit. on p. 6).

[9] Freidberg Jeffrey P. *Plasma physics and fusion energy*. Cambridge university press, 2007 (cit. on p. 9).

[10] Kikuchi Mitsuru, Lackner Karl, and Tran Minh Quang. "Fusion physics". In: (2012). URL: https://inis.iaea.org/search/search.aspx?orig_q=RN:43116796 (cit. on pp. 9, 12).

[11] J.-M. Noterdaeme et al. *Innovations that make Ion Cyclotron Range of Frequency Power suitable for use in Fusion Reactors*. 25th International TOKI conference Toki-city Japan. 2015 (cit. on p. 10).

[12] H et al. Eubank. "Neutral-beam-heating results from the Princeton Large Torus". In: *Physical Review Letters* 43.4 (1979), p. 270 (cit. on p. 11).

[13] F et al. Wagner. "Regime of improved confinement and high beta in neutral-beam-heated divertor discharges of the ASDEX tokamak". In: *Physical Review Letters* 49.19 (1982), p. 1408 (cit. on p. 11).

[14] R. J. et al. Hawryluk. "Confinement and heating of a deuterium-tritium plasma". In: *Phys. Rev. Lett.* 72 (22 1994), pp. 3530–3533. DOI: 10.1103/PhysRevLett.72.3530. URL: http://link.aps.org/doi/10.1103/PhysRevLett.72.3530 (cit. on p. 11).

[15] M. Keilhacker et al. "High fusion performance from deuterium-tritium plasmas in JET". In: *Nuclear Fusion* 39.2 (1999), p. 209. URL: http://stacks.iop.org/0029-5515/39/i=2/a=306 (cit. on p. 11).

[16] V. Toigo et al. "Progress in the realization of the PRIMA neutral beam test facility". In: *Nuclear Fusion* 55.8 (2015), p. 083025. URL: http://stacks.iop.org/0029-5515/55/i=8/a=083025 (cit. on pp. 11, 13).

[17] T Franke et al. "On the Present Status of the EU DEMO H&CD Systems, Technology, Functions and Mix". In: *26th IEEE Symposium on Fusion Engineering (SOFE 2015)*. 2015 (cit. on pp. 11, 83, 103).

[18] M. Bacal. "Physics aspects of negative ion sources". In: *Nuclear Fusion* 46.6 (2006), S250. URL: http://stacks.iop.org/0029-5515/46/i=6/a=S05 (cit. on p. 13).

[19] A.C. Riviere. "Penetration of fast hydrogen atoms into a fusion reactor plasma". In: *Nuclear Fusion* 11.4 (1971), p. 363. URL: http://stacks.iop.org/0029-5515/11/i=4/a=006 (cit. on p. 15).

[20] J.A. Rome et al. "Particle-orbit loss regions and their effects on neutral-injection heating in axisymmetric tokamaks". In: *Nuclear Fusion* 16.1 (1976), p. 55. URL: http://stacks.iop.org/0029-5515/16/i=1/a=006 (cit. on pp. 16, 45).

[21] T H Stix. "Heating of toroidal plasmas by neutral injection". In: *Plasma Physics* 14.4 (1972), p. 367. URL: http://stacks.iop.org/0032-1028/14/i=4/a=002 (cit. on p. 17).

[22] EUROfusion. http://www.euro-fusion.org (cit. on p. 24).

[23] J. Paméla et al. "An ITER-like wall for JET". In: *Journal of Nuclear Materials* 363-365 (2007). Plasma-Surface Interactions-17, pp. 1 –11. ISSN: 0022-3115. DOI: http://dx.doi.org/10.1016/j.jnucmat.2006.12.056. URL: http://www.sciencedirect.com/science/article/pii/S0022311506006283 (cit. on p. 24).

[24] J Hobirk et al. "Improved confinement in JET hybrid discharges". In: *Plasma Physics and Controlled Fusion* 54.9 (2012), p. 095001. URL: http://stacks.iop.org/0741-3335/54/i=9/a=095001 (cit. on p. 24).

[25] P. Batistoni et al. "The JET technology program in support of ITER". In: *Fusion Engineering and Design* 89.7-8 (2014). Proceedings of the 11th International Symposium on Fusion Nuclear Technology-11 (ISFNT-11) Barcelona, Spain, 15-20 September, 2013, pp. 896 –900. ISSN: 0920-3796. DOI: http://dx.doi.org/10.1016/j.fusengdes.2013.12.050. URL: http://www.sciencedirect.com/science/article/pii/S0920379613007643 (cit. on p. 24).

[26] G F Matthews et al. "JET ITER-like wall - overview and experimental programme". In: *Physica Scripta* 2011.T145 (2011), p. 014001. URL: http://stacks.iop.org/1402-4896/2011/i=T145/a=014001 (cit. on p. 24).

[27] G.F. Matthews. "Plasma operation with an all metal first-wall: Comparison of an ITER-like wall with a carbon wall in {JET}". In: *Journal of Nuclear Materials* 438, Supplement (2013). Proceedings of the 20th International Conference on Plasma-Surface Interactions in Controlled Fusion Devices, S2 –S10. ISSN: 0022-3115. DOI: http://dx.doi.org/10.1016/j.jnucmat.2013.01.282. URL: http://www.sciencedirect.com/science/article/pii/S0022311513002900 (cit. on p. 24).

[28] G F Matthews et al. "The second phase of JET operation with the ITER-like wall". In: *Physica Scripta* 2014.T159 (2014), p. 014015. URL: http://stacks.iop.org/1402-4896/2014/i=T159/a=014015 (cit. on p. 24).

[29] F. Romanelli and on behalf of JET Contributors. "Overview of the JET results". In: *Nuclear Fusion* 55.10 (2015), p. 104001. URL: http://stacks.iop.org/0029-5515/55/i=10/a=104001 (cit. on p. 25).

[30] D. Čirić et al. "Performance of upgraded JET neutral beam injectors". In: *Fusion Engineering and Design* 86.6-8 (2011). Proceedings of the 26th Symposium of Fusion Technology (SOFT-26), pp. 509 –512. ISSN: 0920-3796. DOI: http://dx.doi.org/10.1016/j.fusengdes.2010.11.035. URL: http://www.sciencedirect.com/science/article/pii/S0920379610005065 (cit. on p. 25).

[31] M. Romanelli et al. "JINTRAC: A System of Codes for Integrated Simulation of Tokamak Scenarios". In: *Plasma and Fusion Research* 9 (2014), p. 3403023. URL: http://www.jspf.or.jp/PFR/PFR_articles/pfr2014S2/pfr2014_09-3403023.html (cit. on p. 26).

[32] A. Taroni G. Cennachi. *JET Report JET-IR(88)03*. 1988 (cit. on p. 26).

[33] W. A. Houlberg et al. "Bootstrap current and neoclassical transport in tokamaks of arbitrary collisionality and aspect ratio". In: *Physics of Plasmas* 4.9 (1997), pp. 3230–3242. DOI: http://dx.doi.org/10.1063/1.872465. URL: http://scitation.aip.org/content/aip/journal/pop/4/9/10.1063/1.872465 (cit. on p. 26).

[34] G.V. Pereverzev and G. Corrigan. "Stable numeric scheme for diffusion equation with a stiff transport". In: *Computer Physics Communications* 179.8 (2008), pp. 579 –585. ISSN: 0010-4655. DOI: http://dx.doi.org/10.1016/j.cpc.2008.05.006. URL: http://www.sciencedirect.com/science/article/pii/S001046550800218X (cit. on p. 26).

[35] R. Simonini et al. In: *Contribution to Plasma Physics* 34 (1994), p. 368 (cit. on p. 26).

[36] Lauro-Taroni L. *Proc. 21st EPS Conf. on Controlled Fusion and Plasma Physics (Montpelier, France)*. 1994 (cit. on p. 26).

[37] D. Reiter et al. In: *Fusion Science and Technology* 47.2 (2005), pp. 172 –186. URL: http://www.ans.org/pubs/journals/fst/a_698 (cit. on p. 26).

[38] B. Pégourié et al. "Homogenization of the pellet ablated material in tokamaks taking into account the ∇B -induced drift". In: *Nuclear Fusion* 47.1 (2007), p. 44. URL: http://stacks.iop.org/0029-5515/47/i=1/a=006 (cit. on p. 26).

[39] C.D. Challis et al. "Non-inductively driven currents in JET". In: *Nuclear Fusion* 29.4 (1989), p. 563. URL: http://stacks.iop.org/0029-5515/29/i=4/a=002 (cit. on p. 26).

[40] E. Hirvijoki et al. "ASCOT: Solving the kinetic equation of minority particle species in tokamak plasmas". In: *Computer Physics Communications* 185.4 (2014), pp. 1310 –1321. ISSN: 0010-4655. DOI: http://dx.doi.org/10.1016/j.cpc.2014.01.014. URL: http://www.sciencedirect.com/science/article/pii/S0010465514000277 (cit. on pp. 26, 27).

[41] J. Miettunen et al. "Predictive ASCOT modelling of 10Be transport in JET with the ITER-like wall". In: *Journal of Nuclear Materials* 438, Supplement (2013). Proceedings of the 20th International Conference on Plasma-Surface Interactions in Controlled Fusion Devices, S612 –S615. ISSN: 0022-3115. DOI: http://dx.doi.org/10.1016/j.jnucmat.2013.01.128. URL: http://www.sciencedirect.com/science/article/pii/S0022311513001360 (cit. on p. 26).

[42] K. Shinohara et al. "Effects of complex symmetry-breakings on alpha particle power loads on first wall structures and equilibrium in ITER". In: *Nuclear Fusion* 51.6 (2011), p. 063028. URL: http://stacks.iop.org/0029-5515/51/i=6/a=063028 (cit. on p. 27).

[43] B B Kadomtsev. In: *Sov. J. Plasma Phys.* 1 (1975), p. 389 (cit. on p. 28).

[44] T. Koskela et al. *Modelling of the effect of the ITER-like wall on NBI heating in JET*. 40th EPS Conference on Plasma Physics, Espoo, Finland. 2013. URL: http://ocs.ciemat.es/EPS2013PAP/pdf/P1.136.pdf (cit. on p. 29).

[45] J.G. Cordey et al. "Plasma confinement in JET H mode plasmas with H, D, DT and T isotopes". In: *Nuclear Fusion* 39.3 (1999), p. 301. URL: http://stacks.iop.org/0029-5515/39/i=3/a=301 (cit. on p. 30).

[46] E. Righi et al. "Isotope scaling of the H mode power threshold on JET". In: *Nuclear Fusion* 39.3 (1999), p. 309. URL: http://stacks.iop.org/0029-5515/39/i=3/a=302 (cit. on p. 30).

[47] V.P. Bhatnagar et al. "Edge localized modes and edge pedestal in NBI and ICRF heated H, D and T plasmas in JET". In: *Nuclear Fusion* 39.3 (1999), p. 353. URL: http://stacks.iop.org/0029-5515/39/i=3/a=305 (cit. on p. 30).

[48] JET Team (prepared by J.G. Cordey). "H mode power threshold and confinement in JET H, D, DT and T plasmas". In: *Nuclear Fusion* 39.11Y (1999), p. 1763. URL: http://stacks.iop.org/0029-5515/39/i=11Y/a=316 (cit. on p. 30).

[49] J G Cordey et al. "Isotope identity experiments in JET". In: *Plasma Physics and Controlled Fusion* 42.5A (2000), A127. URL: http://stacks.iop.org/0741-3335/42/i=5A/a=312 (cit. on p. 30).

[50] H. Urano et al. "Dimensionless parameter dependence of H-mode pedestal width using hydrogen and deuterium plasmas in JT-60U". In: *Nuclear Fusion* 48.4 (2008), p. 045008. URL: http://stacks.iop.org/0029-5515/48/i=4/a=045008 (cit. on p. 30).

[51] H. Urano et al. "Energy confinement of hydrogen and deuterium H-mode plasmas in JT-60U". In: *Nuclear Fusion* 52.11 (2012), p. 114021. URL: http://stacks.iop.org/0029-5515/52/i=11/a=114021 (cit. on p. 30).

[52] H. Urano et al. "Hydrogen isotope effects on ITG scale length, pedestal and confinement in JT-60 H-mode plasmas". In: *Nuclear Fusion* 53.8 (2013), p. 083003. URL: http://stacks.iop.org/0029-5515/53/i=8/a=083003 (cit. on p. 30).

[53] E. Delabie et al. *L-H threshold results in hydrogen plasmas in JET-ILW*. 57th Annual Meeting of the APS Division of Plasma Physics Savannah Georgia. 2015. URL: http://meetings.aps.org/Meeting/DPP15/Session/GP12.126 (cit. on p. 30).

[54] S Suzuki et al. "Attenuation of high-energy neutral hydrogen beams in high-density plasmas". In: *Plasma Physics and Controlled Fusion* 40.12 (1998), p. 2097. URL: http://stacks.iop.org/0741-3335/40/i=12/a=009 (cit. on pp. 30, 40, 51, 54).

[55] A. Komori et al. "Goal and achievements of large helical device project". In: *Fusion Science and Technology* 58.1 (2010). URL: http://www.ans.org/pubs/journals/fst/a_10788 (cit. on p. 35).

[56] M. Osakabe et al. *Current status of the LHD project and its prospect for deuterium experiment*. 25th International TOKI conference Toki-city Japan. 2015 (cit. on p. 35).

[57] M. Isobe and K. Ogawa. *Development of wide dynamic range neutron flux monitor toward LHD deuterium operation*. Twenty-Sixth Meeting of the ITPA Topical Group on Diagnostics Pohang University of Science and Technology. 2014 (cit. on p. 35).

[58] K. Tanaka et al. *Isotope effects on transport in Compact Helical System*. 41th EPS Conference on Plasma Physics, Berlin, Germany. 2014. URL: http://ocs.ciemat.es/EPS2014PAP/pdf/P4.019.pdf (cit. on p. 36).

[59] M. Isobe and K. Ogawa. *Development of wide dynamic range neutron flux monitor toward LHD deuterium operation*. Twenty-Sixth Meeting of the ITPA Topical Group on Diagnostics Pohang University of Science and Technology. 2014 (cit. on p. 36).

[60] Y. Takeiri et al. "Development of the Heating Scenarios to Achieve High-Ion Temperature Plasma in the Large Helical Device". In: *Plasma and Fusion Research* 10 (2015), p. 1402001. URL: http://www.jspf.or.jp/PFR/PFR_articles/pfr2015/pfr2015_10-1402001.html (cit. on p. 36).

[61] Masayuki YOKOYAMA et al. "Development of Integrated Transport Analysis Suite for LHD Plasmas Towards Transport Model Validation and Increased Predictability". In: *Plasma and Fusion Research* 8 (2013), pp. 2403016–2403016. DOI: 10.1585/pfr.8.2403016 (cit. on p. 37).

[62] S.P. Hirshmann et al. In: *Comp. Phys. Comm.* 43 (1986), p. 143 (cit. on p. 37).

[63] S. Murakami et al. In: *Trans. Fusion Technol.* 27 (1995), p. 256 (cit. on p. 37).

[64] Ryosuke SEKI et al. "Transport Study of LHD High-Beta Plasmas Based on Power Balance Analysis with TASK3D Code Module". In: *Plasma and Fusion Research* 6 (2011), pp. 2402081–2402081. DOI: 10.1585/pfr.6.2402081 (cit. on p. 37).

[65] H Lee et al. "Dynamic transport study of heat and momentum transport in a plasma with improved ion confinement in the Large Helical Device". In: *Plasma Physics and Controlled Fusion* 55.1 (2013), p. 014011. URL: http://stacks.iop.org/0741-3335/55/i=1/a=014011 (cit. on p. 37).

[66] M.H.Hughes and D.E.Post. In: *J. Comput. Phys.* 28.43 (1978) (cit. on p. 37).

[67] M.Yokoyama L.Hedrick et al. *The configuration dependence of ripple transport in LHD by the application of the GIOTA code*. NIFS-810, National Institute for Fusion Science (Feb. 2005). 2005. URL: http://www.nifs.ac.jp/report/NIFS-810.pdf (cit. on p. 37).

[68] V.V. Nemov et al. *Neoclassical transport for LHD in the 1/ν regime analyzed by the NEO code*. 32th EPS Conference on Plasma Physics, Tarragona, Spain. 2005. URL: http://epsppd.epfl.ch/Tarragona/pdf/P1_110.pdf (cit. on p. 37).

[69] C.D. Beidler and W.D. D'Haeseleer. In: *Plasma Phys. Control. Fusion* 37 (1995), p. 463 (cit. on p. 37).

[70] A. Sakai et al. "Integrated Heat Transport Simulation of Multi-Ion-Species Plasma in LHD". In: *Plasma and Fusion Research* 9 (2014), p. 3403124. URL: http://www.jspf.or.jp/PFR/PFR_articles/pfr2014S2/pfr2014_09-3403124.html (cit. on p. 37).

[71] M. Emoto et al. "Automatically processing physical data from LHD experiments". In: *Fusion Engineering and Design* 89.5 (2014). Proceedings of the 9th IAEA Technical Meeting on Control, Data Acquisition and Remote Participation for Fusion Research, pp. 758 –760. ISSN: 0920-3796. DOI: http://dx.doi.org/10.1016/j.fusengdes.2014.02.014. URL: http://www.sciencedirect.com/science/article/pii/S0920379614000982 (cit. on p. 37).

[72] A. Sakai et al. "Integrated Particle Transport Simulation of NBI Plasmas in LHD". In: *Plasma and Fusion Research* 10 (2015), p. 3403048. URL: http://www.jspf.or.jp/PFR/PFR_articles/pfr2015S2/pfr2015_10-3403048.html (cit. on p. 37).

[73] S. Murakami et al. "5-D simulation study of suprathermal electron transport in non-axisymmetric plasmas". In: *Nuclear Fusion* 40.3Y (2000), p. 693. URL: http://stacks.iop.org/0029-5515/40/i=3Y/a=333 (cit. on p. 38).

[74] M. Yokoyama. *TASK3D-a Documentation - version a02*. NIFS internal notes for TASK3D Users-Developers. 2014 (cit. on p. 38).

[75] H C Howe. *Physics Models in the Toroidal Transport Code PROCTR*. Oak Ridge National Laboratory, U.S. Department of Energy. 1990 (cit. on p. 38).

[76] S. Murakami et al. "Effect of neoclassical transport optimization on energetic ion confinement in lhd". In: *Fusion Science and Technology* 46 (2004), p. 241. URL: http://www.ans.org/pubs/journals/fst/a_561 (cit. on p. 38).

[77] Hiroyuki YAMAGUCHI et al. "NBI Heating Analysis of Time-Development Plasma in LHD". In: *Plasma and Fusion Research* 8 (2013), pp. 2403099–2403099. DOI: 10.1585/pfr.8.2403099 (cit. on p. 38).

[78] Ryosuke SEKI et al. "Monte Carlo Study Based on a Real Coordinate System for Tangentially Injected High-Energy Particles in the Large Helical Device". In: *Plasma and Fusion Research* 5 (2010), pp. 027–027. DOI: 10.1585/pfr.5.027 (cit. on p. 38).

[79] Ryosuke SEKI et al. "Monte-Carlo Study Based on Real Coordinates for Perpendicularly Injected High-Energy Ions in the LHD High-Beta Plasma". In: *Plasma and Fusion Research* 5 (2010), pp. 014–014. DOI: 10.1585/pfr.5.014 (cit. on p. 38).

[80] M. Homma, S. Murakami, and H. Yamaguchi. *Estimations of Beam-Beam Fusion Reaction Rates in the Deuterium Experiment Plasma on LHD*. 25th International TOKI conference Toki-city Japan. 2015 (cit. on p. 39).

[81] R.K. Janev, C.D. Boley, and D.E. Post. "Penetration of energetic neutral beams into fusion plasmas". In: *Nuclear Fusion* 29.12 (1989), p. 2125. URL: http://stacks.iop.org/0029-5515/29/i=12/a=006 (cit. on pp. 39, 51, 73).

[82] H.-S. Bosch and G.M. Hale. "Improved formulas for fusion cross-sections and thermal reactivities". In: *Nuclear Fusion* 32.4 (1992), p. 611. URL: http://stacks.iop.org/0029-5515/32/i=4/a=I07 (cit. on pp. 42, 47, 49–51).

[83] A.J. Peres. In: *J. Nucl. Mater.* 50 (1979), p. 5569 (cit. on p. 42).

[84] Masayuki HOMMA et al. "Simulation Study of Energetic Triton Confinement in the D-D Experiment on LHD". In: *Plasma and Fusion Research* 10 (2015), p. 3403050. URL: http://www.jspf.or.jp/PFR/PFR_articles/pfr2015S2/pfr2015_10-3403050.html (cit. on pp. 42, 48).

[85] *Fusion cross section theory*. Wolkenhauer W.C., Ed, 1972 (cit. on pp. 42, 50).

[86] J.D. Huba. *NRL Plasma Formulary*. Naval Research Laboratory, 2002 (cit. on p. 42).

[87] P. Vincenzi et al. *NBI modelling by upgraded TASK3D-a code in preparation of LHD deuterium campaigns*. 42th EPS Conference on Plasma Physics, Lisbon, Portugal. 2015. URL: http://ocs.ciemat.es/EPS2015PAP/pdf/P1.150.pdf (cit. on pp. 51, 102).

[88] P. Vincenzi et al. *Modification of FIT3D code for the analyses of LHD deuterium experiments*. NIFS-MEMO-74, Nov. 19, 2015. 2015 (cit. on pp. 51, 102).

[89] Brower D. L. et al. "Experimental evidence for coupling of plasma particle and heat transport in the TEXT tokamak". In: *Phys. Rev. Lett.* 65 (3 1990), pp. 337–340. DOI: 10.1103/PhysRevLett.65.337. URL: http://link.aps.org/doi/10.1103/PhysRevLett.65.337 (cit. on p. 52).

[90] M. Bessenrodt-Weberpals et al. "Helium and hydrogen isotope fuelling in tokamaks: similarities and differences". In: *Journal of Nuclear Materials* 196,Äì198 (1992). Plasma-Surface Interactions in Controlled Fusion DevicesProceedings of the Tenth International Conference on Plasma-Surface Interactions in Controlled Fusion Devices, pp. 943 – 947. ISSN: 0022-3115. DOI: http://dx.doi.org/10.1016/S0022-3115(06)80172-8. URL: http://www.sciencedirect.com/science/article/pii/S0022311506801728 (cit. on p. 52).

[91] K. Nagaoka et al. *Heat Transport Characteristics of High Temperature Discharges in LHD - Dependence on Hydrogen/Helium Ratio -*. 25th International TOKI conference Toki-city Japan. 2015 (cit. on p. 52).

[92] P. Vincenzi et al. *Analysis of LHD NBI-plasma interaction with upgraded FIT3D module of TASK3D-a analysis transport suite*. 25th International TOKI conference Toki-city Japan. 2015 (cit. on pp. 52, 57, 102).

[93] S. Murakami et al. *Predictions of Plasma Performance and Fusion Reactions in the Deuterium Experiment Plasma of LHD*. 25th International TOKI conference Toki-city Japan. 2015 (cit. on pp. 52, 57).

[94] S. Maeta et al. *Integrated heat transport simulation of the helium-hydrogen plasma of LHD by TASK3D*. 25th International TOKI conference Toki-city Japan. 2015 (cit. on pp. 52, 57).

[95] Goto M. et al. "Determination of the hydrogen and helium ion densities in the initial and final stages of a plasma in the Large Helical Device by optical spectroscopy". In: *Physics of Plasmas* 10.5 (2003), pp. 1402–1410. DOI: http://dx.doi.org/10.1063/1.1566024. URL: http://scitation.aip.org/content/aip/journal/pop/10/5/10.1063/1.1566024 (cit. on p. 53).

[96] Hiroyuki YAMAGUCHI and Sadayoshi MURAKAMI. "Effect of Impurity Ions on NBI Heating in LHD Plasmas". In: *Plasma and Fusion Research* 9 (2014), p. 3403127. URL: http://www.jspf.or.jp/PFR/PFR_articles/pfr2014S2/pfr2014_09-3403127.html (cit. on p. 54).

[97] G. Giruzzi et al. *WP12-SYS02-D04-D06-D07_DEMO Preliminary scenario analysis*. PPPT-SYS02 final report: EFDA_D_2D2EGL v1.0. 2012. URL: https://idm.euro-fusion.org//?uid=2L2F7V&uid=2L2F7V (cit. on pp. 59, 77).

[98] M. Schneider et al. "Self-consistent simulations of the interaction between fusion-born alpha particles and lower hybrid waves in ITER". In: *Nuclear Fusion* 49.12 (2009), p. 125005. URL: http://stacks.iop.org/0029-5515/49/i=12/a=125005 (cit. on p. 59).

[99] M. Schneider et al. "Simulation of the neutral beam deposition within integrated tokamak modelling frameworks". In: *Nuclear Fusion* 51.6 (2011), p. 063019. URL: http://stacks.iop.org/0029-5515/51/i=6/a=063019 (cit. on p. 59).

[100] J.F. Artaud et al. "The CRONOS suite of codes for integrated tokamak modelling". In: *Nuclear Fusion* 50.4 (2010), p. 043001. URL: http://stacks.iop.org/0029-5515/50/i=4/a=043001 (cit. on pp. 59, 72).

[101] Romanelli F. et al. *Fusion Electricity-A Roadmap to the Realisation of Fusion Energy*. 2012. URL: www.euro-fusion.org/wpcms/wp-content/uploads/2013/01/JG12.356-web.pdf (cit. on p. 59).

[102] Rebut P.H. et al. "A program toward a fusion reactor". In: *Physics of Fluids B* 3.8 (1991), pp. 2209–2219. DOI: http://dx.doi.org/10.1063/1.859638. URL: http://scitation.aip.org/content/aip/journal/pofb/3/8/10.1063/1.859638 (cit. on p. 61).

[103] D. Maisonnier et al. "Power plant conceptual studies in Europe". In: *Nuclear Fusion* 47.11 (2007), p. 1524. URL: http://stacks.iop.org/0029-5515/47/i=11/a=014 (cit. on p. 61).

[104] W.E. Han and D.J. Ward. "Revised assessments of the economics of fusion power". In: *Fusion Engineering and Design* 84.2-6 (2009). Proceeding of the 25th Symposium on Fusion Technology(SOFT-25), pp. 895–898. ISSN: 0920-3796. DOI: http://dx.doi.org/10.1016/j.fusengdes.2008.12.104. URL: http://www.sciencedirect.com/science/article/pii/S0920379609000064 (cit. on p. 61).

[105] G. Federici et al. "Overview of EU DEMO design and R&D activities". In: *Fusion Engineering and Design* 89.7-8 (2014). Proceedings of the 11th International Symposium on Fusion Nuclear Technology-11 (ISFNT-11) Barcelona, Spain, 15-20 September, 2013, pp. 882 –889. ISSN: 0920-3796. DOI: http://dx.doi.org/10.1016/j.fusengdes.2014.01.070. URL: http://www.sciencedirect.com/science/article/pii/S0920379614000714 (cit. on p. 62).

[106] ITER Physics Basis Editors et al. "Chapter 1: Overview and summary". In: *Nuclear Fusion* 39.12 (1999), p. 2137. URL: http://stacks.iop.org/0029-5515/39/i=12/a=301 (cit. on p. 62).

[107] H. Zohm et al. "On the physics guidelines for a tokamak DEMO". In: *Nuclear Fusion* 53.7 (2013), p. 073019. URL: http://stacks.iop.org/0029-5515/53/i=7/a=073019 (cit. on p. 62).

[108] Hartmut Zohm. "Assessment of DEMO challenges in technology and physics". In: *Fusion Engineering and Design* 88.6-8 (2013). Proceedings of the 27th Symposium On Fusion Technology (SOFT-27); Liége, Belgium, September 24-28, 2012, pp. 428 –433. ISSN: 0920-3796. DOI: http://dx.doi.org/10.1016/j.fusengdes.2013.01.001. URL: http://www.sciencedirect.com/science/article/pii/S0920379613000021 (cit. on p. 62).

[109] R. Wenninger et al. "Advances in the physics basis for the European DEMO design". In: *Nuclear Fusion* 55.6 (2015), p. 063003. URL: http://stacks.iop.org/0029-5515/55/i=6/a=063003 (cit. on p. 62).

[110] Kunihiko Okano, Gianfranco Federici, and Kenji Tobita. "DEMO design activities in the broader approach under Japan/EU collaboration". In: *Fusion Engineering and Design* 89.9-10 (2014). Proceedings of the 11th International Symposium on Fusion Nuclear Technology-11 (ISFNT-11) Barcelona, Spain, 15-20 September, 2013, pp. 2008 –2012. ISSN: 0920-3796. DOI: http://dx.doi.org/10.1016/j.fusengdes.2014.04.005. URL: http://www.sciencedirect.com/science/article/pii/S0920379614002725 (cit. on p. 62).

[111] Laila A El-Guebaly et al. "Fifty Years of Magnetic Fusion Research (1958-2008): Brief Historical Overview and Discussion of Future Trends". In: *Energies* 3.6 (2010), pp. 1067–1086. URL: http://www.mdpi.com/1996-1073/3/6/1067 (cit. on p. 63).

[112] B.N. Sorbom et al. "ARC: A compact, high-field, fusion nuclear science facility and demonstration power plant with demountable magnets". In: *Fusion Engineering and Design* 100 (2015), pp. 378 –405. ISSN: 0920-3796. DOI: http://dx.doi.org/10.1016/j.fusengdes.2015.07.008. URL: http://www.sciencedirect.com/science/article/pii/S0920379615302337 (cit. on p. 63).

[113] Satoru Tanaka and Hideyuki Takatsu. "Japanese perspective of fusion nuclear technology from ITER to DEMO". In: *Fusion Engineering and Design* 83.7-9 (2008). Proceedings of the Eight International Symposium of Fusion Nuclear Technology ISFNT-8 SI, pp. 865 –869. ISSN: 0920-3796. DOI: http://dx.doi.org/10.1016/j.fusengdes.2008.06.028. URL: http://www.sciencedirect.com/science/article/pii/S0920379608001683 (cit. on p. 64).

[114] R. Hiwatari et al. "Analysis of critical development issues towards advanced tokamak power plant CREST". In: *Nuclear Fusion* 47.5 (2007), p. 387. URL: http://stacks.iop.org/0029-5515/47/i=5/a=003 (cit. on p. 64).

[115] M. Kikuchi. "Steady state tokamak reactor based on the bootstrap current". In: *Nuclear Fusion* 30.2 (1990), p. 265. URL: http://stacks.iop.org/0029-5515/30/i=2/a=006 (cit. on p. 64).

[116] K. Tobita et al. "Design study of fusion DEMO plant at JAERI". In: *Fusion Engineering and Design* 81.8-14 (2006). Proceedings of the Seventh International Symposium on Fusion Nuclear Technology ISFNT-7 Part B Proceedings of the Seventh International Symposium on Fusion Nuclear Technology, pp. 1151 –1158. ISSN: 0920-3796. DOI: http://dx.doi.org/10.1016/j.fusengdes.2005.08.058. URL: http://

www.sciencedirect.com/science/article/pii/S0920379605006411 (cit. on p. 64).

[117] K. Tobita et al. "Compact DEMO, SlimCS: design progress and issues". In: *Nuclear Fusion* 49.7 (2009), p. 075029. URL: http://stacks.iop.org/0029-5515/49/i=7/a=075029 (cit. on p. 64).

[118] A. Sagara et al. "Helical reactor design FFHR-d1 and c1 for steady-state DEMO". In: *Fusion Engineering and Design* 89.9-10 (2014). Proceedings of the 11th International Symposium on Fusion Nuclear Technology-11 (ISFNT-11) Barcelona, Spain, 15-20 September, 2013, pp. 2114 –2120. ISSN: 0920-3796. DOI: http://dx.doi.org/10.1016/j.fusengdes.2014.02.076. URL: http://www.sciencedirect.com/science/article/pii/S0920379614001732 (cit. on p. 64).

[119] Kenji Tobita. *Concept development of compact DEMO reactor*. IEA/LT Workshop (W59) combined with DOE/JAERI Technical Planning of Tokamak Experiments (FP1-2) 'Shape and Aspect Ratio Optimization for High Beta Steady-State Tokamak', San Diego, GA. 2005. URL: fire.pppl.gov/iea59_optimiz_tobita.ppt (cit. on pp. 64, 65).

[120] Jinhua Huang et al. "Overview of Fusion-Fission Hybrid Reactor Design Study in China". In: *Fusion Science and Technology* 42.1 (2002), pp. 138–145. URL: http://www.ans.org/pubs/journals/fst/a_221 (cit. on p. 65).

[121] Y. Wu. "Conceptual design activities of FDS series fusion power plants in China". In: *Fusion Engineering and Design* 81.23-24 (2006). Proceedings of the Fifteenth International toki Conference on "Fusion and Advanced Technology" ITC-15 SI, pp. 2713 –2718. ISSN: 0920-3796. DOI: http://dx.doi.org/10.1016/j.fusengdes.2006.07.068. URL: http://www.sciencedirect.com/science/article/pii/S0920379606002687 (cit. on p. 65).

[122] Y. Wu et al. *The Fusion-Fission Hybrid Reactor for Energy Production: A Practical Path to Fusion Application*. 22nd IAEA Fusion Energy Conference FEC. 2008. URL: http://www-pub.iaea.org/mtcd/meetings/fec2008/ft_p3-21.pdf (cit. on p. 66).

[123] "DEMO development strategy based on China FPP program". In: *Fusion Engineering and Design* 83.7-9 (2008). Proceedings of the Eight International Symposium of Fusion Nuclear TechnologyISFNT-8 SI, pp. 877 –882. ISSN: 0920-3796. DOI: http://dx.doi.org/10.1016/j.fusengdes.2008.05.035. URL: http://www.sciencedirect.com/science/article/pii/S0920379608001130 (cit. on p. 66).

[124] K.M. Feng et al. "Conceptual design study of fusion DEMO plant at SWIP". In: *Fusion Engineering and Design* 84.12 (2009), pp. 2109 –2113. ISSN: 0920-3796. DOI: http://dx.doi.org/10.1016/j.fusengdes.2009.01.104. URL: http://www.sciencedirect.com/science/article/pii/S0920379609001136 (cit. on p. 66).

[125] Yun Tao Song et al. "Concept Design of CFETR Tokamak Machine". In: *Plasma Science, IEEE Transactions on* 42.3 (2014), pp. 503–509. ISSN: 0093-3813. DOI: 10.1109/TPS.2014.2299277 (cit. on p. 66).

[126] Chen Dehong et al. "Preliminary Cost Assessment and Compare of China Fusion Engineering Test Reactor". In: *Journal of Fusion Energy* 34.1 (2015), pp. 127–132. ISSN: 0164-0313. DOI: 10.1007/s10894-014-9770-x. URL: http://dx.doi.org/10.1007/s10894-014-9770-x (cit. on p. 66).

[127] M. Kwon et al. "A strategic plan of Korea for developing fusion energy beyond ITER". In: *Fusion Engineering and Design* 83.7-9 (2008). Proceedings of the Eight International Symposium of Fusion Nuclear Technology ISFNT-8 SI, pp. 883 –888. ISSN: 0920-3796. DOI: http://dx.doi.org/10.1016/j.fusengdes.2008.06.009. URL: http://www.sciencedirect.com/science/article/pii/S0920379608001567 (cit. on p. 66).

[128] Keeman Kim et al. "A preliminary conceptual design study for Korean fusion DEMO reactor". In: *Fusion Engineering and Design* 88.6-8 (2013). Proceedings of the 27th Symposium On Fusion Technology (SOFT-27); Liége, Belgium, September 24-28, 2012, pp. 488 –491. ISSN: 0920-3796. DOI: http://dx.doi.org/10.1016/j.fusengdes.2013.02.123. URL: http://www.sciencedirect.com/science/article/pii/S092037961300238X (cit. on p. 66).

[129] K. Kim et al. "Design concept of K-DEMO for near-term implementation". In: *Nuclear Fusion* 55.5 (2015), p. 053027. URL: http://stacks.iop.org/0029-5515/55/i=5/a=053027 (cit. on p. 66).

[130] Yu.A. Sokolov. "Overview of the Russian Demo plant study". In: *Fusion Engineering and Design* 29 (1995), pp. 18 –27. ISSN: 0920-3796. DOI: http://dx.doi.org/10.1016/0920-3796(95)80001-E. URL: http://www.sciencedirect.com/science/article/pii/092037969580001E (cit. on p. 67).

[131] Yu.A. Sokolov et al. "Russian DEMO plant study". In: *Fusion Engineering and Design* 41.1-4 (1998), pp. 525 –533. ISSN: 0920-3796. DOI: http://dx.doi.org/10.1016/S0920-3796(98)00301-9. URL: http://www.sciencedirect.com/science/article/pii/S0920379698003019 (cit. on p. 67).

[132] G. Shatalov et al. "Russian DEMO-S reactor with continuous plasma burn". In: *Fusion Engineering and Design* 51-52 (2000), pp. 289 –298. ISSN: 0920-3796. DOI: http://dx.doi.org/10.1016/S0920-3796(00)00262-3. URL: http://www.sciencedirect.com/science/article/pii/S0920379600002623 (cit. on p. 67).

[133] B.N. Kolbasov et al. "Russian concept for a DEMO-S demonstration fusion power reactor". In: *Fusion Engineering and Design* 83.7-9 (2008). Proceedings of the Eight International Symposium of Fusion Nuclear Technology ISFNT-8 SI, pp. 870 –876. ISSN: 0920-3796. DOI: http://dx.doi.org/10.1016/j.fusengdes.2008.07.041. URL: http://www.sciencedirect.com/science/article/pii/S0920379608002342 (cit. on p. 67).

[134] B.V. Kuteev et al. "Development of DEMO-FNS tokamak for fusion and hybrid technologies". In: *Nuclear Fusion* 55.7 (2015), p. 073035. URL: http://stacks.iop.org/0029-5515/55/i=7/a=073035 (cit. on p. 67).

[135] A.Yu. Dnestrovskij et al. "Integrated modelling of DEMO-FNS current ramp-up scenario and steady-state regime". In: *Nuclear Fusion* 55.6 (2015), p. 063007. URL: http://stacks.iop.org/0029-5515/55/i=6/a=063007 (cit. on p. 67).

[136] R. Srinivasan and S.P. Deshpande. "Strategy for the Indian DEMO design". In: *Fusion Engineering and Design* 83.7-9 (2008). Proceedings of the Eight International Symposium of Fusion Nuclear TechnologyISFNT-8 SI, pp. 889 –892. ISSN: 0920-3796. DOI: http://dx.doi.org/10.1016/j.fusengdes.2008.07.038. URL: http://www.sciencedirect.com/science/article/pii/S0920379608002366 (cit. on p. 67).

[137] Kernbichler W et al. "D-3He in Field Reversed Configurations-Ruby: an International Reactor Study". In: *Plasma Physics and Controlled Nuclear Fusion Research* 3 (1991), p. 555 (cit. on p. 67).

[138] Miley GH et al. "SAFFIRE-A D-3He Pilot Unit for Advanced-Fuel Development". In: *Electric Power Research Institute Report ER-645-1* (1979) (cit. on p. 67).

[139] Momota Hiromu et al. "Conceptual design of the D-3He reactor Artemis". In: *Fusion Science and Technology* 21.4 (1992), pp. 2307–2323 (cit. on p. 67).

[140] Najmabadi F. et al. "The ARIES-III D-3He tokamak-reactor study". In: *Fusion Engineering, 1991. Proceedings., 14th IEEE/NPSS Symposium on*. 1991, 213–218 vol.1 (cit. on p. 67).

[141] Kulcinski GL et al. "Summary of Apollo, A D-3He Tokamak Reactor Design". In: *Fusion Science and Technology* 21.4 (1992), pp. 2292–2296 (cit. on p. 67).

[142] F. Romanelli and G. Giruzzi. "A D-3He fusion reactor with an edge radiating layer". In: *Nuclear Fusion* 38.1 (1998), p. 103. URL: http://stacks.iop.org/0029-5515/38/i=1/a=309 (cit. on p. 68).

[143] P E Stott. "The feasibility of using D-3He and D-D fusion fuels". In: *Plasma Physics and Controlled Fusion* 47.8 (2005), p. 1305. URL: http://stacks.iop.org/0741-3335/47/i=8/a=011 (cit. on p. 68).

[144] M. Kovari et al. ""PROCESS": A systems code for fusion power plants-Part 1: Physics". In: *Fusion Engineering and Design* 89.12 (2014), pp. 3054 –3069. ISSN: 0920-3796. DOI: http://dx.doi.org/10.1016/j.fusengdes.2014.09.018. URL: http://www.sciencedirect.com/science/article/pii/S0920379614005961 (cit. on p. 68).

[145] G. Giruzzi et al. *DEMO physics assumptions and scenario modelling*. 2nd IAEA DEMO PROGRAMME WORKSHOP,17-20 December 2013, IAEA Headquarters, Vienna, Austria. 2013 (cit. on p. 68).

[146] G. Giruzzi et al. "Modelling of pulsed and steady-state DEMO scenarios". In: *Nuclear Fusion* 55.7 (2015), p. 073002. URL: http://stacks.iop.org/0029-5515/55/i=7/a=073002 (cit. on pp. 68, 74, 76, 80–82, 103).

[147] E. Surrey et al. "The influence of neutral beam optimization for DEMO on injector design". In: *Fusion Engineering and Design* 87.4 (2012), pp. 373 –383. ISSN: 0920-3796. DOI: http://dx.doi.org/10.1016/j.fusengdes.2012.03.028. URL: http://www.sciencedirect.com/science/article/pii/S0920379612002311 (cit. on pp. 71, 83, 87).

[148] Zohm H et al. "Assessment of H&CD System Capabilities for DEMO". In: 40^{th} *EPS Conference on Plasma Physics, Finland* (2013). URL: http://ocs.ciemat.es/EPS2013PAP/pdf/O3.108.pdf (cit. on pp. 71, 78, 90).

[149] Jenkins I et al. "Scoping studies for NBI launch geometry on DEMO". In: *Fusion Engineering (SOFE), 2013 IEEE 25th Symposium on*. IEEE. 2013, pp. 1–6. DOI: 10.1109/SOFE.2013.6635445 (cit. on p. 71).

[150] R. Albanese, R. Ambrosino, and M. Mattei. "CREATE-NL+: A robust control-oriented free boundary dynamic plasma equilibrium solver". In: *Fusion Engineering and Design* 96-97 (2015). Proceedings of the 28th Symposium On Fusion Technology (SOFT-28), pp. 664 –667. ISSN: 0920-3796. DOI: http://dx.doi.org/10.1016/j.fusengdes.2015.06.162. URL: http://www.sciencedirect.com/science/article/pii/S0920379615302167 (cit. on p. 72).

[151] Artaud J.F. *METIS user's guide*. Tech. rep. CEA/IRFM/PHY/NTT-2008.001, 2008 (cit. on p. 72).

[152] K. Okano et al. "NON-LINEAR INCREMENT OF BEAM STOPPING CROSS-SECTION BY CIRCULATING FAST IONS". In: 28^{th} *EPS Conference on Plasma Physics, Madeira, Portugal* (2001). URL: http://www.cfn.ist.utl.pt/EPS2001/fin/pdf/P2.088.pdf (cit. on p. 73).

[153] MH Li et al. *Modeling of EAST scenarios with the upgraded H/CD systems using METIS code*. 41^{th} EPS Conference on Plasma Physics, Berlin, Germany. 2014. URL: http://ocs.ciemat.es/EPS2014PAP/pdf/P5.024.pdf (cit. on p. 74).

[154] M Irishkin et al. *Automated comparison of profile reconstruction from measurements with integrated models*. 41^{th} EPS Conference on Plasma Physics, Berlin, Germany. 2014. URL: http://ocs.ciemat.es/EPS2014PAP/pdf/P5.002.pdf (cit. on p. 74).

[155] X. Litaudon et al. "Modelling of hybrid scenario: from present-day experiments towards ITER". In: *Nuclear Fusion* 53.7 (2013), p. 073024. URL: http://stacks.iop.org/0029-5515/53/i=7/a=073024 (cit. on p. 74).

[156] JF Artaud et al. *Simulation of present-day Tokamak Discharges Mimicking a Fully non-Inductive Burning Plasma*. 35^{th} EPS Conference on Plasma Physics, Hersonissos, Greece. 2008. URL: http://epsppd.epfl.ch/Hersonissos/pdf/P5_068.pdf (cit. on p. 74).

[157] P. Vincenzi et al. "Fuelling and density control for DEMO". In: *Nuclear Fusion* 55.11 (2015), p. 113028. URL: http://stacks.iop.org/0029-5515/55/i=11/a=113028 (cit. on pp. 74, 79, 102).

[158] Artaud JF and Kim SH. "A new free-boundary equilibrium evolution code FREEBIE". In: *39th European Physical Society Conference on Plasma Physics,(Stockholm, Sweden)*. Vol. 4. 2012, p. 023 (cit. on p. 83).

[159] G. Giruzzi et al. *Final Report on DEMO scenario modelling 2014, Task PMI-7.2.1-1 (2LMSDR v1.0)*. PPPT WP-PMI final report: EFDA_D_2LMSDR. 2014. URL: https://idm.euro-fusion.org/?uid=2LMSDR&version=v1.0&action=get_document (cit. on p. 83).

[160] A.R. Polevoi et al. "Assessment of plasma parameters for the low activation phase of ITER operation". In: *Nuclear Fusion* 53.12 (2013), p. 123026. URL: http://stacks.iop.org/0029-5515/53/i=12/a=123026 (cit. on pp. 83, 91, 94).

[161] P. Vincenzi and T. Bolzonella. *Final-Report WPPMI Scenario Modelling ENEA-RFX*. PPPT WP-PMI final report: EFDA_D_123456. 2014. URL: https://idm.euro-fusion.org/?uid=2LMSDR&version=v1.0 (cit. on pp. 90, 103).

[162] Y R Martin, T Takizuka, and the ITPA CDBM H-mode Threshold Database Working Group. "Power requirement for accessing the H-mode in ITER". In: *Journal of Physics: Conference Series* 123.1 (2008), p. 012033. URL: http://stacks.iop.org/1742-6596/123/i=1/a=012033 (cit. on pp. 91, 94, 97).

[163] M. Mattei, R. Albanese, and R. Ambrosino. *PPPT Final-Report WPMI 7.2.3.1_ED Mattei*. PPPT WP-PMI final report: EFDA_D_2MG9LF. 2014. URL: https://idm.euro-fusion.org/?uid=2MA2HJ&version=v1.0 (cit. on p. 93).